SYNTHESIS AND CHARACTERIZATION OF CdSe AND In_2S_3 NANOPARTICLES AND THEIR SURFACE MODIFICATION USING $Ru(bipy)_2Cl_2$ COMPLEX

By

DATTATRI JOIS
KUDANALLI NAGESHA

Bachelor of Science
Madras University
Chennai, India
1995

Master of Science
Indian Institute of Technology
Chennai, India
1997

Submitted to the Faculty of the
Graduate College of the
Oklahoma State University
in partial fulfillment of
the requirements for
the Degree of
DOCTOR OF PHILOSOPHY
December, 2002

SYNTHESIS AND CHARACTERIZATION OF CdSe AND In_2S_3 NANOPARTICLES AND THEIR SURFACE MODIFICATION USING $Ru(bipy)_2Cl_2$ COMPLEX

Thesis Approved:

Thesis Advisor

Dean of the Graduate College

ACKNOWLEDGEMENTS

I would like to thank my advisor, Dr. Nicholas A. Kotov for the wonderful experience of doing research under his guidance. The guidance, support, encouragement and research have been great. I would like to take this opportunity to thank him for all that he has done to help me pursue my career. I would like to thank my graduate committee - Dr. Knobbe, Dr. Apblett, Dr. Materer and Dr. Rosenberger, for their support and encouragement throughout my stay here. I would like to extend a special note of thanks to Dr. Lagadic for all the help and guidance.

Research was possible with the cooperation of my fellow group members. I would like to thank all group members – past and present. Ms. Ni Tong, Mr. Arif Mamedov, Ms. Nataliya Mamedova and Mr. Todd Crisp have provided me good support and friendship over the course of this work. A very special thanks to Ms. Ludy Avila for been a very good friend. Of course, I would like to dedicate this work to my loving parents for all their encouragement.

I would like to acknowledge the Chemistry Department for providing financial support during my stay here and an opportunity to pursue my research.

On a lighter note, this work would not have been completed but for the great atmosphere and the over-friendly owners and *baristas* at Aspen Coffee Company, Downtown, Stillwater. Thank you everybody.

TABLE OF CONTENTS

Chapter Page

I. INTRODUCTION.....1

A. Introduction.....1

B. Applications of nanoparticles.....1
1. Catalysis.....2
2. Biological.....3
3. Optoelectronics.....4
4. Energy Conversion and Storage.....4

C. Synthesis of Nanoparticles.....5
1. Reverse-micelle method 5
2. Sonication.....6
3. Capping agent or wet-chemical route.....6
4. Sol-gel methods.....7
5. Syntheses in a structured medium.....8

D.Characterization.....9
1. Transmission electron microscopy.....9
2. X-ray diffraction or powder X-ray powder diffraction.....10
3. Nuclear Magnetic Resonance.....11
4. X-ray Photoelectron Spectroscopy.....13
5. UV-vis Spectroscopy.....15
6. Luminescence.....16

E. Surface Modification.....17
1. Organic capping.....18
2. Inorganic capping.....19

F. Purpose.....21

II. SYNTHESIS OF CdSe, CdS NANOPARTICLES, RuBP COMPLEX..... AND THEIR CHARACTERIZATION.....23

A. Introduction.....23

B. Materials.....23

C. Instrumentation.....24

D. Preparation of nanoparticles.....26
1. Synthesis of CdSe nanoparticles stabilized by sodium citrate.....26
2. Synthesis of CdS nanoparticles stabilized by sodium citrate.....26
3. Synthesis of Ru(2,2'-bipyridyl-N,N')$_2$Cl$_2$ and (2,2'-bipyridyl-N,N') (malonate-O,O')copper (II) monohydrate.....27

E. Characterization.....27
1. UV-vis absorption.....28
2. Luminescence.....33
3. Transmission electron microscopy.....37

F. Conclusions.....38

III. SYNTHESIS OF In_2S_3 NANOPARTICLES AND THEIR CHARACTERIZATION.....39

A. Introduction.....39
B. Instrumentation.....41

C. Preparation of nanoparticles.....43
1. Synthesis of In_2S_3 nanoparticles stabilized by thioglycerol.....43
2. Synthesis of In_2S_3 nanoparticles stabilized by 1-amino-2-methyl-2-propanethiol hydrochloride.....44
3. Synthesis of In_2S_3 nanoparticles stabilized by sodium citrate.....44

D. Characterization.....44
1. UV-vis absorption.....44
2. Transmission electron microscopy.....48
3. Nuclear Magnetic Resonance.....51
4. Luminescence.....54
5. Time Resolved Photoluminescence.....60

D. Conclusions.....62

IV. CHALCOGEN SITE SURFACE MODIFICATION OF CdSe NANOPARTICLES WITH RuBP, CdS NANOPARICLES WITH CuBM AND In_2S_3 NANOPARTICLES WITH RuBP....63

A. Introduction....63

B. Modification reactions....68
1. CdSe_citrate nanoparticles modified with RuBP....68
2. CdS_citrate nanoparticles modified with CuBM....68
3. In_2S_3_citrate nanoparticles modified with RuBP....68

C. Results of RuBP modified CdSe_citrate nanoparticles....69
1. Structure of modified nanoparticles....69
a. Optical absorption spectrum....69
b. Transmission electron microscopy....75
2. Optical properties of RuBP-modified CdSe nanoparticles....78
a. Steady state luminescence....78
b. Time Resolved Photoluminescence....84
c. Molecular Modeling Studies....88

D. Results of RuBP modified In_2S_3_citrate nanoparticles....93
1. Structure of modified nanoparticles....93
a. Optical absorption spectrum....93
2. Optical properties of modified nanoparticles....98
a. Steady state luminescence....98
b. Time Resolved Photoluminescence....101

E. Conclusions....103

V. REFERENCE....112

LIST OF FIGURES

Figure Page

Chapter I

1. Reverse micelle synthesis of semiconductor NPs.....5
2. Colloidochemical synthesis of semiconductor NPs.....7
3. HREM images of CdSe NP and CdSe/ZnS core-shell NP.....10
4. X-ray diffraction images of thioglycerol stabilized CdS NPs.....11
5. ^{1}H NMR of thiophenol stabilized CdS NPs.....13
6. XPS of TOPO stabilized CdSe NPs.....14
7. Optical absorption spectra of II-VI semiconductor nanoparticles.....16
8. Luminescence spectrum of ZnS/CdSe NPs stabilized by TOP/TOPO.....17
9. Schematic for organic and inorganic type of modification.....19

Chapter II

10. UV-vis of citrate stabilized CdSe NPs.....29
11. UV-vis of citrate stabilized CdS NPs.....30
12. Luminescence of CdSe NPs.....34
13. Luminescence of CdS NPs.....35
14. Luminescence of CdSe NPs after dialysis.....36
15. TEM images of citrate stabilized CdSe NPs.....37

Chapter III

16. UV-vis of Tg stabilized In_2S_3 NPs.....45
17. UV-vis of AMPT stabilized In_2S_3 NPs.....46
18. UV-vis of citrate stabilized In_2S_3 NPs.....47
19. TEM of In_2S_3 NP.....49
20. Electron diffraction of In_2S_3 NP.....50
21. NMR of In_2S_3 NP.....52
22. Luminescence of Tg stabilized In_2S_3 NPs.....55
23. Luminescence of AMPT stabilized In_2S_3 NPs.....56
24. Luminescence of citrate stabilized In_2S_3 NPs.....57
25. Luminescence of In_2S_3 NP after dialysis.....58
26. Time resolved photoluminescence of In_2S_3 NP.....61

Chapter IV

27. Structure of RuBP.....65
28. UV – vis of CdSe-RuBP modification reaction.....70
29. UV – vis of modification reaction – evolution with time.....71
30. UV – vis of CdSe (30:1) with different ratios of RuBP.....73
31. UV of RuBP + selenourea.....74
32. UV of CdSe, CdSe + RuBP before and after dialysis.....76
33. TEM of CdS and CuBM modified CdS.....77
34. Structure of CdSe – RuBP supramolecule.....78
35. Luminescence of CdSe (30:1) + 60 µl RuBP.....80
36. Luminescence of CdSe with different ratios of RuBP.....81
37. Luminescence of different size CdSe + RuBP.....82
38. Luminescence of RuBP modified CdSe before and after dialysis.....83
39. Excitation spectrum of RuBP modified CdSe.....86
40. Excitation spectrum of RuBP modified CdSe.....87
41. Molecular Modeling.....89
42. UPS spectra of CdS and CdS modified with CuBM.....91
43. UV of In_2S_3 modified with RuBP.....94
44. UV of RuBP + Na_2S.....96
45. UV of In_2S_3 with different ratios of RuBP.....97
46. Luminescence of RuBP modified In_2S_3 NPs.....99
47. Luminescence of In_2S_3 NPs modified with different ratios of RuBP.....100

LIST OF TABLES

Table Page

1. Particle size vs absorption edge of citrate stabilized CdSe nanoparticles.....31
2. Particle size vs absorption edge of citrate stabilized CdS nanoparticles.....32
3. Lifetime of CdSe and RuBP modified CdSe nanoparticles.....84
4. Lifetime of In_2S_3 and RuBP modified In_2S_3 nanoparticles.....101

NOMENCLATURE

A	Angstrom
AMPT	1-amino-2-methyl-2-propanethiol hydrochloride
AOT	Aerosol-OT
CuBM	(2,2'-bipyridyl-N,N')(malonate-O,O')copper (II)monohydrate
DMF	N,N-dimethylformamide
E	Chalcogen atom in general
EDAX	Element detection and analysis by X-rays
eV	Electron volt
HOMO	Highest occupied molecular orbital
λ	Wavelength
LUMO	Least occupied molecular orbital
μ	micro
NP	Nanoparticles
nm	Nanometer
NMR	Nuclear magnetic resonance
ns	Nanosecond
OD	Optical density
φ	Quantum yield
RuBP	Ruthenium $(2,2'\text{-bipyridyl-N,N'})_2Cl_2$
τ	Lifetime
TEM	Transmission electron microscopy
Tg	Thioglycerol
TOP	Trioctyl phosphine
TOPO	Trioctyl phosphine oxide
TRPL	Time resolved photoluminescence
UPS	Ultra violet photoelectron spectroscopy
UV	Ultra violet
XPS	X-ray photoelectron spectroscopy
XRD	X-ray diffraction

CHAPTER I

INTRODUCTION

A. Nanoparticles: Introduction

During the past few decades, the field of chemistry has seen a new area emerge known as nanoparticle/nanomaterial research. It could be said that this new field gained recognition when Arnim Henglein wrote the first review on these materials in 1989.[7] In this paper, Henglein states: " By 'small particles' are meant clusters of atoms or molecules of metals and semiconductors, ranging in size from <1 nm to almost 10 nm or having agglomeration numbers from <10 up to a few hundred, i.e., species representing the neglected dimension between single atoms or molecules and bulk materials". Initially starting out with colloidal semiconductor and metals, this field has now branched out to a variety of other fields.[1,2,3,4,5,6,7]

The NPs have the same interior geometry as a known bulk material, yet exhibit variations in their phase transition pressures, melting points, optical, optoelectrical, catalytic, magnetic and electrical properties with size.[4] The important effect seen in the case of NPs is know as the quantum size effects which is due to changes in the density of electronic states with particle size.[1] Thus, nanocrystals can be said to represent a new class of materials with a hybrid molecular and bulk properties.[1,4,7]

B. Applications of nanoparticles:

Nanoparticles of a variety of materials ranging from metals,[8] metal oxides,[9] polymers[10] and metal chalcogenides [4,6,13,14,15,16] in a wide range of sizes have been synthesized and characterized. But the semiconductor chalcogenide NPs are the one for

which the quantum confinement or quantum size effect is most pronounced and has been extensively studied. The ability to control the properties of the materials by controlling the size of the NP has lead to wide variety to applications for the nanomaterials. The fields of applications are very diverse, from materials chemists to biochemists.[1,4] Going into the details of all the applications is beyond the scope of this work; here, they will be discussed briefly.

1) Catalysis: NPs find applications as sensitizers and catalysts for photochemical reactions as a result of the small size, which results in a high surface area-to-volume ratio. The size quantization effect results in formation of different energy levels as compared to bulk material. Upon light absorption, the charge carrier migrates to the surface to these new levels where they can reduce or oxidize surface-bound chemical species. A number of studies on this type of chemistry have been reported. It has been reported that ZnS NPs have been used for the oxidation of alcohols and the reduction of CO_2 to formic acid.[17] There have been reports of hydrogen production by illumination of aqueous colloids of PbSe (50 Å) or HgSe (50 Å) [17] particles; a reaction not observed when bulk PbSe is used. Similarly, CO_2 reduction to formic acid, from CO_2-saturated aqueous solutions has been reported to occur in the presence of CdSe (50 Å), whereas no reaction is observed if larger particles are used.[17] There has been great interest in the use of TiO_2 NPs as sensors, for the detection of O_2, NO_2, and organic molecules.[18,19] The selectivity of the sensor depends on the method used to produce TiO_2 NPs, with the efficiency of the chemical sensor increasing as particle size decreases.

2) Biological: A new direction of NP research that has received a lot of attention lately is the conjugation of biological molecules such as antibodies and peptides [11] on the surface of semiconductor and metal NPs. Depending on the method of synthesis, nanocrystals can have a hydrophobic, hydrophilic, cationic, anionic, or neutral faces to the surrounding environment for the required applications. Therefore, NPs can be considered as groups that resemble proteins and can undergo chemical reactions similar to proteins.[20] Biomodified NPs have also been used for luminescence tagging,[20] drug delivery,[12] and for assembling hybrid protein - NP units.[12] Semiconductor quantum dots (CdS, CdSe, CdSe/ZnS) are becoming favored as robust luminescent probes for biological applications.[20] CdSe-CdS core-shell nanocrystals enclosed in a silica shell has been reported as a potential biological staining material.[20a] Since the semiconductor nanocrystals have narrow, tunable, symmetric emission spectrum and are photochemically stable, they are suitable fluoroscent probe over the conventional fluorophores.[20]

Another potential application for NPs is as a drug delivery agent for cancer treatment. Isotopes of ^{67}Cu, ^{111}In, ^{212}Bi, ^{213}Bi, ^{186}Re, ^{153}Sm and ^{90}Y have been used for cancer treatment.[21] The present methodology involves the use of a chelating agent to couple the radioisotope to the antibodies, which specifically target the tumor cells. One of the disadvantages of using chelating agents is the weak bond between the chelate and the isotope, which results in easy release of the isotope in the body before reaching the tumor cells. This is not a desired property since the radioisotopes are not specifically targeting the tumor cells. Since, NPs forms a strong bond with the antibodies they can be used instead of the chelating agents to make the radioisotopes specifically target the tumor

cells. In principle, NPs made with the radioisotopes can be conjugated to antibodies instead of the chelating agents and introduced in the human body to specifically target the tumor cells for cancer treatment.

3) Optoelectronics: Electroluminescent materials have been made using NPs and semiconducting polymers. Light emitting diodes have been fabricated from a hybrid cadmium selenide nanocrystallites and semiconducting *p*-paraphenylene vinylene (PPV) mateial.[24] The color of emission is dependent on the size of the nanocrystal used. The importance of these kinds of devices is the degree of voltage tunability with the size of the nanocrystal. Mn^{2+} doped ZnS is another important electroluminescent material that is extensively used in the electronics industry.[23] The Mn^{2+}can be introduced either as a doped ZnS:Mn (interstitial Mn^{2+}) or activated ZnS:Mn (surface Mn^{2+}) particles. A design for a solid-state laser, based on the luminescence properties of metal chalcogenide quantum dots (CdSe, CdTe, ZnSe, ZnTe), in a host material such as poly (methyl methacrylate) has been described recently in the literature.[24] The wavelength of the emitted light is determined by the size of the nanocrystallites chosen.

4) Energy Conversion and Storage. Grätzel and co-workers [25,26] reported the construction of a novel solar cell device, based on the sensitization of highly porous nanocrystalline TiO_2 with organic dyes. Another semiconductor nanocrystalline material of interest for thin film solar cell device is CdTe [27a], suitable as a light absorber.

C. Synthesis of Nanoparticles:

One of the fundamental challenges in the study of NP is their synthesis. The synthesis and characterization of these NPs can be an involved and complex task. There are a variety of methods to make these NPs, each with its advantages and limitations. Considering semiconductor NPs, some of the desired properties include narrow size distribution, good crystallinity, and high luminescence quantum yield.

1) Reverse-micelle method: In this method of synthesis, a microemulsion is first made by dissolving the surfactant Aerosol-OT (AOT) in heptane, followed by the addition of water. An aliquot of the metal salt is added to this microemulsion and then the solution of sulfide or selenide, depending on the type of semiconductor NP being synthesized.[28, 29, 30] This is illustrated in Figure 1. The size of the colloid so obtained depends on the "water-pool" size, governed by the ratio (ω) of AOT/H_2O, as well as the

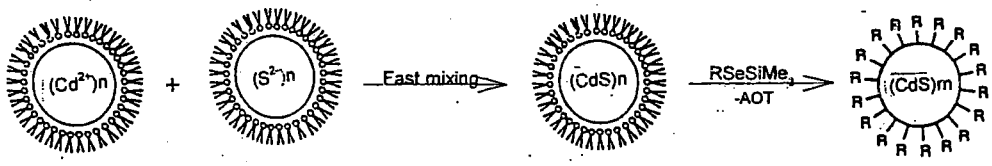

Figure 1. Reverse micelle synthesis of semiconductor NPs
(Adapted from reference 28)

ratio of metal ion/AOT. The drawback of this method is the difficulty in controlling the size of the "water pool" and hence the size of NP formed. Examples of semiconductor colloids synthesized by this method are CdS, CdSe and ZnS.[28, 30, 31]

2) Sonication: Ultrasound has been used to synthesize nanocolloids from powdered bulk semiconductor materials.[32,33] The procedure involves dispersing the semiconductor material in water (or suitable solvent) and introducing it in a sonicator in an atmosphere of H_2. Hydrogen acts as a scavenger of OH radical that is formed from water and thus prevents the degradation of the formed colloidal NP. The main drawback of this method is the difficulty in controlling the size of the formed nanocolloid. MoS_2 and WSe_2 are examples of NPs synthesized by this method.[32,33]

3) Capping agent or wet-chemical route: In colloidochemical route, the precipitation reaction is carried out in homogeneous solution in the presence of the so-called stabilizers.[6,13,16,34] The stabilizers prevent the colloids from agglomerating or growing further, thus allowing the particles to remain in solution. Stabilizers generally used are thiols, polyphosphates, sulfonic acids, trioctyl phosphine (TOP) and trioctyl phosphine oxide (TOPO). A typical synthesis is illustrated Figure 2. To synthesize a metal sulfide NP, the metal salt (chloride, acetate, perchlorate) is first dissolved in water followed by the addition of a stabilizer. The pH is adjusted to a suitable value and the chalcogen source (hydrogen sulfide, sodium sulfide, hydrogen telluride, thiourea, selenourea) is rapidly injected. Depending on the source of chalcogen, the reaction mixture might be heated. The NP stays in solution and can be precipitated as a powder by a variety of solvents such as acetone and alcohols. The advantage of this type of preparation is its versatility. A variety of semiconductor [35,36] NPs (CdS, CdSe, ZnS, HgTe), metal oxide [9]

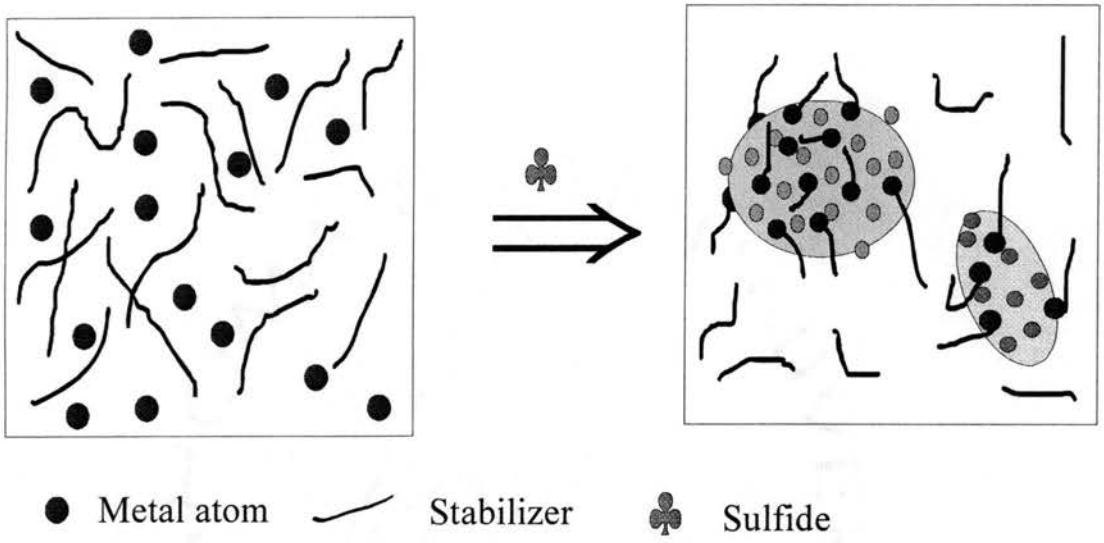

Figure 2. Colloidochemical synthesis of semiconductor NPs

(TiO_2, SnO_2) and metal [8] NPs (Pt, Pd, Au, Ag) have been synthesized by this method. The versatility of this method lies in the ability to control the size of the nanocrystal formed. This is accomplished by changing the metal ion to stabilizer ratio, pH, starting materials, chemical structure of stabilizer molecule, solvent, reaction atmosphere, heating temperature and heating time. Most of the syntheses are done in relatively low temperature and this could lead to formation of defects in the structure, resulting in poor crystallinity of the sample.[5] This form of synthesis is also not applicable to moisture sensitive materials like GaAs and InSb.

4. Sol-gel methods: This method is used to synthesize metal oxide NP like TiO_2 and Fe_2O_3.[22] In a typical synthesis, the metal salt (chloride or isopropoxide) is dissolved in ethanol and ammonia is added to help the hydrolysis to form the corresponding hydroxide. The resulting sol is generally dried in air or under inert atmosphere to form

the gel. The product may be subsequently calcined at higher temperatures to improve the mechanical properties of the nanostructured materials. This method has also been used to incorporate semiconductor NPs like CdS and CdSe in the framework of the glass or TiO_2. The limitation of this method is in the inability to produce NPs other than metal oxides and the difficulty in controlling the size of the resulting metal oxide NPs.

5. Syntheses in a structured medium: A large number of matrices such as zeolites,[37,38] layered solids,[39] molecular sieves,[40] micelles,[41] gels,[42] polymer,[43] and glasses [44] have been used to synthesize semiconductor nanoparticles. The matrices limit the size to which a nanocrystallite can grow. One example of the synthesis of CdS nanocrystallites in a structured medium, namely zeolite, is mentioned below. Zeolites are aluminosilicate materials with pores and channels that are very small (in nanometer regime) and have been used to synthesize NPs. To prepare NPs encapsulated in zeolites,[37] the sodium salts in the zeolites are first ion-exchanged with the cadmium salt. This is then calcined in a nitrogen atmosphere, followed by a flow of hydrogen sulfide at controlled pressure and flow rate. The excess hydrogen sulfide is evacuated. Generally a 1:1 metal to sulfur ratio and a low loading level (1 %) of metal is used, but levels up to 28 % have been reported.[37] The presence of matrix greatly complicates optical studies and hence the utilization of NPs. Since the matrixes have pores and channels of various sizes, it broadens the NP size distribution during the synthesis. Examples of NPs prepared by this method include CdS, CdSe and ZnS. [37, 38]

There are a few post-synthesis procedures that can be used to further purify the prepared NPs. They are size exclusion chromatography,[45] gel electrophoresis [46] and size-

selective precipitation [6] to name a few. Thus, limitations in one method of synthesis can, to some extent be overcome by these post-synthesis techniques.

D: Characterization:

The synthesized nanoparticles are characterized by standard procedures to elucidate the structure, optical and surface properties. Size, morphology and crystallinity can be found from the transmission electron microscopy (TEM) [13,14,16,47] and X-ray diffraction (XRD) [6,33,47] data. Surface properties can be investigated using X-ray photoelectron spectroscopy (XPS) [48] and nuclear magnetic resonance (NMR) techniques.[49,50,51] The optical and electronic properties are studied by UV-vis absorbance,[6,13,16,45] luminescence [36,47,52,53,54] and time resolved photoluminescence (TRPL) experiments.[36,50,51]

D.1 Transmission electron microscopy (TEM):

The most direct way to determine the size of nanoparticles is by analyzing the TEM images.[2,16,47] This technique also allows imaging of individual crystallites and the development of a statistical distribution of the size and shape of the particle in a given sample. This is clearly seen in Figure 3. High magnification imaging with lattice contrasts allows for the determination of individual crystalline morphology. TEM can also be used for observing the ordering of crystallites into secondary structures. Electron microscopy is generally coupled with EDAX (Element Detection and Analysis by X-rays) measurement to determine the composition.[15,16] The main limitation of TEM for determining the size of NPs is that the results are inconsistent and not reliable for small sized clusters.[6] This can be overcome by using small angle X-ray diffraction techniques.

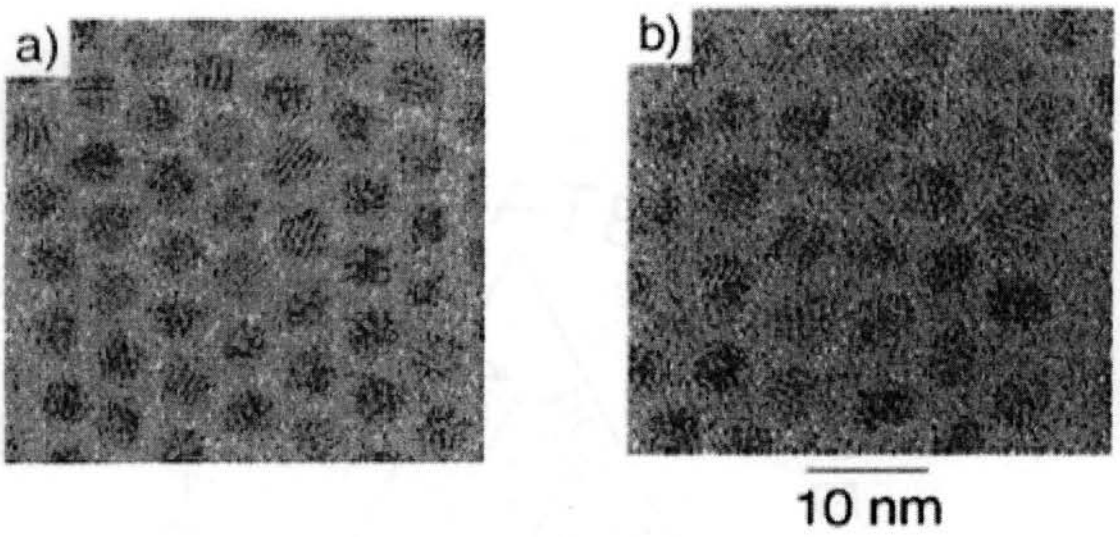

Figure 3. HRTEM images of a) CdSe NP and b) CdSe/ZnS core-shell NP
(Adapted from reference 47)

D.2 X-ray diffraction or powder X-ray powder diffraction (XRD):

This technique is used to estimate the size of small NPs, which is difficult to approximate from the TEM technique. XRD can be used to determine the crystallinity and the crystal phase of the NPs.[6,33] The peak angle maxima can be converted to the nearest neighbor distances of the clusters in the powdered samples using the Bragg equation:

$$2d \sin \theta = n\lambda$$

where θ is the angle of incidence or the Bragg angle, λ is the X-ray wavelength and d is the distance between the adjacent planes, also known as the d-spacing. These distances can be used to measure the mean particle size, taking into account the ligand shell.

The particle size is determined using the Scherrer formula:

$$t = 0.9\ \lambda / B \cos \theta_B$$

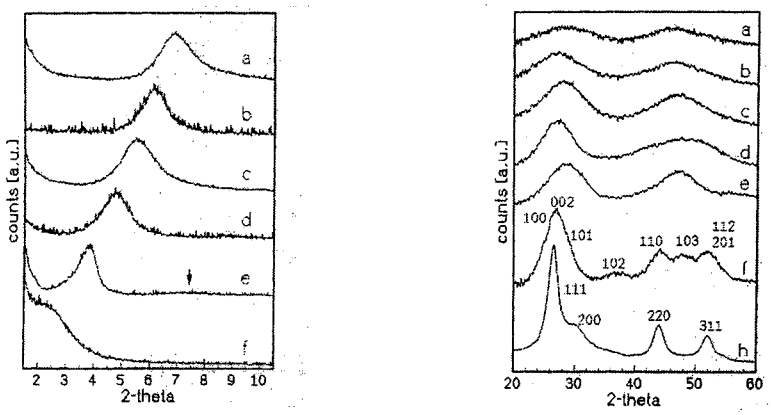

Figure 4. X-ray diffraction 1) small angle and 2) wide angle pattern of 1-thioglycerol stabilized CdS nanoparticles (Adapted from reference 6)

where t is the thickness of the crystal (in angstroms), λ the X-ray wavelength and θ_B the Bragg angle.

Due to the small particle size, the diffractograms exhibit very broad diffraction peaks and this is typical for particles of such small sizes. The appearance of a reflection maximum in the small-angle region of the X-ray diffraction patterns is due to the periodicity of their arrangement. The appearance of such peaks provides further confirmation for the narrow size distribution of the particles. In case of large particles, the crystalline structure can be readily derived from the diffractograms as seen in Figure 4.

D.3 Nuclear Magnetic Resonance (NMR):

NMR has been used to study the surfactant molecules absorbed on the NP surface and this in turn is useful to understand the structure of the NP. ^{1}H, ^{13}C, ^{31}P, ^{113}Cd NMR techniques[49,50,51] both in liquid state and solid state have been used. In general, homogeneous broadening of the lines is observed in NMR spectra of the molecules

bounded to or absorbed on the surface. The broadening is rationalized as slowing down of the molecule tumbling motion at the surface, low motional average and fast T_2 relaxation. Thus, NMR can distinguish the molecules that are attached to the surface from molecules that are free in solution.

Surface coverage of the organic molecule on the NP can be quantified by comparing the integrated signal of the stabilizers with that of an internal standard of known concentrations. The broadening effect and the chemical shift may or may not be dependent upon the particle size, which can be determined by the nature of the capping agent. For example, in the case of thiophenol stabilized CdS NPs [49], the NMR signals of the aromatic ring has been used to investigate the surface as shown in Figure 5. It can be seen that as the size decreases, the surface area and hence the surface coverage increases. The ring molecules experience more steric hindrance and faster T_2 relaxation. As a result, there is an increase in the signal intensity with decreasing size. In addition to the increase in signal intensity of the thiophenol signals there is also size dependence of the line widths of these peaks. This broadening of the signals is homogeneous as a result of changes in the mechanism of motional narrowing of the lines. The selective transverse relaxation time (T_2) measurements were used to study the broadening.

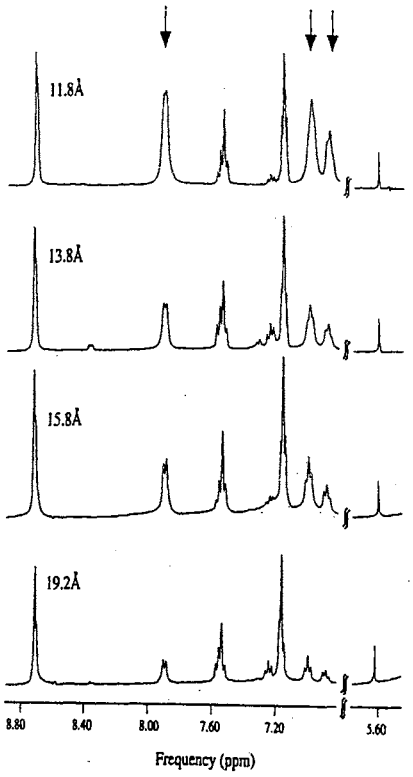

Figure 5. ^{1}H NMR spectra of solutions of thiophenol stabilized CdS nanoparticles of different sizes. The arrows indicate the thiophenol resonance.
(Adapted from reference 49)

D.4 X-ray Photoelectron Spectroscopy (XPS):

XPS measurements have been used to study the atoms on the surface of the nanocrystals.[48] Typically, a few layers of the NPs are coated onto a Si or Au substrate and introduced into XPS chamber for measurements. It can be seen in the XPS spectrum in Figure 6a the presence of Au from the substrate, Cd, Se, and P from the nanocrystals and

the surfaces, and C and O from the nanocrystals surfaces and from the adsorbed gaseous molecules. The spectrum also gives an idea on the coverage of the surface- when Cd 3d signal is larger than that from Au 4f signal which indicates a uniform monolayer

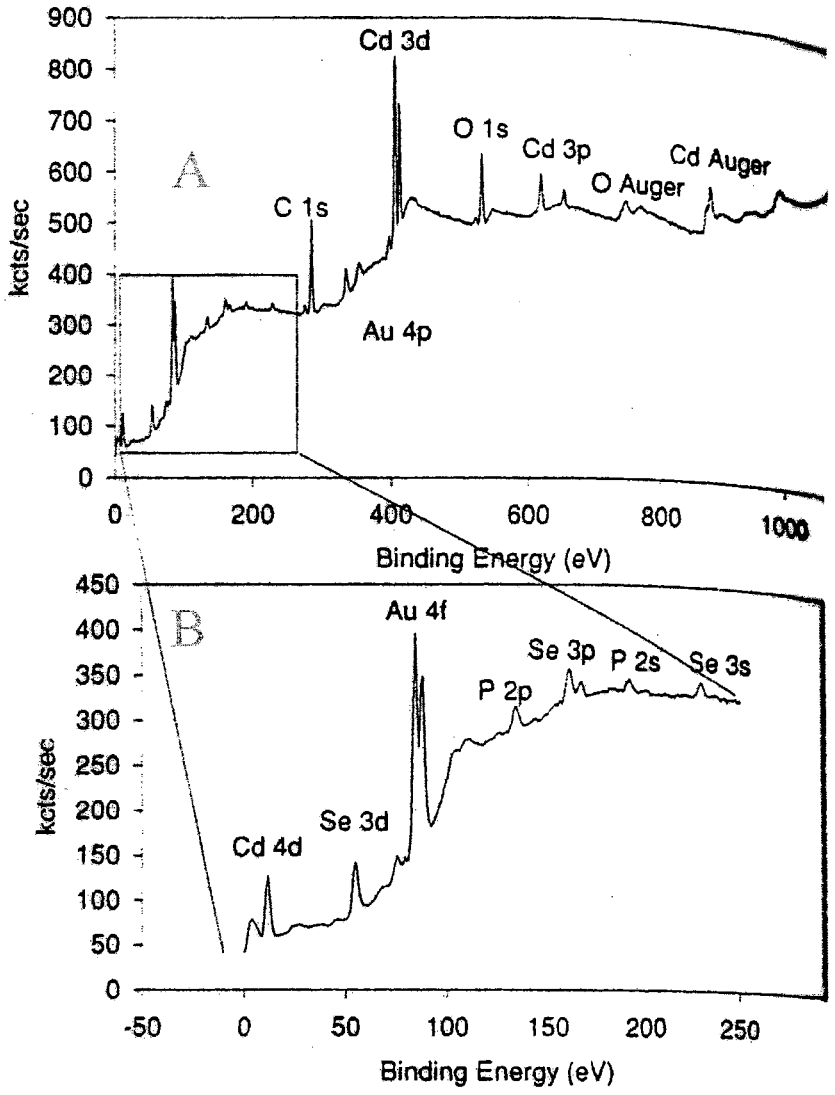

Figure 6. XPS survey spectrum of (a) TOPO-stabilized CdSe nanoparticles bonded on gold using Mg X-ray source and (b) close up of the lower binding energy area (Adapted from reference 48)

on the surface. High-resolution survey Figure 6b of the samples shows no peaks other than Cd and Se cores. The peak position of Cd $3d_{5/2}$, Se 3d and the difference between these peak positions can be used to characterize the surface of the nanocrystallites. The peak area of Cd and Se cores can be measured and used to calculate the ratio of Cd:Se in a given crystallite. The XPS signal of the stabilizer molecules can also be seen and is used to determine the extent of coverage of nanocrystallite surface with the stabilizer molecules. For example, in the case of TOPO covered CdSe NPs,[48] the ratio of Cd: P signal is used to determine the surface coverage of ligand.

D.5 UV-vis spectroscopy:

The most characteristic feature seen in the UV spectrum of NPs is the blue shift of the absorption band as compared to the bulk semiconductor, which is consistent with widening of the band gap in quantum confinement.[6,13,16] This is clearly demonstrated in Figure 7a, where the absorption of CdS, CdSe and CdTe are shifted dramatically from the 512, 716 and 827 nm bulk band gaps, respectively.[5,6] This well-developed maximum near the onset of absorption is ascribed to the first excitonic transition, and other peaks in the spectrum correspond to higher energy transitions. Another observation from the UV spectrum is the evolution of optical spectrum with size. This is seen in Figure 7b for the trioctylphosphine/trioctylphosphine oxide (TOP/TOPO) stabilized CdSe crystallites ranging from ~ 12 to 115 Å in diameter.[13] It can be seen that with decreasing particle size the transition energies shift to higher values. The series span a range of sizes, from near molecular species containing fewer than 100 atoms to fragments of the bulk lattice containing more than 30,000 atoms.[13]

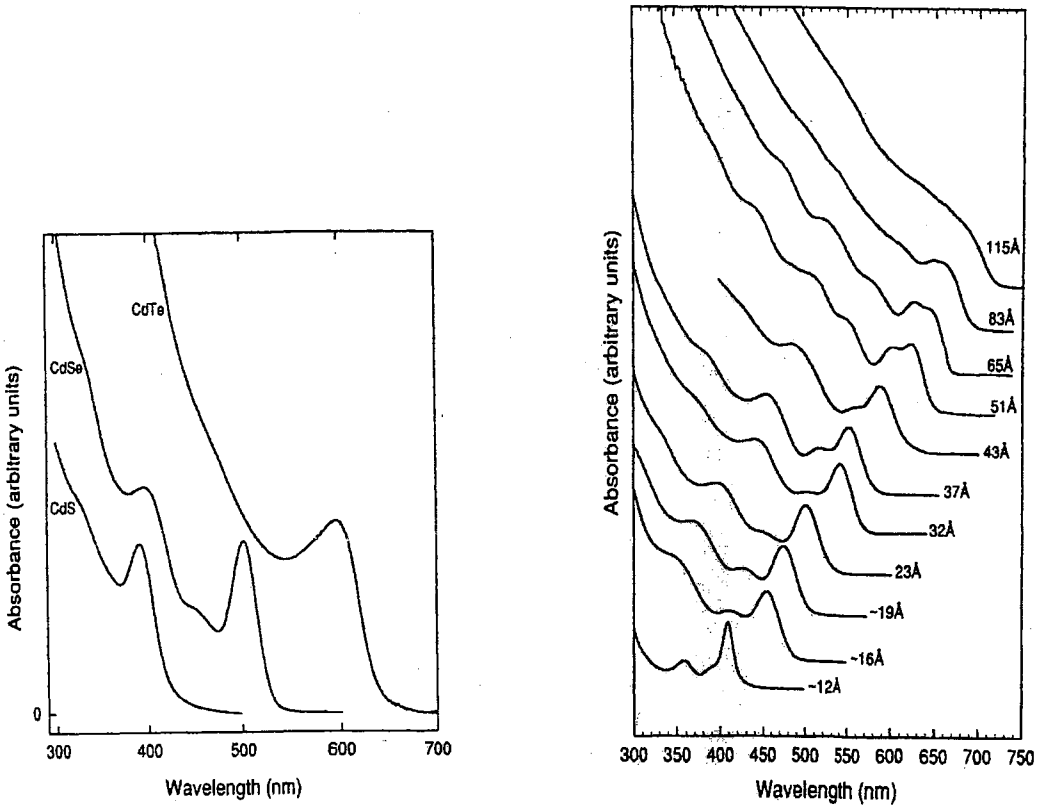

Figure 7. Optical absorption spectra of II-VI semiconductor nanoparticles. a) 20-30 Å diameter CdS, CdSe, and CdTe nanocrystals. b) TOPO stabilized CdSe nanocrystals ranging in size from ~ 12-115 Å (Adapted from reference 13)

D.6. Luminescence

One of the characteristic properties observed in semiconductor NPs is luminescence. Luminescence property, like the UV-vis absorption, is size dependent. As the particle size increases, the luminescence peaks are red shifted.[6,13,55] This is clearly seen in Figure 8. Semiconductor NPs generally exhibit two kinds of luminescence peaks, excitonic emission and trapped emission. The general opinion on the origin of the excitonic emission is due to the e^- - h^+ recombination, which is red shifted with respect to the absorption onset. The trapped emission is due to the e^- and h^+ trapped on the surface

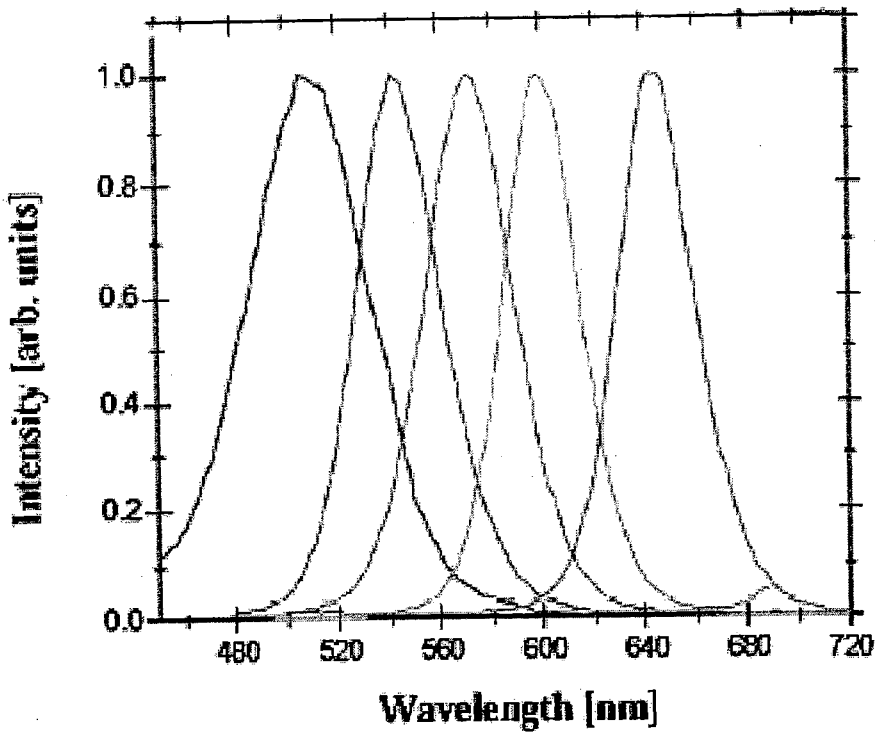

Figure 8. Luminescence spectrum of CdSe/ZnS NPs stablilized by TOP/TOPO. (Adapted from reference 52)

defects. Semiconductor NPs synthesized either have both the excitonic and trapped emission peaks or one of them, depending on the material and method of preparation. For example, citrate stabilized CdS NPs synthesized in our lab show a strong trapped emission peak with a weak excitonic emission band,[55] whereas similarly prepared CdSe NPs have a very strong excitonic emission with a very weak trapped emission.[14]

E: Surface Modification:

The unique properties of the nanoparticles are attributed to the large number of atoms on the surface. For clusters in such a small size regime, a large percentage of the atoms are in or near the surface. For example, a 50Å CdS cluster has approximately 15% of the atoms on the surfaces.[1,2,3,4] The existence of this vast interface between the cluster

and the surrounding medium can have a profound effect on the cluster properties. Irrespective of the synthetic route to make the nanoparticles, there are always defects on the surface of the NPs. This invariably leads to new levels within the energetically-forbidden gap of the bulk solid. These levels, also known as the surface states, act as traps for electrons or holes and tend to degrade the electrical and optical properties of the material. Hence understanding the surface and modifying it will be crucial in altering the properties of the NPs. Surface modification [5] of the NPs can be divided into two different types namely, organic and inorganic based on the nature of modifying group. This is illustrated in Figure 9 and both of these methods are briefly described below.

E.1. Organic capping

Colloidal nanocrystals generally have a stabilizer molecule on the surface and this prevents the NP from agglomerating in the solvent. In the case of semiconductor NPs, CdSe has been extensively studied and CdSe stabilized by TOP/TOPO is a good example for demonstrating the surface modification reaction.[6,13] These colloids are synthesized in a TOPO which acts both as solvent and the stabilizer. The NP is formed with a layer of TOPO on the surface, which coordinates to the Cd sites. The nanocrystals are soluble in nonpolar solvents, like toluene due to presence of TOPO on the surface of NP. Coordinating solvent, such as pyridine, can readily displace TOPO from the surface without affecting the stability of the NP. Thus replacing one stabilizer with another is known as the organic capping type of surface modification.

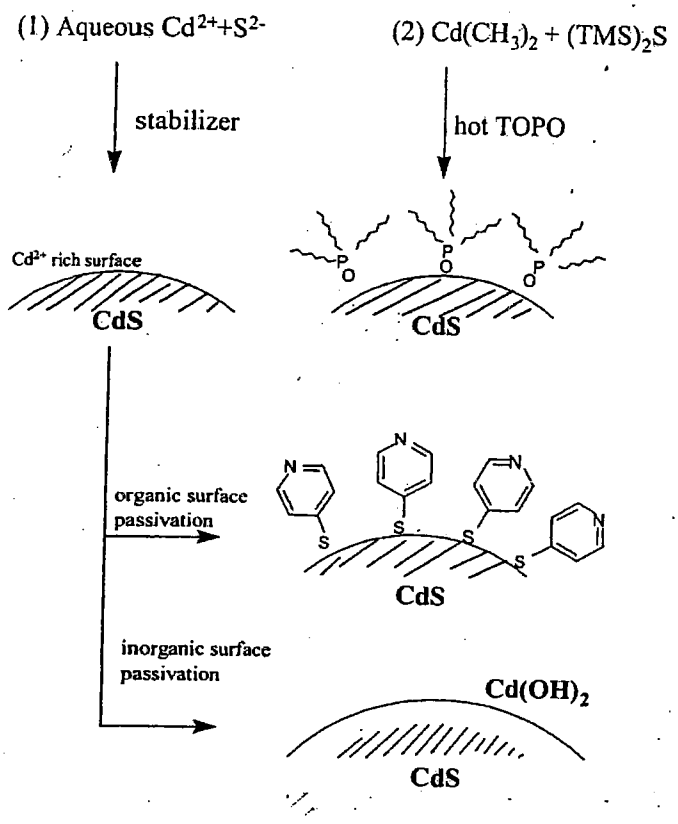

Figure 9. Schematic for organic and inorganic type of surface modification of semiconductor nanoparticles (Adapted from reference 5)

E.2. Inorganic capping

Another approach for surface modification is through the use of inorganic molecules as the capping agent.[36,47,56,57,58] This type of modification is also known as the core-shell type of modification or epitaxial deposition method. A semiconductor NP is first synthesized to constitute the core and on the surface of this, another inorganic material is grown to from a shell. The organic stabilizer molecule is now bonded to the metal atom on the surface of the shell. This type of modification not only allows for the lattice matching but also electronically passivates the surface of the NP; while at the same

time does not sacrifice the solubility and chemical manipulation of the NP. This type of modification has lead to improved properties in semiconductor NPs. One such system is the ZnS-capped CdSe nanocrystals [36,47], which showed enhanced luminescence quantum yields. Another possible application is development of faceted nanocrystals.[1,58] By careful manipulation, it is possible to grow a particular face of the crystal that has special properties.[58]

Another type of inorganic capping of NP using the core-shell methodology is the formation of a silica coating on the NP surface.[14,59,60] L.Liz-Marzan suggested to first form a NP core and on the surface of this core grow a layer of silica as a shell.[59] The silica shell is usually 4-5 nm thick and therefore does not compromise the optical properties of the NP significantly, but at the same time improves the stability of the NP.

It is evident from the above two approaches to the surface modification of NPs, the metal site is the one that is primarily involved while the chalcogen atom is either not utilized (TOP/TOPO) or partially engaged (core-shell) in NP modification. It has been shown that there is a substantial energy mismatch between the surface cadmium ions and the conduction band of the semiconductor NPs, [77] creating energy hurdles that prevent effective interaction between the carrier levels. This barrier is much lower for corresponding sulfur and selenium sites as the energy states of surface sulfur or selenium atoms are partially mixed with the valence band of CdS and CdSe respectively,[55,77] making them more suitable for the preparation of conjugated electronic systems. The drawbacks of the conventional surface modification reactions challenged us to attempt to modify the surface of the semiconductor NPs via the chalcogen atoms, or E-sites. This

approach of surface modification is of special interest from both a fundamental and practical point of view. Details of this approach will be discussed in a later chapter.

F. Purpose:

The discussion above provided a brief account of what has been learned in the synthesis and surface modification of semiconductor NPs. The various synthetic pathways and the surface modification to enhance the luminescence properties are emphasized. Even though, a great deal of progress has been achieved in the preparation of NPs, there is always a search for new synthetic routes to achieve narrow size distribution and better luminescence properties. The research is divided into two main parts, the first part involves synthesis of NPs and the second part will cover the surface modification.

In the first part, investigate new synthetic routes to make stable NPs will be investigate. The synthetic part of the research is divided into two parts; the synthesis of CdSe NPs and In_2S_3 NPs. The syntheses of the two systems are different due to difference in the number of metal and chalcogen atoms in the unit cells. This work will constitute Chapters II and III.

The second part of the research involves the surface modification of the synthesized NPs. The surface modification reactions that have been investigated so far are through the metal atoms. This approach of surface modification is far from optimal to achieve the effective interaction with aromatic electronic systems of organic chromophors due to the mismatch of the electronic levels involved. Thus, extending the surface modification reaction utilizing the free chalcogen sites will be more suitable for

effective electronic interactions. This approach of surface modification was achieved using mixed ligand complexes and the results of this work will be covered in Chapter IV. Two NP systems with different number of chalcogen atoms on the surface were modified to study the effect of modification with the type of surface. The results from this work will constitute the final chapter.

CHAPTER II

II. Synthesis of CdS, CdSe nanoparticles, RuBP complex and their characterization

A. Introduction

Semiconductor NPs have received a lot of attention in the study of NP chemistry. The compounds that have been extensively studied are the II-VI class of compounds and in this class, CdS and CdSe NPs are the ones for which there is a good understanding on the physical and chemical properties of these materials. In the case of CdS and CdSe NPs, the synthetic method developed by Murray, C.B., in Reference 13 is the most common cited paper for the synthesis of NPs. This method results in the formation of monodisperse, stable NPs in non-aqueous medium. The disadvantage of this method is the inability to transfer the NPs to aqueous medium. The dispersion of NPs in water is a desired property in NPs for a variety of applications. The goal of this research is to develop new synthetic routes to make stable, monodisperse CdSe NPs in aqueous medium with a narrow size distribution.

This chapter is based on Reference 14 and 55. Tong Ni synthesized the CdS NPs and this work is described in detail in Reference 55 and 76. Michael Giersig at Hahn-Meitner-Institiu, Abt. Physikalische Chemie, Glienickerstr, Berlin, Germany performed the TEM work. CdS NPs were synthesized as part of this research to compare the properties of CdS and CdSe NPs.

B. Materials

Cadmium perchlorate [$Cd(ClO_4)_2.4H_2O$](Aldrich), sodium citrate [$Na_3C_6H_5O_7.2H_2O$] (EM Science), thiourea [CH_4N_2S](Aldrich), N,N,dimethylselenourea [$C_3H_8N_2Se$](Strem),

indium chloride [$InCl_3.xH_2O$](Strem), sodium sulfide [$Na_2S.9H2O$](Fluka), copper(I)chloride [$CuCl.xH_2O$](Strem), 1-thioglycerol [C_3H_8OS](Aldrich), 1-amino-2-methyl-2-propanethiol hydrochloride (Aldrich), thioacetamide [C_2H_5NS](Aldrich), 2,2'-bipyridine (Sigma), bismuth nitrate pentahydrate [$Bi(NO_3)_2.5H_2O$](Strem), ruthenium chloride [$RuCl_3.7H_2O$](Aldrich), lithium chloride [LiCl](Sigma), copper carbonate [$CuCO_3{\cdot}Cu(OH)_2$](Aldrich), malonic acid [$CH_2(COOH)_2$](Aldrich), RhodamineB (Aldrich), *p*-quaterphenyl (Aldrich), N,N,Dimethylformamide (EM Science), pyridine (Aldrich), glacial acetic acid [CH_3COOH](EM Science), chloroform (Fisher Scientific), hexane (Fisher Scientific), acetone (Pharmaco), isopropyl alcohol (Pharmaco), sodium hydroxide [NaOH](Fisher), D_2O (99.9% D, Aldrich). All chemicals were of A.C.S. reagent grade and were used without further purification. Dialysis membranes with a molecular weight cut off (MWCO) of 15000Da and 2000Da (Spectrum) were used. Nanopure water from a Barnstead E-pure system (18.2 MΩ) was used in all preparations.

C. Instrumentation

1. UV-vis absorption. Optical measurements were performed on a Hewlett Packard 8453 diode array spectrophotometer. All measurements were done in 1 cm quartz cuvettes at room temperature, using air as blank.

2. Steady-State Emission. Fluorescence spectra were recorded on a Fluorolog-3 - Tau 11 and Fluoromax-3 (Jobin Yvon) spectrofluorometer in 1 cm quartz cuvettes. The light source was a 450 W xenon lamp, the increment set at 0.5 nm and the integration time of 0.1 sec. The slit widths for excitation and emission monochromators, expressed in band pass units, were adjusted from 5-10 nm depending on the sample's signal intensity. Emission of each batch of samples was first analyzed for different excitation wavelengths

to separate excitation-energy-independent peaks from excitation-energy-dependent peaks, namely the Raman and Rayleigh scattering. The excitation wavelength was chosen to minimize the interference of the latter with the luminescence signals. Optical long pass band filters were used to cut-off the interfering water Raman peak. Right angle registration mode with no intermediate filters was utilized for the measurements.

3. Quantum yield measurement: The quantum yield of the prepared NPs was measured using the formula described in Reference 15:

$$\varphi_{NP} = \varphi_S (I_{NP}/ I_S) \times (OD_S/OD_{NP})$$

where, NP and S stand for NPs and the standard respectively, φ stands for the quantum yield, I the integrated area of luminescence and OD is the optical density at the excitation wavelength. The standards used were Rhodamine B for CdS NPs and *p*-quarterphenyl for the In_2S_3 NPs with quantum yields of 1.0 [88] and 0.71 [89] respectively.

4. Transmission Electron Microscopy (TEM). A Phillips CM 300 operating at 200 kV was used for transmission electron microscopy (TEM). The samples for TEM were prepared by placing a drop of the aqueous solution of NP onto a carbon coated aluminum grid (200 mesh). The samples were allowed to dry on the grid for a minute and then the excess was removed by using a filter paper. The dried grids were transferred into a nitrogen-filled container and then to a cell compartment of the TEM microscope, equipped with a Phillips EDAX 9800 analyzer.

5. Electron diffraction. A JEOL 2000-FX scanning transmission research electron microscope (200k eV, bright LaB6 source) was used for obtaining an electron diffraction pattern. It was registered at 200,000/300,000 magnification and calibrated by the diffraction spacings of gold obtained at identical conditions.

D. Preparation of nanoparticles

1. Synthesis of CdSe nanoparticles stabilized by sodium citrate

This procedure is described in detail in Reference 14. In brief, in 45 ml deionized water, 0.05 g of sodium citrate and 2 ml of 1 x 10^{-2} M aqueous solution of $Cd(ClO_4)_2$ was added. The solution was degassed by argon gas bubbling. To this, 2 ml of freshly made aqueous solution of 1 x 10^{-2} N,N-dimethylselenourea was added and the pH adjusted to 9.4 using 0.1 M NaOH solution. This solution was then introduced in a 1000 W microwave (Sharp) for 55 seconds. When the ratio of Cd^{2+} to Se^{2-} was 1:1, it resulted in a pale brown colored solution with an absorption edge at 598 nm and a CdSe particle size estimated to be 46 Å. Different sizes of CdSe NPs were obtained by adjusting the Cd^{2+} to Se^{2-} ratio. The size of nanoparticles decreased from 46 Å to 22 Å when the ratio of Cd^{2+}: Se^{2-} was increased from 1:1 to 30:1. A series of CdSe NPs of different sizes were synthesized and is shown in Figure 10. The Se^{2-} concentration and the pH remained the same in all the syntheses, but the citrate concentration was increased to 0.10g for the 30:1 ratio synthesis. The prepared CdSe NPs are stable for months when stored at 20° C in a refrigerator and protected from light.

2. Synthesis of CdS nanoparticles stabilized by sodium citrate

The synthetic procedure is described in detail in Reference 14 and 55. To 45 ml de-ionized water, 0.25 g of sodium citrate and 2 ml of 1 x 10^{-2} M aqueous solution of $Cd(ClO_4)_2$ were added. The solution was degassed by argon gas bubbling. To this, 2.5 ml of freshly made aqueous solution of 8 x 10^{-3} M thioacetamide was added and the pH adjusted to 9.2 using 0.1M NaOH solution. Aliquots of this solution were introduced in a 1000 W conventional microwave oven for 55 seconds. For the 1:1 ratio of Cd^{2+} to S^{2-}, the

absorption edge was around 445 nm and the resulting solution is yellow in color. When the ratio Cd^{2+}: S^{2-} was 1:1, 2:1, 4:1 and 6:1, they resulted in 44, 35, 30 and 26 Å sized CdS NPs. These are plotted in the graph as shown in Figure 11.

3. Synthesis of Ru(2,2′-bipyridyl-N,N′)$_2$Cl$_2$ (Abr. as RuBP) and (2,2′-bipyridyl-N,N′)(malonate-O,O′)copper(II)monohydrate (Abr. as CuBM)

The synthesis of the RuBP and CuBM complexes was followed as described in detail in Reference 61 and 62 respectively.

In brief, the synthesis of RuBP was done by mixing together 1.37 g ruthenium chloride, 1.56 g 2,2′-bipyridine and 1.4 g lithium chloride in 8.5 mL dimethyl formamide in a three-necked round bottom flask. The reaction mixture was refluxed for 8 hours at 80° and then cooled to room temperature. 50 mL acetone was then added to this mixture. The solution was stored at 0°C overnight. RuBP crystals were filtered out in a crucible as black crystal and washed 3 times with 5 mL distilled water and ethyl ether.

In brief, the CuBM complex was synthesized by mixing 178 mg basic copper carbonate, 43 mg sodium hydroxide, 83 mg malonic acid and 124 mg 2,2′-bipyridine in 40 mL distilled water and refluxed for 3 hours. The solution was concentrated in a rotary evaporator until small crystals appeared. The reaction vessel was then cooled and the solid was allowed to precipitate. The blue crystalline product was washed 3 times in acetone then dried under vacuum to remove traces of solvent. The yield was 48.3%.

E. Characterization of CdSe, CdS nanoparticles

The synthesized NPs were characterized by the standard methods of UV-vis absorption, TEM and luminescence.

E.1. UV-vis absorption

The main characteristics of the NPs that can be interpreted from the UV-vis spectrum are:

a) well developed maximum near the absorption onset which is ascribed to the first excitionic transition.

b) the transition energy shift to higher values with decreasing particle size which is attributed to the size quantization effect.

c) increase in the absorption coefficient with decreasing particle size.

These characteristics are clearly seen in the UV-vis spectrum of the citrate stabilized CdSe and CdS NPs in Figure 10 and 11. The steplike feature of the absorption band in the UV-vis spectrum is attributed to the valence-to-conduction-band transition in CdS and CdSe NPs. In the bulk CdS and CdSe, the band gap (E_g) is reported to be 2.42 eV and 1.73 eV respectively [5]. Considering the position in the UV-vis onsets at 498 – 600 nm for CdSe in [5,13] Figure10, the band-gap equals 2.49 –2.07 eV. Similarly, for CdS NPs from Figure 11, the absorption edge at 445 – 395 nm corresponds to band gap of 2.79-3.14 eV. This observation indicates the strong quantum confinement of the excitonic transitions for the nanoparticles. It is also seen that with increasing metal to chalcogen ratio in the synthesis, the particle size of both CdS and CdSe nanoparticle decreases. This could be ascribed as the result of the increase of surface charge on the nanoparticle and the related electrostatic adsorption of citrate stabilizer.

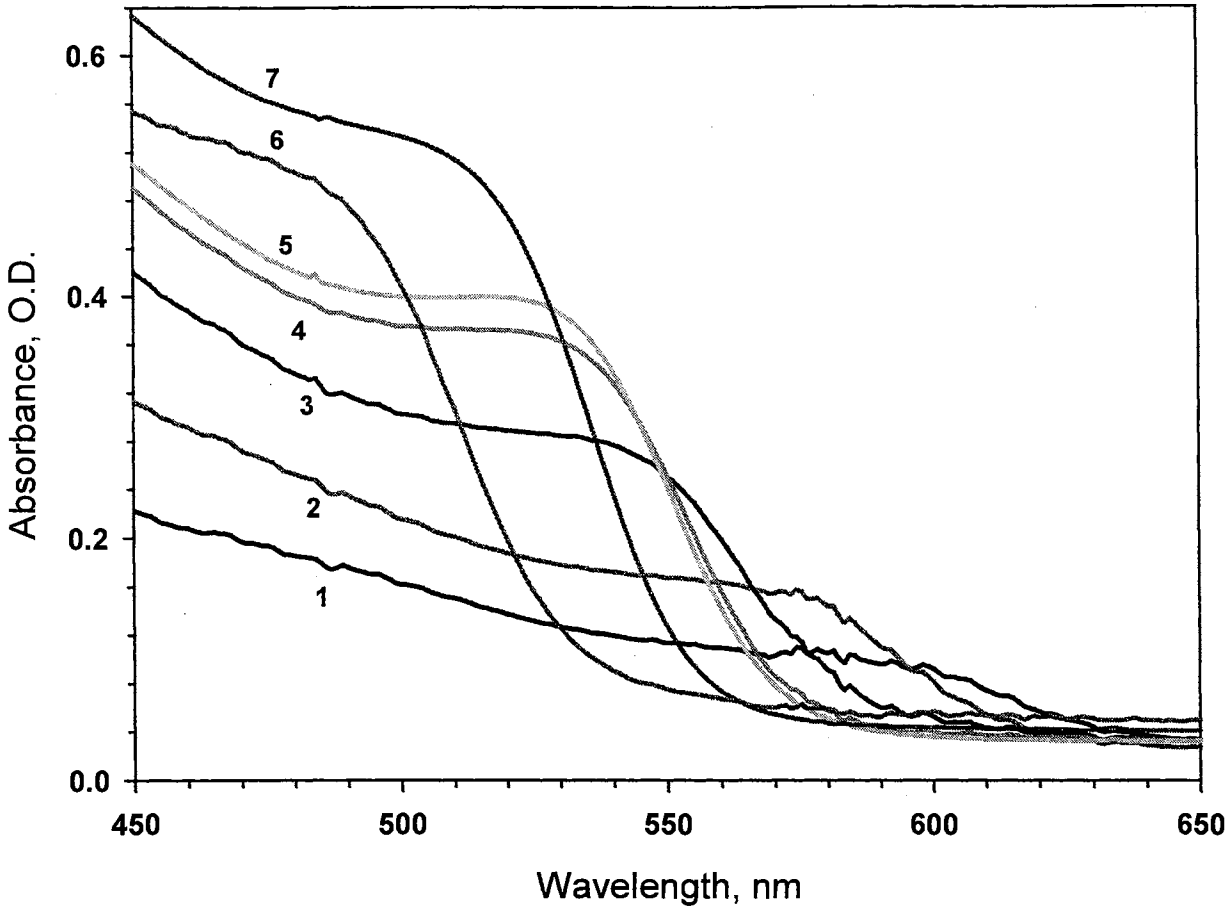

Figure 10. Optical absorption spectrum of different sized citrate stabilized CdSe. The ratio of Cd^{2+}:Se^{2-} for the different samples was 1) 1:1, 2) 2:1), 3) 4:1,4) 6:1, 5) 10:1, 6) 30:1 and 7) 20:1

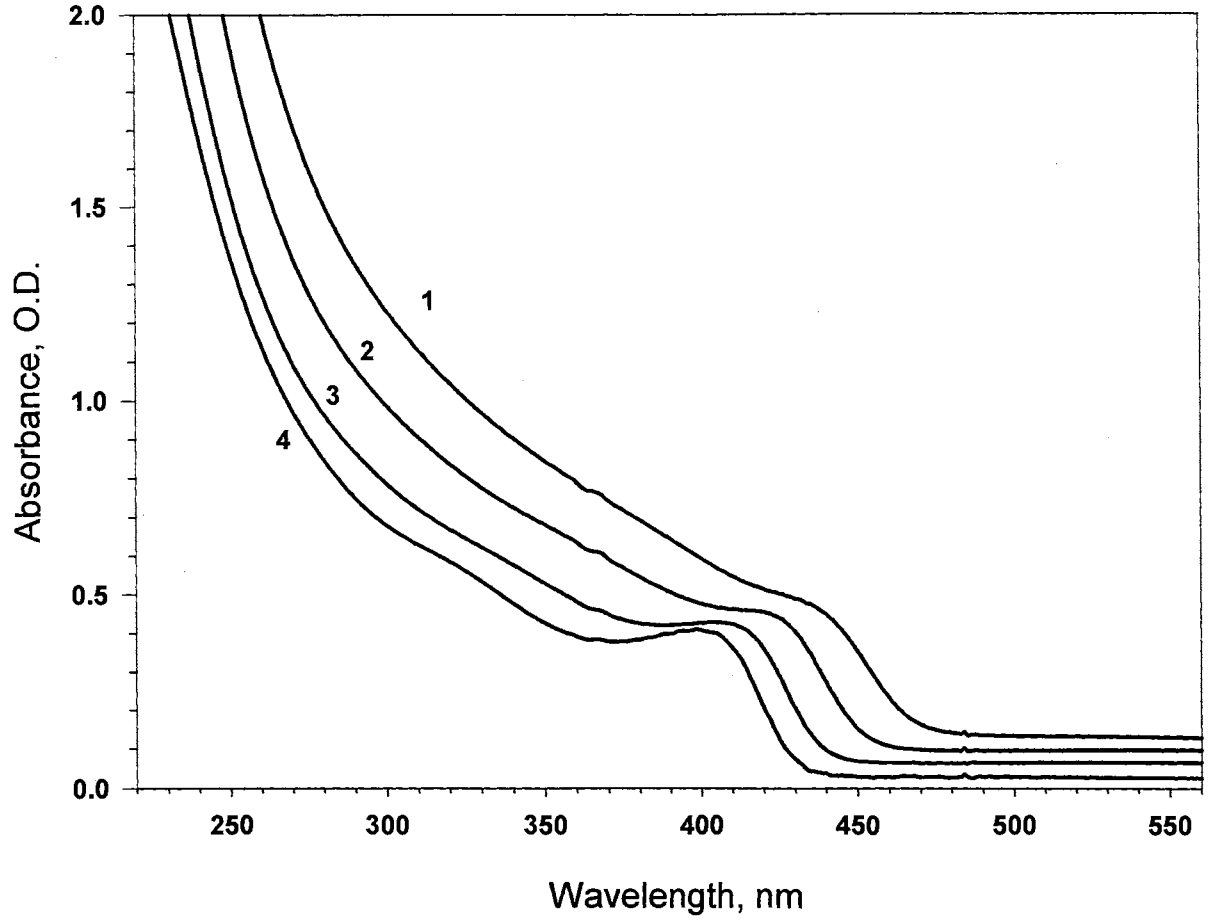

Figure 11. Optical absorption spectrum of different sized citrate stabilized CdS. The ratio of Cd^{2+}:S^{2-} for the different samples was 1) 1:1, 2) 2:1), 3) 4:1, and 4) 6:1. (Adapted from Reference 55)

The diameter of the particles was evaluated on the basis of the UV-vis spectra, using the correlation between the absorption onset and the particle diameter. This method of evaluation is based on the work of T. Vossmeyer, described in Reference 6. The size quantization effect was studied by plotting the band gap energies *vs* cluster radius. The experimental values of the first electronic transition energies were compared with the pseudopotential calculations and the results of tight-binding theory. The results showed that there was good agreement between the theory and experimental results.

Based on the results from the above-mentioned work, the particle size of the NPs in our synthesis was estimated by comparing the absorption onset between the CdS NPs in Reference 6 and those in Figure 11. This is shown in Table 2 for CdS NPs. Similarly, the size of CdSe NPs was estimated by comparing the absorption onset in Reference 13 and those in Figure 10. This is shown in Table 1 for CdSe NPs. This method of determining the size is not accurate but is still very useful to estimate the rough size of the NP during the synthesis. The more accurate sizes of NPs were obtained from the transmission electron microscopy images. There was a good agreement between the values in Table 1 and 2 with the values obtained by the TEM method.[14,55]

Table 1. Particle radius vs absorption edge for citrate stabilized CdSe NPs

Abs. of CdSe (nm)	600	580	560	545	535	524	512	498
Band gap (eV)	2.07	2.14	2.22	2.28	2.32	2.37	2.42	2.49
Radius (Å)	23	19.8	16.9	15.2	14.3	13.2	12.3	11.1

Table 2. Particle radius *vs* absorption edge for citrate stabilized CdS NPs

Abs. of CdS (nm)	395	410	425	445
Band gap (eV)	3.14	3.03	2.92	2.79
Radius (Å)	13.1	14.7	17.0	21.9

Stabilization by thiols is an established route of synthesis of semiconductor nanoparticles [16,6]. It was demonstrated earlier in our group that there is interference of the modification reaction in case of thiol and phosphine stabilized colloids [55]. (See, Chapter IV). The limitation of thiols as a stabilizer was overcome by the use of a different kind of stabilizer – sodium citrate. Sodium citrate has been used successfully as a stabilizer for CdS nanoparticles with good size control and size distribution.[14,59] Even though the carboxyl group does not form a strong covalent bond with the transition metal as the thiols do but while acting together they are able to arrest the growth of nanoparticles. The source of selenide was N,N-dimethyl selenourea instead of TOPSe generally used in the synthesis of CdSe nanoparticles. Thioacetamide was used as the sulfide source for the synthesis of CdS instead of sodium sulfide used previously. It has been reported previously in the synthesis of TOPO-stabilized CdSe nanoparticles that the birth of numerous nucleation centers simultaneously resulted in relatively narrow size distribution for the nanoparticles [13,78]. In our synthesis, instead of conventional heating, a microwave oven was used to decompose the chalcogen source. The microwave assisted decomposition of the chalcogen source results in fast and uniform formation of the chalcogen ions in the solution, which promotes the crystal growth on numerous nucleation sites at the same time. This resulted in narrow size distribution and better size

control and this can be seen in the UV spectrum of CdSe and CdS NPs in Figure 10 and 11.

E.2. Luminescence

The prepared nanoparticles exhibit relatively strong luminescence, as shown in Figure 12 and 13. Optical spectra of the formed nanoclusters may be affected by the interference of the byproducts of the reaction. Complexes may be formed as a side product by the reaction of Cd^{2+} with the stabilizer molecules or sulfide source. Thus to verify the origin of luminescence, the redispersed aqueous nanocolloid solution was extensively dialyzed against deionized water for 36 hours (3 x 12 h). The molecular weight cut off for the dialysis membrane was 15 kDa, which was large enough to allow the complexes of Cd^{2+} to escape and, at the same time, small enough to retain the nanoclusters inside. The luminescence spectra of CdSe virtually remain the same before and after dialysis, as seen in Figure 14. Even though the UV-vis spectrum of CdS and CdSe look similar, the luminescence spectra of CdSe and CdS are very different. The luminescence spectra of CdSe have two distinct peaks, namely the excitonic and the red shifted trapped emission. The excitonic emission in case of CdS nanoparticles is seen but is significantly reduced in intensity when compared to the trapped emission. The quantum yields of trapped and excitonic emission bands of CdS nanoparticles are 6.0-7.5% and 0.10-0.15 % respectively. In case of CdSe, these values are 0.05-0.1% and 5.5-7.0%. Thiol stabilized CdS and CdSe NPs without any special epitaxial coatings have been reported to have similar quantum yields [30,36,63]. The closeness of the emission peak to the absorption onset indicates that the emission comes from an interband electron-hole recombination.

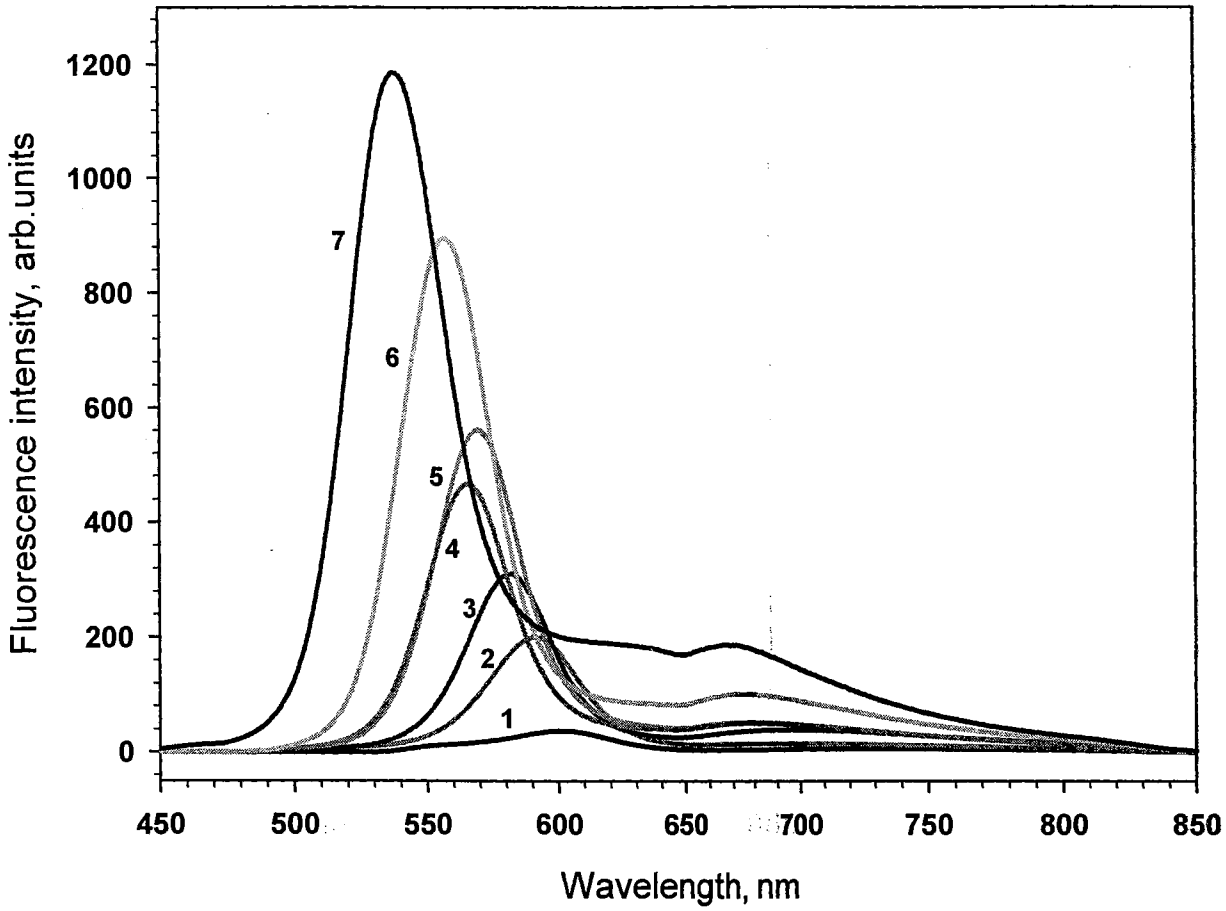

Figure 12. Steady state luminescence of citrate stabilized CdSe NPs. The ratio of Cd^{2+}:Se^{2-} for the different sizes were 1) 1:1, 2) 2:1), 3) 4:1, 4) 10:1, 5) 6:1, 6) 20:1 and 7) 30:1

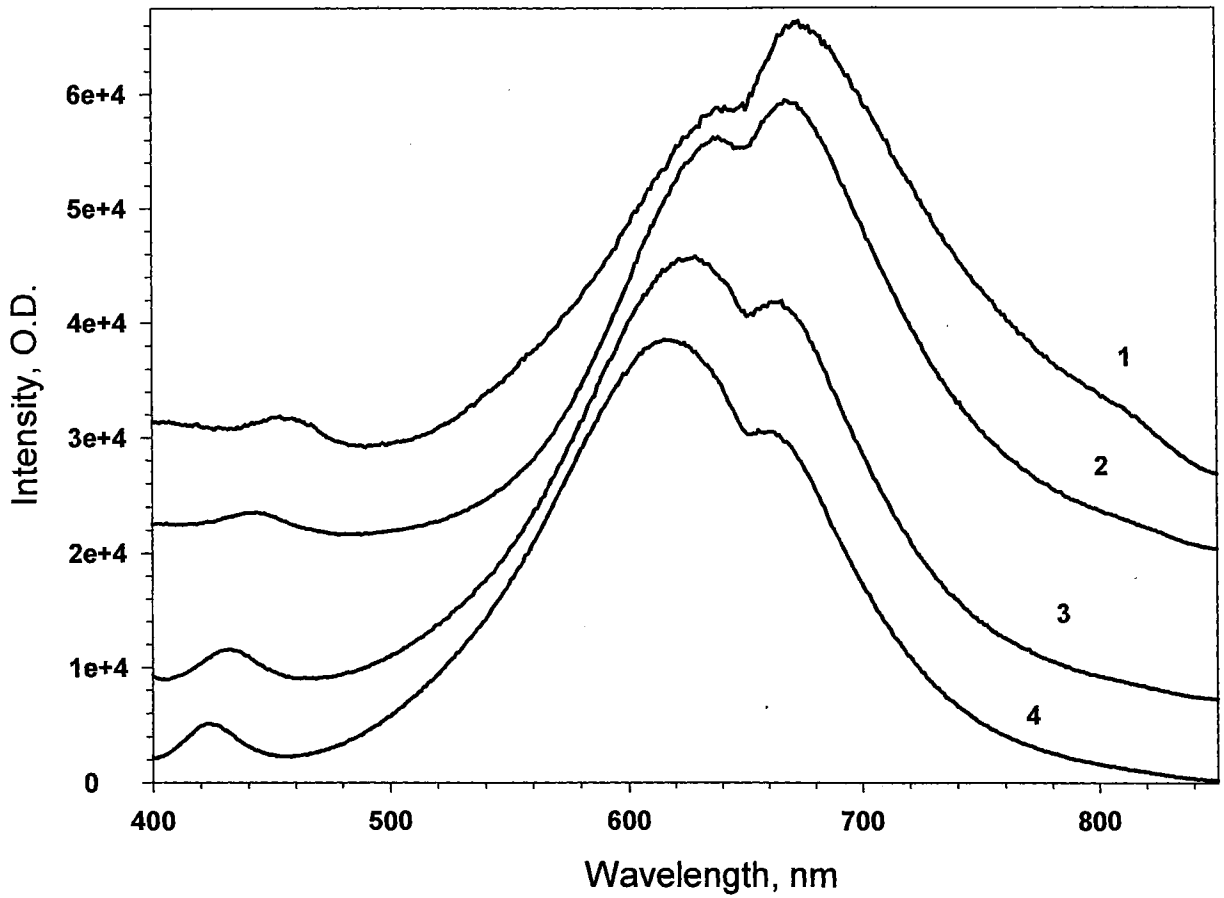

Figure 13. Steady state luminescence of citrate stabilized CdSe NPs. The ratio of Cd^{2+}:S^{2-} for the different sizes were 1) 1:1, 2) 2:1), 3) 4:1, and 4) 6:1. (Adapted from Reference 55)

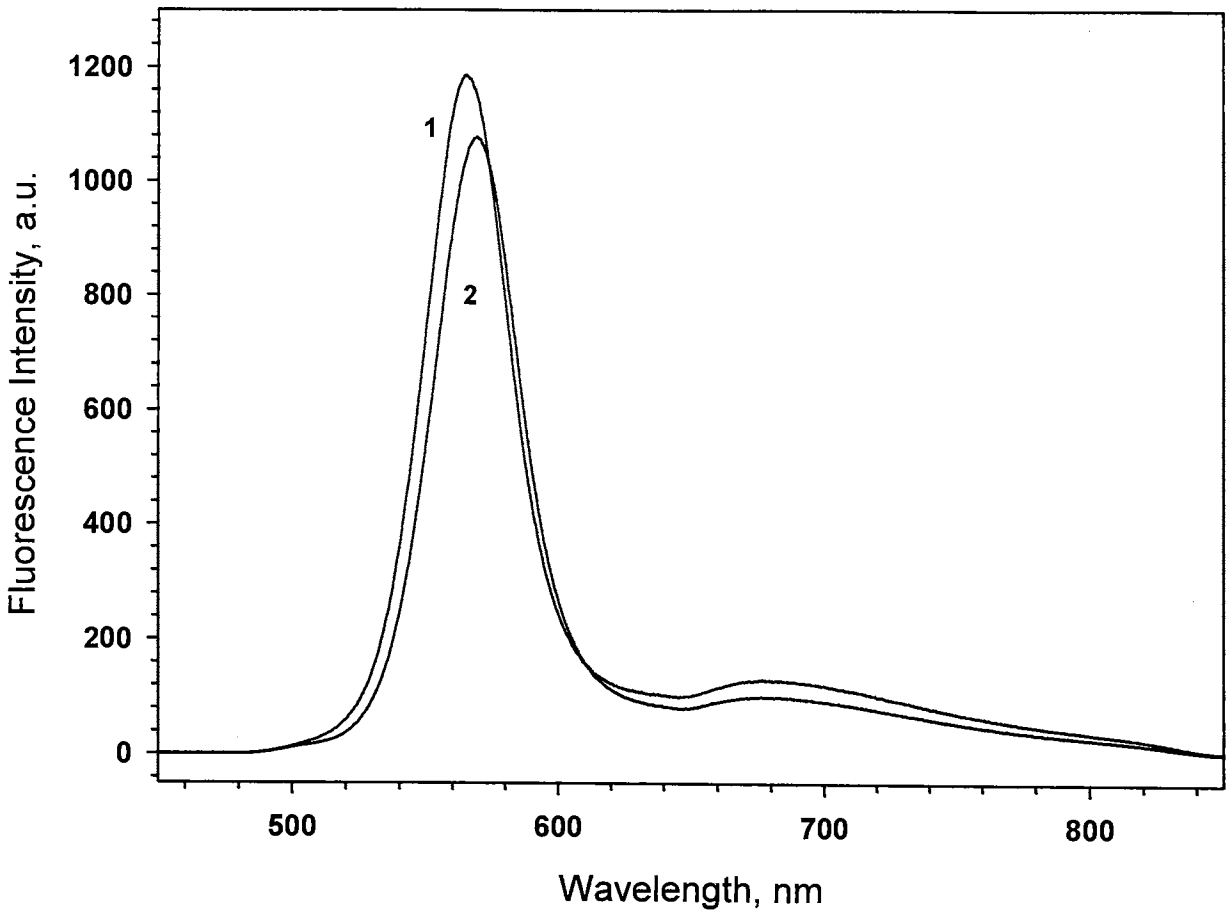

Figure 14. Steady state luminescence of CdSe NPs, 1) before and 2) after dialysis

The trapped emission is typically attributed to the emission of the charge carriers trapped in the surface states undergoing a recombination between themselves and/or with the carriers on the conduction and valence bands [14,55].

E.3 Transmission Electron Microscopy:

The TEM images of citrate stabilized CdSe NPs in Figure 15 revealed that the nanocolloids are crystalline in nature. The diameter of NP was calculated to be 24 Å. The diameter of the semiconductor core does not significantly change upon repeated redispersion. The NPs tend to aggregate on the TEM grid and the isolated spots where the NP did not aggregate was imaged to estimate the size of the nanocluster.

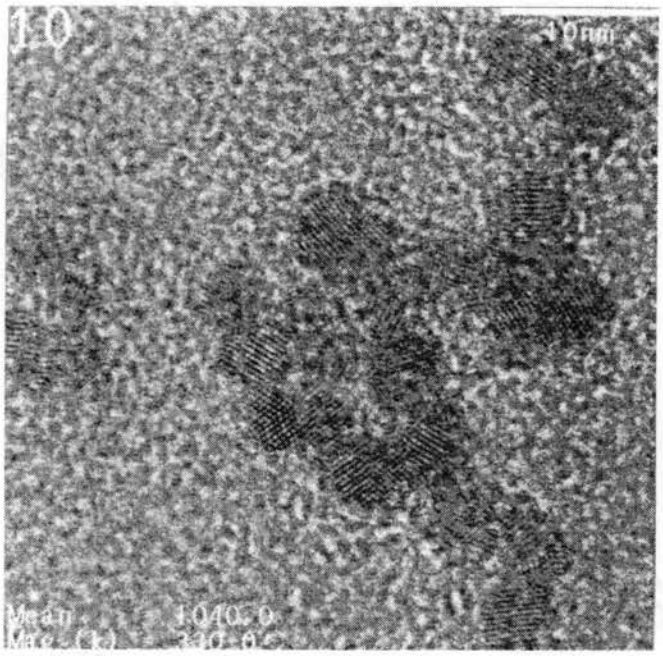

Figure 15. TEM images of citrate stabilized CdSe NPs

F. Conclusions:

A new synthetic route to the preparation of CdSe NPs was successfully attempted. The useful feature of sodium citrate as a stabilizer is the relatively narrow size distribution and lability of the stabilizer, which has been used for surface modification reaction [14]. The luminescence properties of the CdSe NPs are quite exceptional as they exhibit both the excitonic and the trapped emission bands that are not generally associated with these types of NPs. The major advantage of this method of synthesis is the relatively easy way to control the size of the NPs formed. Since all the properties of the NPs are size dependent, the ability to control the size during the synthesis is a very important property. Therefore, these CdSe NPs are quite unique and open up new applications for these materials. (See Chapter IV).

CHAPTER III

III. Synthesis of In_2S_3 nanoparticles and their characterization

This chapter is based on Reference 15. This work was done in collaborations with Michael Giersig at Hahn-Meitner-Institiu, Abt. Physikalische Chemie, Glienickerstr, Berlin, Germany and Gordon Gainer, Jin-Joo Song at Center for Laser and Photonics Research, Oklahoma State University, Stillwater, Oklahoma.

A. Introduction

Semiconductor nanoparticles that have received a lot of attention are the II-VI class of compounds (CdS, CdSe, ZnS, etc.) for which some understanding of the nature of electronic processes has been attained. In this class of compounds, there are an equal number of metal and chalcogen on the surface of the particle. Other semiconductor nanoparticles that have been studied are III-V [64,65] (InP, GaAs etc.), I-VI [66] (Ag_2S, Cu_2S, etc.), and I-VII [67] class of compounds (AgI, AgCl, etc.). All these compounds have either 1:1 or greater stoichiometric ratio of the metal atom to chalcogen atom in the unit cell. In most of these NPs, the stabilization is achieved through the use of organic Lewis bases such as thiols, phosphines, acids or amines as stabilizer molecules.

There is another class of semiconductor compounds for which the number of chalogen atoms is greater than the metal atoms in the unit cell. Examples of such compounds are MoS_2, WS_2, ReS_2, Sb_2S_3, In_2S_3 and Bi_2S_3. All of them exhibit special optical, mechanical, and catalytic properties. In_2S_3 and Bi_2S_3 in particular, are of special interest to us since the isotopes of these metals have been used in cancer treatment for diagnostics purposes (See Chapter I - Introduction). Literature search revealed that In_2S_3

and Bi_2S_3 NP have only been synthesized in the presence of polymers or in physically constrained environments such as porous solids and reverse micelles [68,69]. The disadvantage of this methodology is that the polymeric matrix interferes with the optical properties and broadens the size distribution. The importance of chalcogen dominance on the surface lies in the fact that these compounds will lead to:

(a) different photophysical behavior of electron/hole pairs in the quantum dots and,

(b) novel surface chemistry, including new ways of building nanoparticle supramolecules.

Therefore, synthesis of these compounds as stable redispersible nanocolloids would be significant in understanding the fundamental properties of these types of chalcogen-rich compounds.

The first compound to be synthesized was In_2S_3 nanocolloids. In addition to the increase in the number of chalcogen atoms on the surface, In_2S_3 posses some other unique properties:

a) In_2S_3 is a case of ordered crystalline material with a large amount of vacant interstitial cationic sites [70,71]. Owing to tetragonal sites formed by incompletely coordinated sulfur atoms, indium sulfide can serve as a host lattice for a number of metal ions to form semiconducting and/or magnetic materials. Doping In_2S_3 produces materials with exceptional optical, electrical, and magnetic properties, which can be adjusted not only by the particle diameter, but also by the concentration of the guest ion. This is in contrast to II-VI class of nanoparticles, which tend to expel guest ions [72,73].

b) Unlike most of the semiconductors nanocolloids currently being investigated, In_2S_3 and related materials display both direct [79] and indirect [80] conduction-to-valence band transitions, which can be observed by different modalities of UV-vis spectroscopy at 2.0-2.2 and 1.0-1.1 eV respectively. This opens the door for investigation of the effect of quantum confinement on direct and indirect excitonic transitions.

c) In_2S_3 nanoparticle bioconjugates can have medical applications, such as in cancer diagnosis [21b].

In this context, the synthesis and characterization of In_2S_3 and other chalcogen rich semiconductor nanocolloids are unique and the results of this work are discussed below.

B. Instrumentation:

The details of the instrumentation for the UV-vis absorption, steady state luminescence, TEM, electron diffraction are described in detail in Chapter II.

Margaret Eastman (Department of Chemistry, Oklahoma State University, Stillwater, Oklahoma) performed the NMR measurements and the details are described in Reference 15. Gordon Gainer at the Center for Laser and Photonics Research, (Oklahoma State University, Stillwater, Oklahoma), performed the time-resolved photoluminescence studies and the details are described in Reference 15 and 55.

1. Powder X-ray Diffraction (XRD). The XRD pattern was obtained on a Bruker AXS D-8 Advance X-ray powder diffractometer using Cu K_α radiation, operating at 40 kV tension and 30 mA current. The pattern was recorded over the 2θ range from 2° to 60°, with increments of 0.2° and a scanning rate of 4s per step. Indium sulfide NPs were precipitated as powder from mother liquor using isopropyl alcohol. The samples were

first air dried and then under vacuum to completely remove the solvent. The sample was finely powdered before X-ray diffraction measurements.

2. Nuclear Magnetic Resonance Spectroscopy (NMR). Proton nuclear magnetic resonance spectra were obtained on a Varian Inova 400 MHz instrument operating at ^1H frequency of 399.96 MHz. The In_2S_3 NP sample was obtained by sedimentation with isopropyl alcohol and thoroughly washed in excess solvent. These were then dried under vacuum and then dissolved in 99.9% D_2O to produce a clear saturated solution. Residual water peak at 4.80 ppm was used as an internal standard.

3. Molecular modeling. All calculations (Semiempirical PM3 and Density Functional Theory) were carried out on a Silicon Graphics Octane Workstation. Spartan V5.1 software packages were also employed. (Spartan version 5.1, Wavefunction, Inc., CA.)

4. Time Resolved Photoluminscence: Time-resolved photoluminescence were also made on a Fluorolog-3 Tau 11 (Jobin Yvon), which uses cross-correlation frequency domain measurements of the phase shift, and demodulation factors (phase shift and ratio of modulated anisotropy) across a frequency range. The phase modulation method measures the response functions of a fluorescent sample from a sinusoidally modulated by a Pockels cell continuous wave source of excitation from 450 W Xenon lamp. Diluted Ludox dispersion was used as a scattering standard for all measurements. The lifetime of emission is calculated by fitting phase shift *vs* frequency curve by using the software provided by ISA SPEX for frequencies between 0.1 and 300 MHz.

5. Ultraviolet Photoelectron Spectroscopy (UPS). The surface analytical apparatus consists of a ultrahigh vacuum chamber pumped by a 330-L/s ion pump coupled to a load-lock chamber via long stroke manipulator. Typical base pressure is 1×10^{-5} Pa and

rises to 1 x 10^{-3} Pa during He (I) UPS. The sample was placed at a 45 ° angle with respect to the front of the energy analyzer to avoid photoelectron contributions from the sample holder. A double-pass cylindrical mirror analyzer with a pass energy of 5 eV was used to measure the photoelectrons. This analyzer accepts all electrons within a cone around 42 ° from the sample normal. A He discharge source was differentially pumped using a mechanical pump as the first stage and a turbomolecular pump as the second and final stage. The source pressure was adjusted to optimize the He (I) emission that provides photons with energy of 21.21 eV. The discharge source was positioned slightly less than perpendicular from the face of the analyzer. Thus, the sample was illuminated at glancing incidence. To allow direct comparisons between the various modified surfaces, the binding energies were calculated with respect to the vacuum level.

C. Preparation of nanoparticles

1. Synthesis of In_2S_3 nanoparticles stabilized by thioglycerol (TG)

The synthesis is described in Reference 15. To 25 ml de-ionized water, 0.050 g indium chloride and 0.18 mL of thioglycerol was dissolved. The pH was adjusted to 3-3.5 using 0.1 M sodium hydroxide. Under vigorous stirring, 3.39 mL of 0.1 M aqueous solution of sodium sulfide was added. The nanoparticles are formed in the solution as a pale yellow - white turbid suspension that is stable for a few days when stored in the dark. Indium sulfide nanoparticles were separated as a pale yellow powder from the mother liquor using isopropyl alcohol.

2. Synthesis of In_2S_3 nanoparticles stabilized by 1-amino-2-methyl-2-propanethiol hydrochloride (AMPT)

The synthesis is explained in detail in Reference 15. In_2S_3 nanoparticles stabilized with AMPT was prepared similar to the Tg stabilized nanoparticles by dissolving 0.05 g indium chloride and 320 mg of AMPT in 25 ml de-ionized water. The pH of the solution was adjusted to 3-3.5 using 0.1 M NaOH. Under vigorous stirring 0.39 mL of 0.1 M aqueous solution of sodium sulfide was added. Stable indium sulfide nanoparticles, as white suspension, were formed in the solution.

3. Synthesis of In_2S_3 nanoparticles stabilized by sodium citrate

The nanoparticles were synthesized by first dissolving 0.05 g indium chloride and 0.66 g of sodium citrate in 45 mL de-ionized water that was degassed with argon gas for 15 minutes. The pH of the solution was adjusted to 3.5 using 0.1 M NaOH solution. This was followed by addition of 3.39 mL of 0.1 M aqueous solution of sodium sulfide under vigorous stirring. Indium sulfide nanoparticles were formed in the solution as a pale white suspension.

D. Characterization of nanoparticles

The synthesized nanoparticles were characterized by the general methods of UV-vis absorption, luminescence, XRD, TEM, EDAX and NMR. The instrumentation for these techniques was discussed previously in Chapter II.

D.1. UV-vis absorption

Different stabilizers were used to synthesize In_2S_3 nanocolloids. Figure 16, 17, 18 are the UV-vis spectrum of In_2S_3 stabilized by thioglycerol, AMPT and citrate, respectively. The characteristic absorption band was at 265-285 nm for thioglycerol, 275-

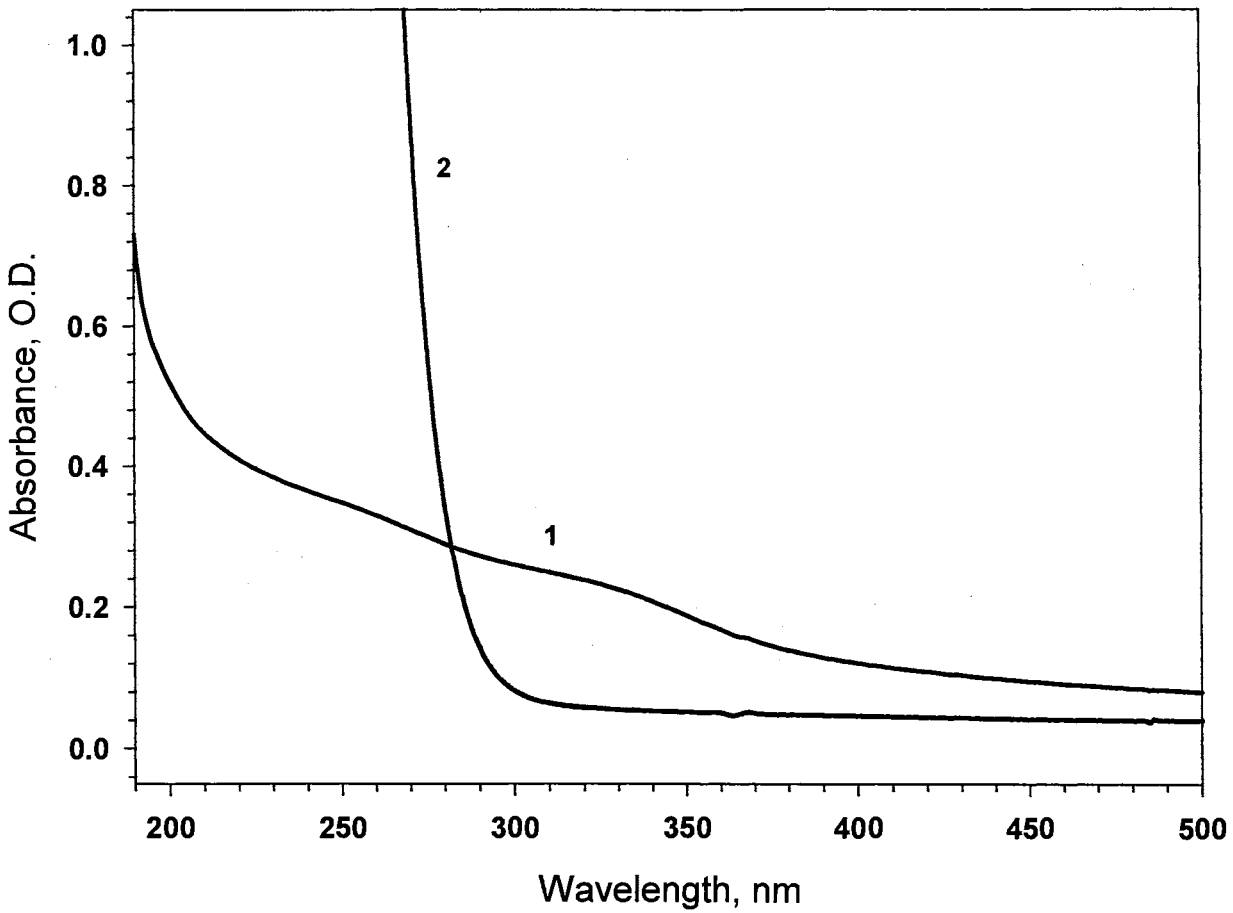

Figure 16. Absorption spectrum of 1) thioglycerol stabilized In_2S_3 NPs and 2) mixtureof $InCl_3$ and thioglycerol

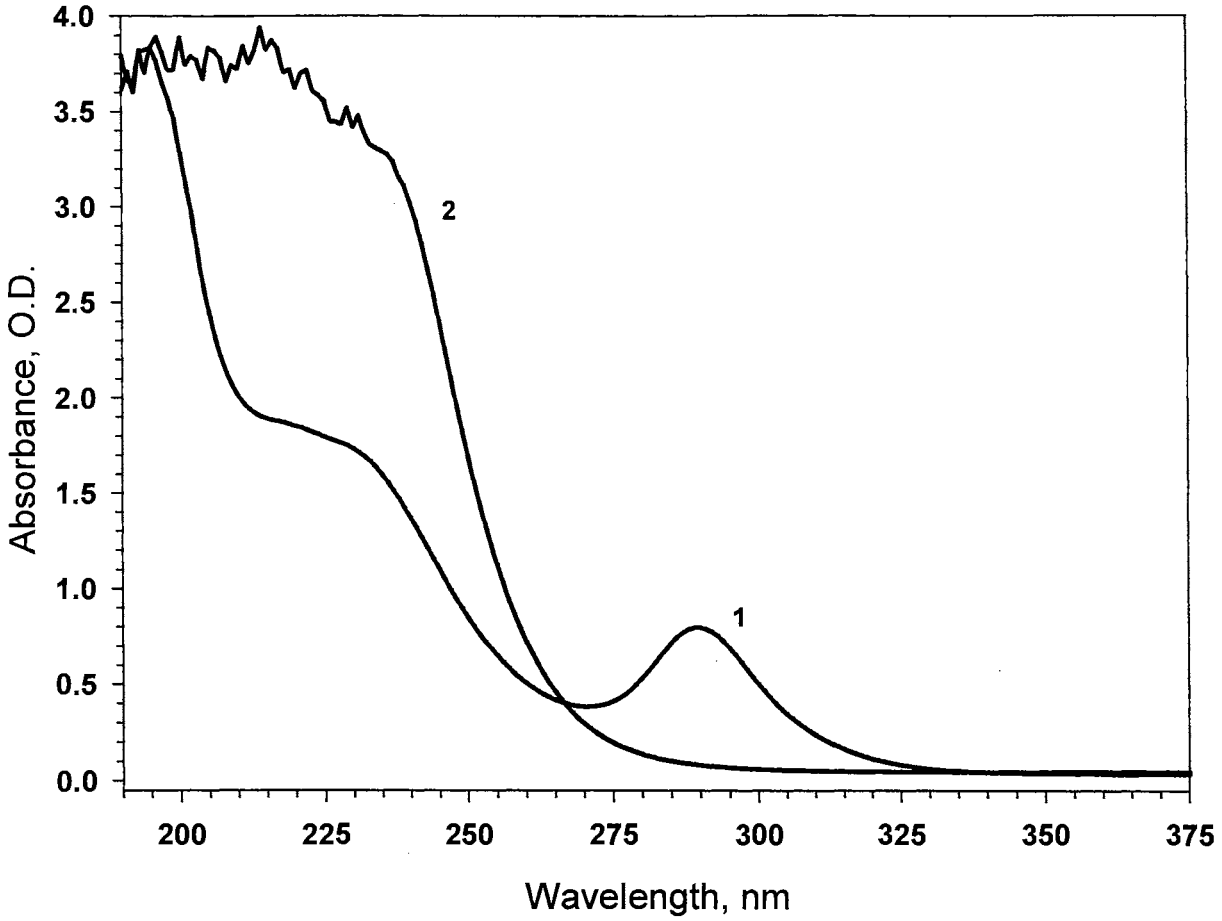

Figure 17. Absorption spectrum of 1) AMPT stabilized In_2S_3 NPs and 2) mixtureof $InCl_3$ and AMPT

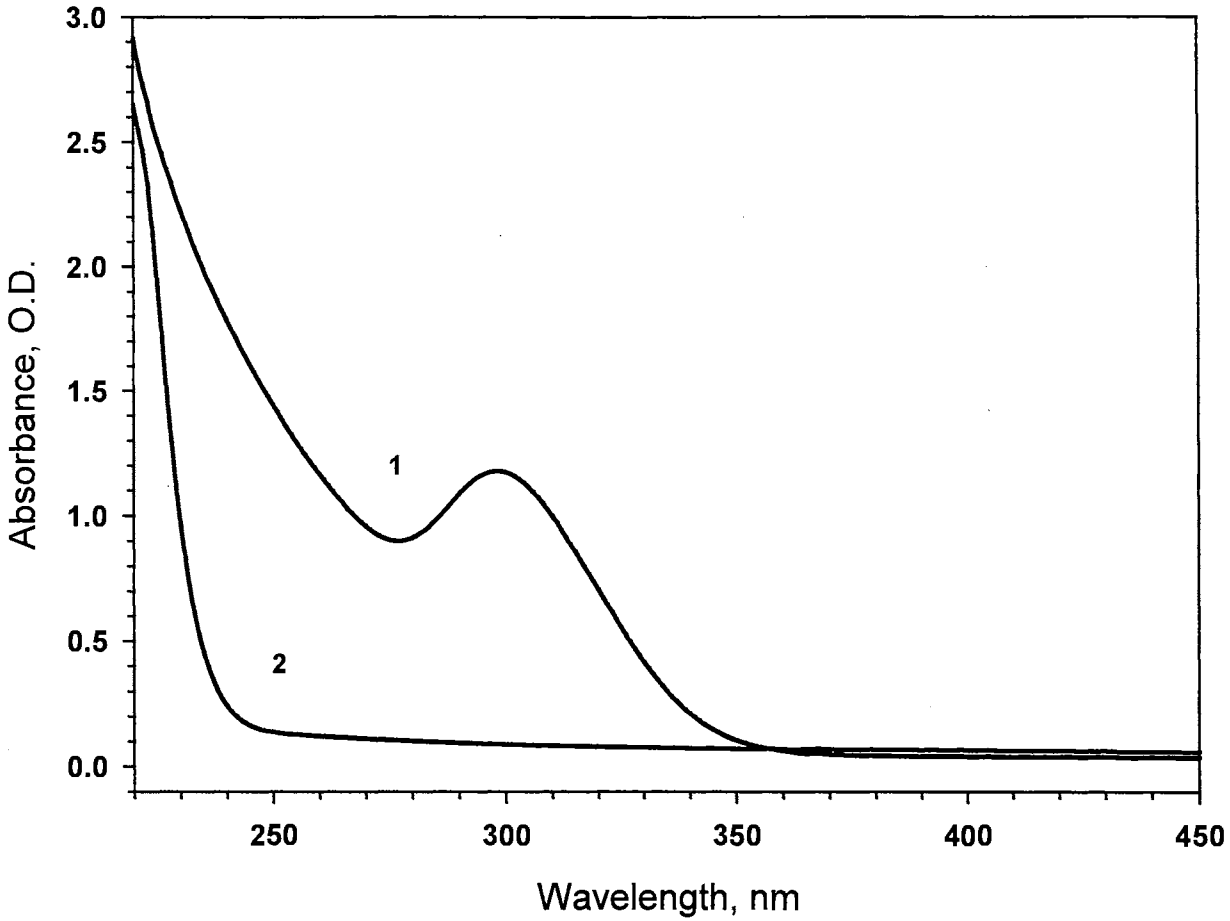

Figure 18. Absorption spectrum of 1) citrate stabilized In_2S_3 NPs and 2) mixtureof $InCl_3$ and citrate

310 nm for AMPT and 290-315 nm for citrate stabilized nanocolloids. The step like shape of the bands indicates that these correspond to the valence-to-conduction band transitions in indium sulfide. In the case of bulk In_2S_3 the band gap (E_g) is reported to be in the vicinity of 2.0-2.2 eV with corresponding UV-vis onsets at 620-550 nm. Correspondingly, from the absorption onset in the UV-vis spectra, the band gaps of In_2S_3 nanoparticles are 3.5, 3.6 and 3.8 eV for TG, AMPT and citrate stabilized nanoparticles respectively. The increase in band gap is typical for the nanocolloids and indicates the strong quantum confinement [6]. The position of the absorption onset is well within the range that was observed for similar In_2S_3 nanocolloids synthesized in the presence of polymers and solid matrices [68,69].

D.2. Transmission electron microscopy (TEM):

The TEM images of the redispersed nanoparticles are shown in Figure 19. The crystalline nature of the prepared nanocolloid was observed in the high resolution TEM as seen in Figure 19. The EDAX data indicate the ratio of indium to sulfur in the particle as 4.1:5.9, which is close to the expected ratio of 2:3 for In_2S_3. The Fourier transforms of the crystalline areas show lattice spacings equal to 2.6 and 2.9 Å. These spacings correspond to (220) and (206) crystal planes of the tetragonal β-In_2S_3 [81,82]. Figure 20 shows the electron diffraction data of the nanoparticles and it reveals the presence of lattice spacings of 2.09, 1.21, 1.05, 0.79, 0.70 Å. The diffraction circles at 2.09 and 1.21 Å correspond to the expected 2.06 and 1.20 reflexes with relatively intensity of 75 and 67 originating from (309) and (840) lattice planes in β-In_2S_3 [83]. The 1.90, 1.64 and 1.40 Å lattice planes in β-In_2S_3 with relative intensity of 100, 58 and 88, respectively, is not seen in the nanoparticles. The other possible modification of indium sulfide is the α-In_2S_3

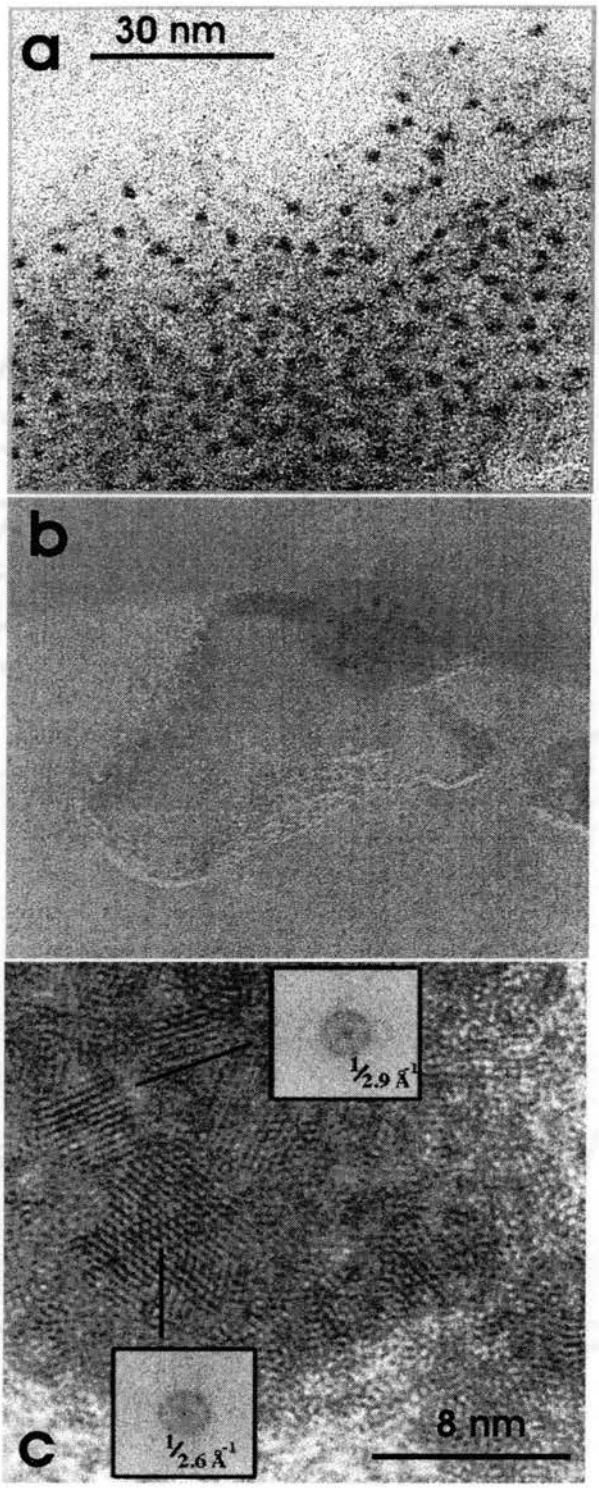

Figure 19. Survey a), b) and c) high resolution transmission electron microscopy images of thioglycerol stabilized In_2S_3 NPs.

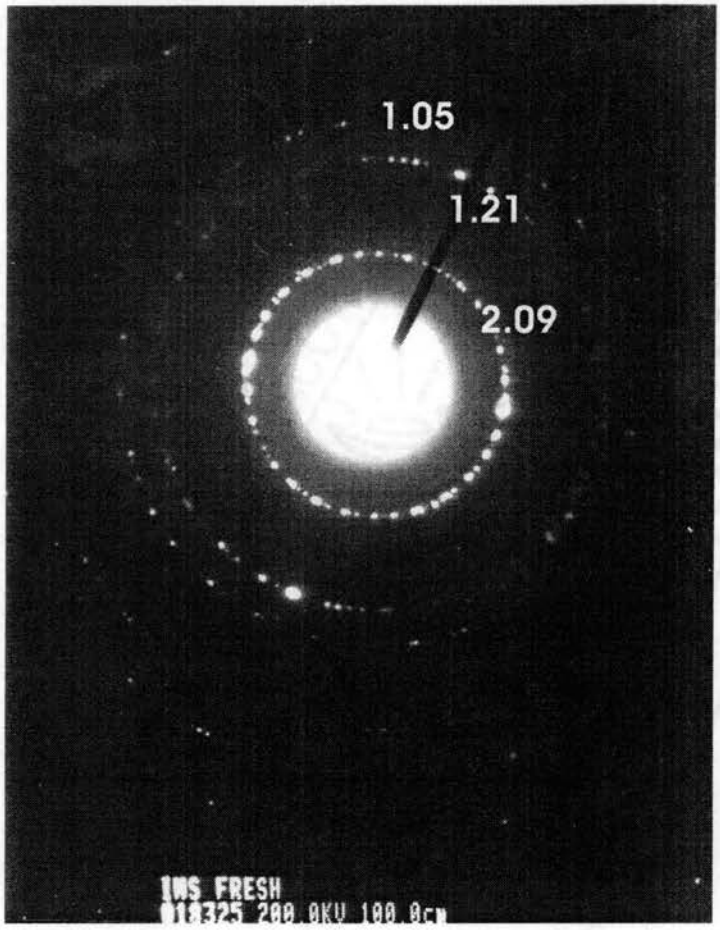

Figure 20. Electron diffraction pattern of thioglycerol stabilized indium sulfide NPs.

form [83], which has strong signals at 1.89, 1.55, 1.09 and 0.94 Å with relative intensities of 100, 50, 80, and 50. Since there are no signals from this form of indium sulfide in the electron diffraction pattern, α-In_2S_3 form is ruled out. The single-crystal diffraction pattern could not be obtained, as the nanoparticles are unstable under the electron beam.

D.3. Nuclear magnetic resonance (NMR):

The NMR study was carried out in the liquid state so that the dynamic behavior of thiol stabilizers adsorbed to the nanoparticle surface can be characterized. The ^{1}H NMR spectrum of unbound TG consists of five groups of peaks representing the protons on methylene and methane carbons Figure 21, trace 1. Assignment of the peaks is based on their relative position and the observed multiplet structure. Protons of –OH and –SH groups are not visible in these spectra due to their fast exchange with D_2O. The quintet at 3.75 ppm represents the middle –CH(OD)- group because it is split by the two adjacent pairs of protons. The multiplets at 2.57 and 2.69 ppm correspond to CH_2SD protons, while those at 3.56 and 3.64 ppm correspond to –CH_2-OD signal.

Upon binding to the In_2S_3 nanoparticle surface, signals from all the protons in TG become broader, as seen in Figure 21, trace 2. Additionally, the bands of –CH_2S-In_2S_3 undergo a shift from 2.70 to 2.85 ppm and that of –CH(OD) undergoe a shift from 3.77 to 3.83 ppm. The protons of –CH_2OD broaden, without significant shift in its position. The magnitude of shift correlates well with the distance between the protons and the In_2S_3 surface. The protons in the immediate proximity to the surface, i.e., -CH_2S-In_2S_3, experience the strongest shift of 0.15 ppm. The signal of the protons in the next hydrocarbon group, -CH(OD)-, is shifted by 0.06 ppm, while the frequency of the

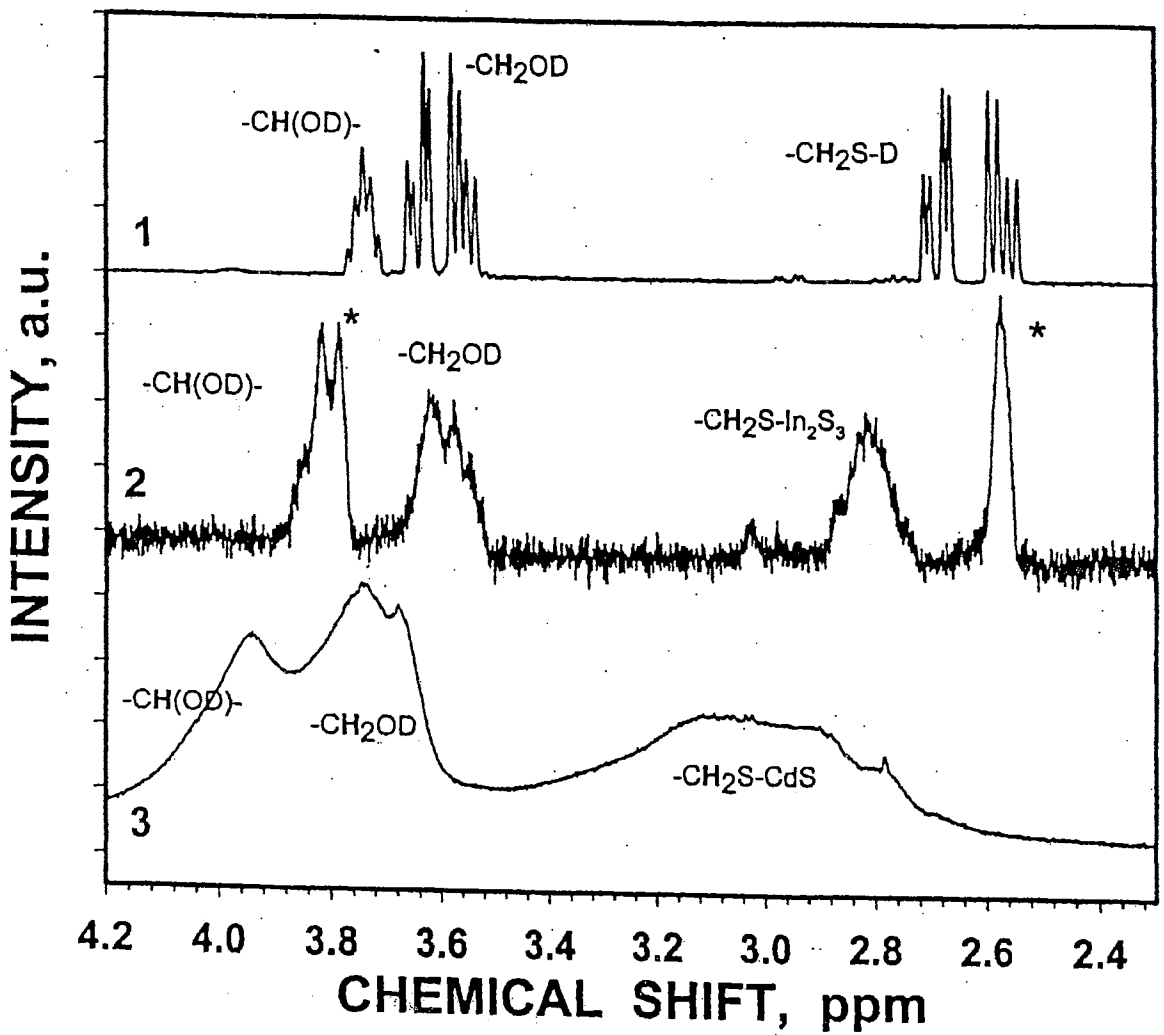

Figure 21. NMR spectrum of 1) thioglycerol, 2) In_2S_3 NPs stabilized by thioglycerol, and 3) 3.0 nm CdS NPs stabilized by thioglycerol. Stars mark the signals from residual amounts of 2-propanol used for the precipitation of In_2S_3 NPs.

terminal end protons, -CH_2OD, remains virtually unchanged. This effect could be a direct consequence of binding to the positively charged metal centers on the nanoparticle surface with the high positive charge of indium withdrawing electrons from the thiol headgroup and a resulting depletion of the electron density along the chain of σ-bonds affecting the first two carbon atoms and deshielding the associated protons. The broadening of the proton NMR for the bound TG could be attributed to the frustration of rotational and vibrational moment of the stabilizer when adsorbed to heavy nanoparticles. With limited motion of the bound TG, the rotational correlation time of the nanoparticles would be more influential in determining NMR relaxation parameters. The larger rotational correlation time of the coated nanoparticles in comparison to that of the free TG molecule would be associated with a shorter transverse relaxation time, T_2, and hence a broader line.

The NMR spectrum of TG coating on the In_2S_3 quantum dots can be compared to the one obtained for a similar sized CdS nanocrystal Figure 21, trace 3 [15]. The shift pattern –CH_2SH > -CH(OH) > -CH_2OH is consistent with the one observed for In_2S_3. On the other hand, the broadening of the TG signals on 3.0 nm CdS is much greater than for TG on In_2S_3. The bands partially merge, which is also accompanied by the complete loss of the fine structure. Since, as noted above, the width of the NMR signal largely depends on the mobility of the TG moiety, the motion of the stabilizer molecules on CdS is significantly more hindered than on the In_2S_3. This result can be understood by recalling the difference in crystal lattices of the two solids. In the case of CdS, the number of metal and chalcogen atoms forming the unit cell is equal. Unlike the group II-VI quantum dots, the metal atoms are in the minority in In_2S_3. In β-In_2S_3, indium atoms are accommodated

in all octahedral sites and two-thirds of the tetrahedral sites of the basic cubic lattice produced by sulfur atoms. Note that in cubic CdS, the structural motif of small CdS clusters, all of these sites are filled by Cd atoms. The number of metal centers available for binding the stabilizer is naturally smaller in In_2S_3 than in CdS. The coating of the stabilizer becomes less dense, and therefore, the greater mobility of the adsorbed TG moieties lengthens T_2, resulting in less broadening of the NMR lines. It is worth pointing out that the mobility of the TG group on the surface of both types of nanoparticles studied here is significantly lower than that of thiophenyl moiety previously investigated [49]. This can be attributed to the multiple hydrogen bonds that the TG group can form with adjacent stabilizer molecules, as well with the semiconductor surface.

D.5. Luminescence

The prepared In_2S_3 nanocolloids exhibited relatively strong luminescence, as shown in Figure 22, 23 and 24, which had not been reported for the previously made indium sulfide nanocomposites [27,74,75,76,85,86]. The origin of the luminescence peaks had to be verified as the indium ions might form complexes with the various stabilizers and sulfur molecule that could interfere with the optical spectra of the nanocolloids. The origins of the peaks were confirmed by the dialysis experiment. Aqueous solution of indium sulfide nanoclusters was dialyzed against deionized water for 24 hours (3 x 12 hours) in a 15 kDa molecular weight cut off (MWCO) dialysis membrane. It is clearly seen in Figure 25 that there is no significant change in the peaks before and after dialysis, and thus confirming the origin of luminescence peaks. The slight red shift in the peak from 365 nm to 375 nm is attributed to the aggregation of the nanocolloid due to the partial removal of the protective layer of the stabilizer from the nanoparticle surface. A

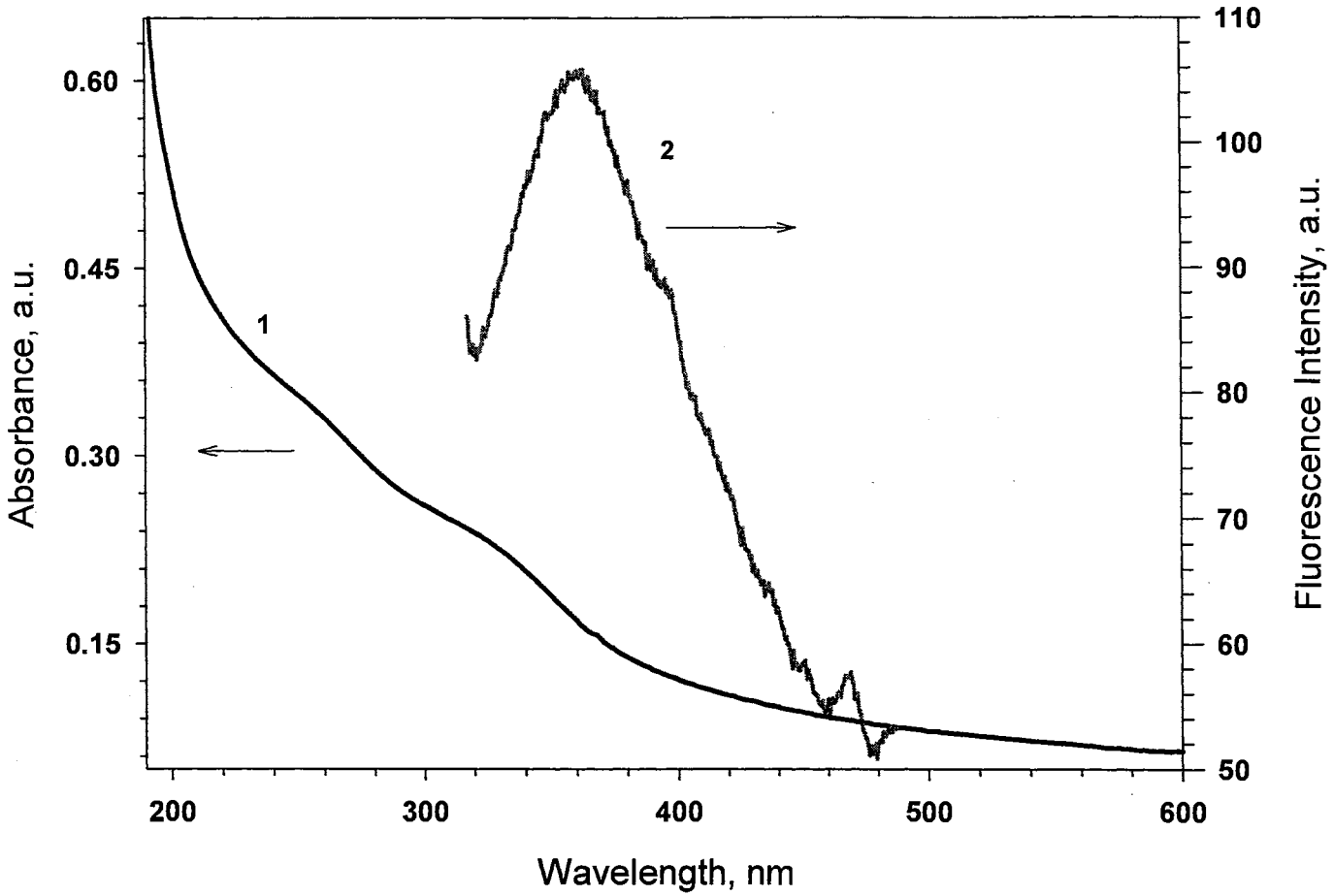

Figure 22. Optical properties of In_2S_3 NPs stabilized by thioglycerol. 1) UV-vis absorption spectra and 2) Luminescence spectra

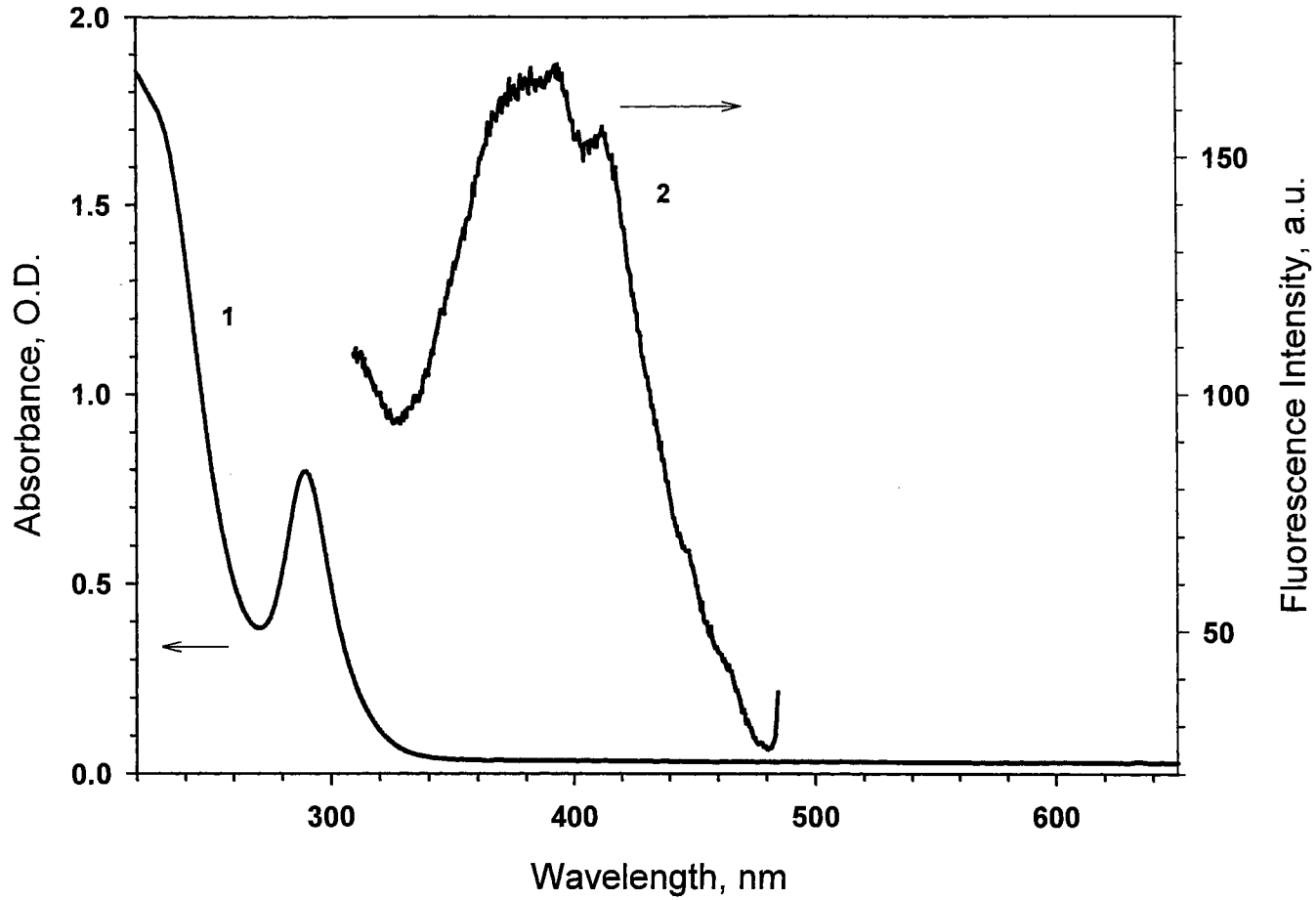

Figure 23. Optical properties of In_2S_3 NPs stabilized by AMPT. 1) UV-vis absorption spectra and 2) luminescence spectra.

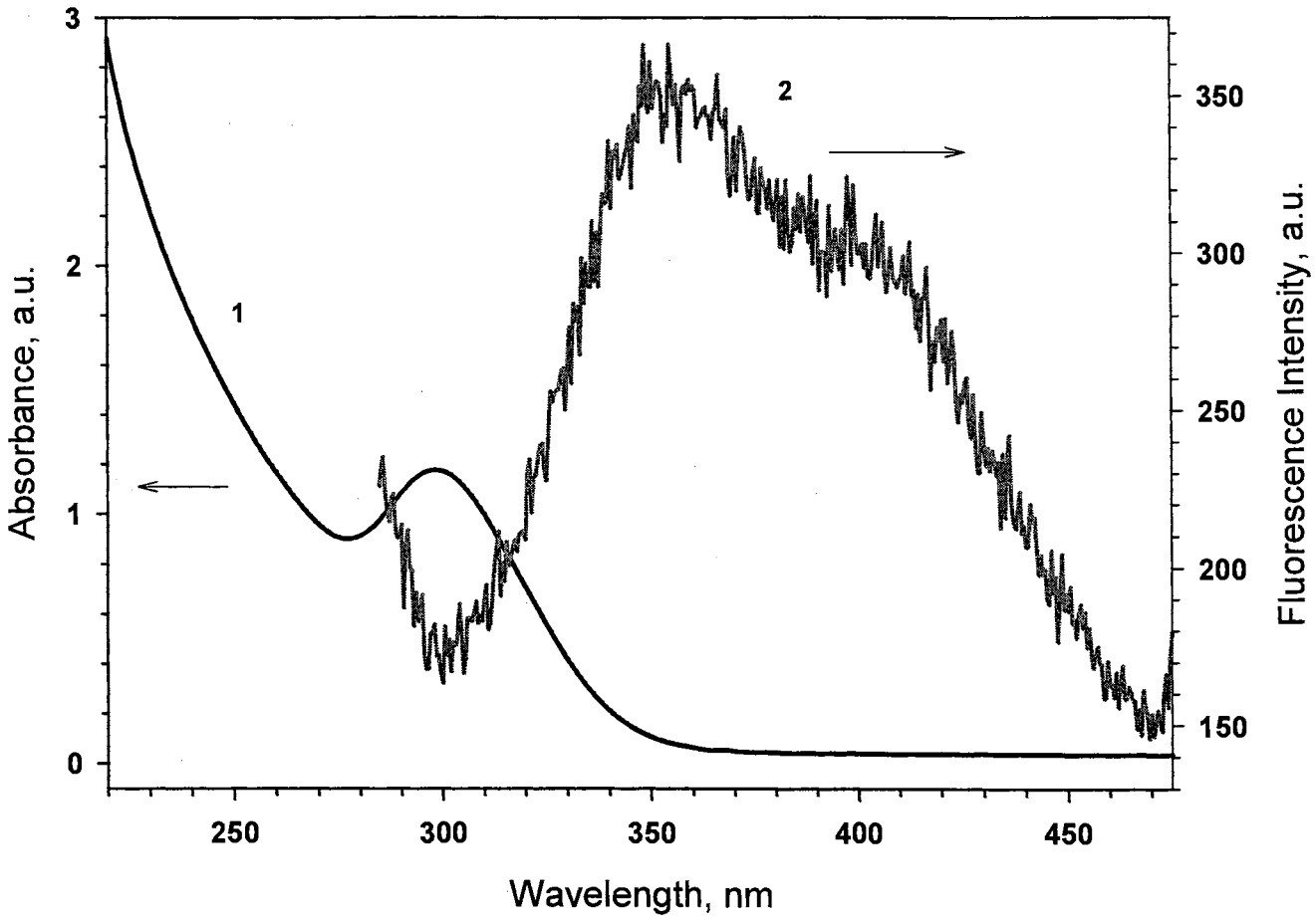

Figure 24. Optical spectrum of citrate stabilized In_2S_3 NPs. 1) UV-vis absorption spectra and 2) luminescence spectra

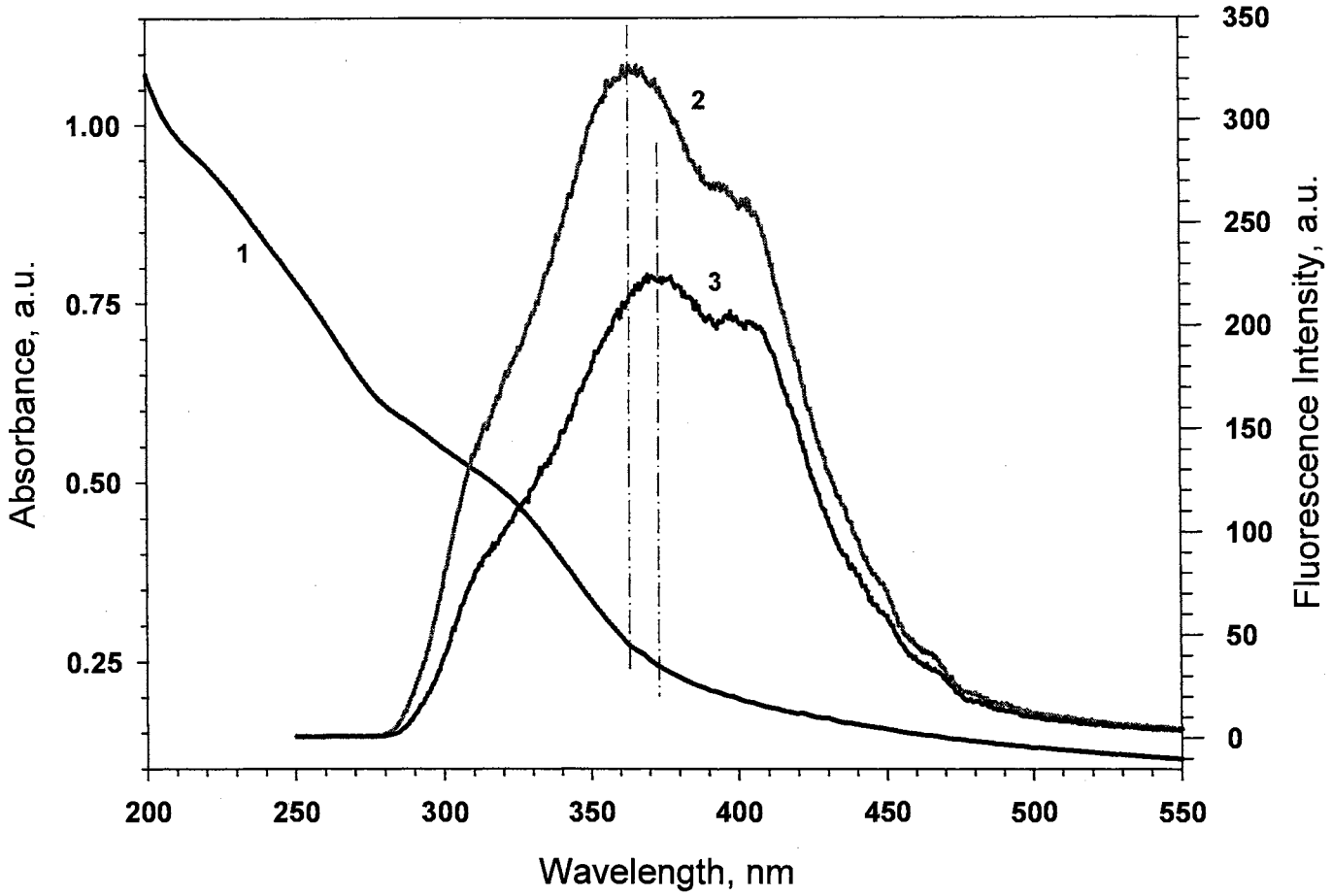

Figure 25. Optical properties of thioglycerol stabilized In_2S_3 NPs. (1)UV-vis absorption spectra, (2) and (3) luminescence spectra before and after dialysis respectively

small amount of the nanoparticles collapsed to form a white solid precipitate on the walls of the dialysis membrane.

The closeness of the emission peaks to the absorption onset of the semiconductor indicates that this emission comes from the interband electron-hole recombination. The luminescence of In_2S_3 does not show the characteristic second luminescence peak or the trapped emission [55]. This lack of trapped emission is a useful feature of the prepared nanocolloids.

The quantum yield of the In_2S_3 nanocolloids was measured with respect to Rhodamine B and *p*-quaterphenyl as standards. The quantum yield of the nanoclusters was calculated using the formula:

$$\varphi_{NP} = \varphi_S (I_{NP}/ I_S) \times (OD_S/OD_{NP})$$

where, NP and S stand for nanoparticles and the standard respectively, φ stands for the quantum yield, I is the integrated area of luminescence and OD is the optical density at the excitation wavelength. The peak position of the standard should approximately be in the same region of the spectrum as that of the nanoparticle whose quantum yield is being determined. Rhodamine B, which has a luminescence peak maximum at 585 nm, has been used as a standard for CdS and CdSe nanoparticles that have peaks in the 550-650 nm region [14,55]. Since the peak maxima for the various In_2S_3 nanoparticles are in the 360-380 nm range, the choice of rhodamine B as the standard would result in slight errors in the calculated values of the quantum yield. In order to minimize this error, *p*-quaterphenyl (peak maxima at 365 nm) was selected as the standard [88,89]. The quantum yield (φ) value for Rhodamine B in ethylene glycol is 1.0 and that of *p*-quaterphenyl in ethanol is 0.71. The quantum yield for the prepared nanocolloids was found to be in the

range of 1.2-1.5%. This value is comparable to similarly synthesized thiol stabilized CdS and CdSe nanoclusters without any special epitaxial coating [36,91,92].

D.6. Time resolved photoluminescence (TRPL):

The most important observation in the lifetime measurement experiments is the relatively short lifetime for the NPs when compared to the same bulk material [36,92]. The electron-hole pairs generated in the case of bulk materials are well separated. The electrons are highly localized and the excited states have long lifetimes. In the case of NPs, the recombination of the electron-hole is very much favored due to the size confinement. Because of this, the excited states have a relatively short lifetime. The lifetime obtained for the In_2S_3 nanocolloids was 5.3 ± 0.5 ns. It can be seen in Figure 26 that the luminescence decay is monoexponential, unlike CdS or CdSe NPs that have a multiexponential decay profile [36,53,54].

The nature of the valence-to-conduction-band transition in bulk In_2S_3 is a topic of debate. It is believed to be associated with an indirect electronic transition [80]. There are some who consider it as a direct allowed transition [79a-f] and some even consider it to be a direct forbidden transition [79g]. Indirect band gap transitions are ruled out based on the following reasons. Phonons, which are quanta of the vibrational energy of the semiconductor crystal lattice, are involved in the indirect band gap transitions. These transitions are nonemissive [90] in nature due to the fast non radiative recombination via vibrational states.

The lifetime of an emissive state is determined by two factors namely, the radiative and radiationless transitions to the ground states [75]. The nature of the radiationless process is not taken into consideration here. It is assumed that there is only

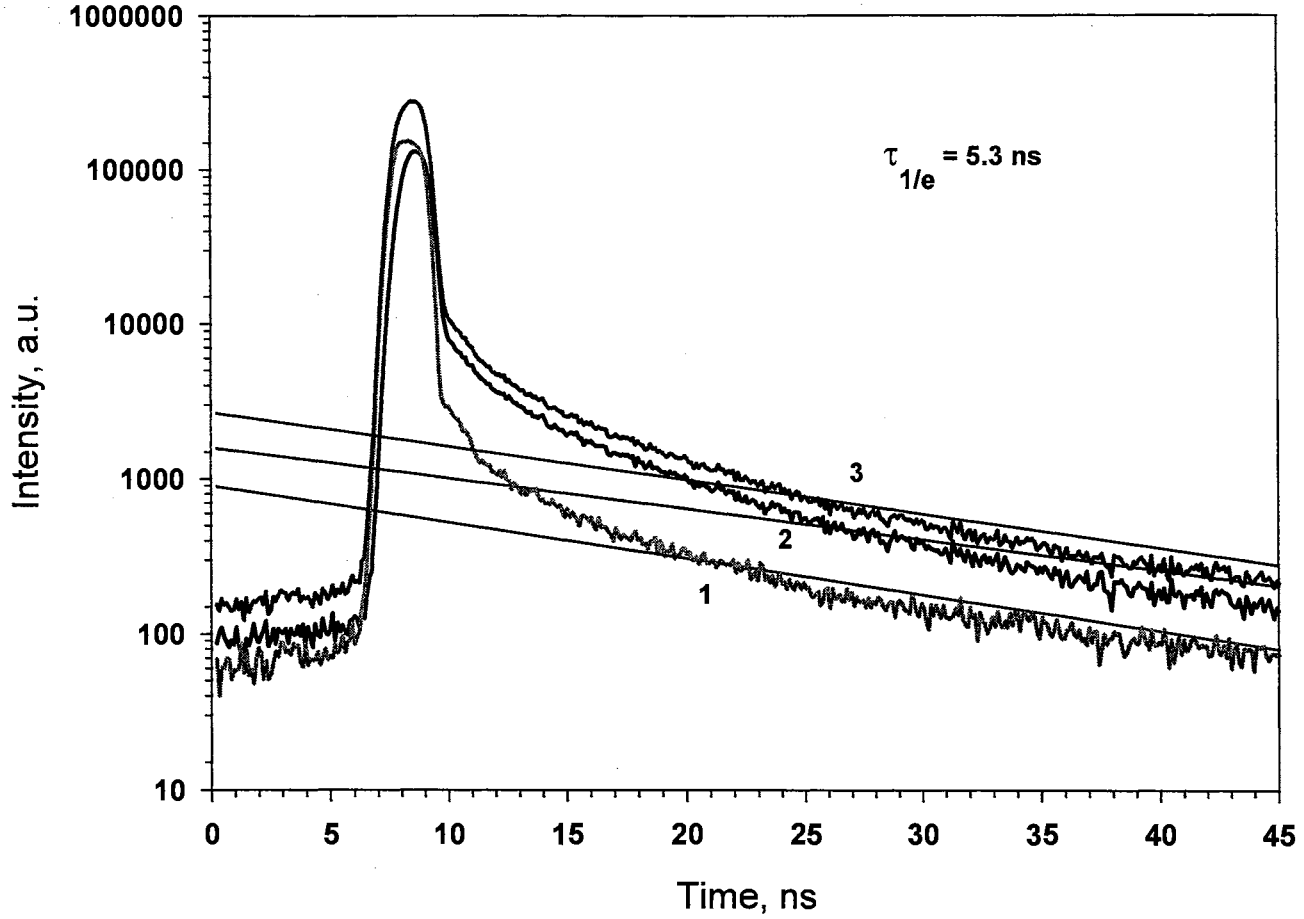

Figure 26. Time resolved photoluminescence spectrum of In_2S_3 NPs, excited at 330nm and measured from (1) 356-390nm, (2) 390-445nm and (3) 356-445nm

one emissive state, which correlates with the monoexponential decay of the luminescence kinetics, the

observed lifetime τ, true radiative lifetime τ_0, and the quantum yield φ are related by [75]

$$\varphi = \tau/\tau_0$$

Using the above equation, the true radiative lifetime for In_2S_3 NPs was determined to be τ_0 = 350 ns. For a blue-emitting CdS NPs, using similar calculations [75], the true radiative lifetime τ_0 = 1200 ns. The radiative lifetime of In_2S_3 NPs is significantly shorter than that of forbidden transitions. For instance, in oxidized silicon, it is in the range of microseconds [93]. Therefore, due to the shorter radiative lifetime and strong near band-edge luminescence, it is concluded that the electron-hole recombination in these NPs occur through a direct allowed transition.

E. Conclusions:

New synthetic pathways to prepare In_2S_3 nanoparticles in colloidal form were achieved with considerable control on the optical properties. The structure, morphology, optical properties are significantly different from the II-VI class of NPs that was discussed in Chapter II. The observation of direct band-gap transition is quite significant for these types of semiconductor NPs. The strong luminescence in the 350-400 nm region had not been previously reported for In_2S_3 and therefore this opens up a new possible application for these materials. The ability of In_2S_3 to accommodate guest ions is a very significant property and allows this to be doped with other metals to improve the magnetic properties.

CHAPTER IV

IV. Chalcogen site surface modification of CdSe and In_2S_3 nanoparticles with RuBP

A. Introduction

Semiconductor NPs due to their small size have a very high surface area with a large percentage of atoms on the surface. Therefore modification of the surface can greatly influence the properties of the semiconductor NPs. As mentioned in the introduction in Chapter I, there are two main types of surface modifications – organic and inorganic surface modification. The organic capping involves the replacement of one organic stabilizer molecule with another stabilizer molecule. Since the stabilizer molecule is bound to the metal atom on the surface, this type of modification does not utilize the chalcogen atoms on the surface. The inorganic capping of NP involves formation of a layer of the inorganic material on the surface of a preformed NP. The stabilizer molecule now binds to the metal atom on the surface of the new layer of NP. Thus, in both types of modification, only the metal atom is utilized for the modification reaction.

It has been reported previously that in CdSe NPs, the surface HOMO band consists of lone pairs of Se atoms and this level lies within the band gap [1,77]. Therefore, for an effective modification reaction the Se or the chalcogen atoms on the surface could be used. This was the main purpose of the work; to exploit the chalcogen atom on the surface for modification reaction.

The present method of modification reaction through the metal sites is convenient as the metal atoms are readily available on the surface. The metal atom has a high affinity to a variety of complimentary Lewis bases (thiols, amines, phophines, etc.) and the replacement of the stabilizer does not cause the NPs to grow [55,56,57]. Using the same

Lewis acid-base chemistry, the chalcogen atom (which is a Lewis base) can react with Lewis acids in the surface modification reaction. Since the probability of finding the metal and chalcogen on the surface is nearly the same, the reaction through the chalcogen atoms should be feasible. However, finding a suitable Lewis acid to react with the chalcogen atom is quite difficult. The solvents generally used in the synthesis have a considerable electron donor activity and hence could compete with the chalcogen atom for the Lewis acids. To avoid this, a mild Lewis acid is used that will react only with the chalcogen atoms and not with the stabilizer or solvent molecules.

Some of the properties that are desired in the Lewis acid to be used in the surface modification reaction are:

1) presence of aromatic or π-conjugated systems to allow electronic interactions between the NP and the modifier.

2) weak labile groups in the modifier that they can be readily displaced during the modification reaction.

3) the atom (transition metal) that links the modifier with the NP should be able to form a strong bond with the chalcogen atom.

4) the optical spectrum of the modifying group should not overlap with the bands of the NP so that changes of the modification reaction can be monitored by UV-vis absorption spectrum.

Based on the above consideration for the choice of a mild Lewis acid, the weak labile ligands could be Cl^-, H_2O, NH_3 and similar groups. The strong ligand with a distinct UV signature could be organic groups like bipyridine, phenanthroline, pyridine and similar groups. The modifier selected for this research work was a mixed ligand

complex with bipyridine groups, labile chloride ions and a transition metal, ruthenium. The molecule was ruthenium *bis*-bipyridine dichloride, which for brevity will be referred to as RuBP, and is shown in Figure 27.

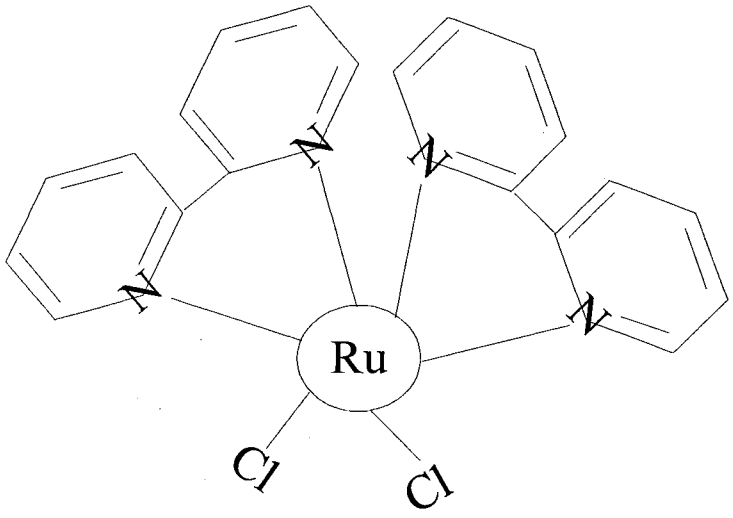

Figure 27. Structure of RuBP

A similar mixed ligand complex that was first attempted, in our research group, for the chalcogen site surface modification of NPs was a copper complex - CuBM where, CuBM is (2,2′-bipyridyl-N,N′)(malonate-O,O′) copper(II) monohydrate. CuBM was used to modify the surface of citrate stabilized CdS NPs [55,76]. The Cu – S bonding is strong and the spectral signature of CuBM is very distinct and does not overlap with the NP spectrum. The advantages of RuBP for the modification reaction in comparison with CuBM are the following:

1) Greater volume of electron density is located in aromatic π-systems of the two bipyridine rings compared to only one in the case of CuBM,

2) This complex has absorption in the visible region of the spectrum, 490 nm, which simplifies the observation of electronic effects,

3) The ruthenium atom can potentially form two bonds with the chalcogen atoms, therefore strengthening the supramolecule.

One of the important observations during this modification reaction was the role of stabilizer molecules. The initial experiments used thiol stabilized NPs for the modification reaction. It was noticed that there was a competitive reaction between the chalcogen atoms and S atom on the stabilizer for the modifier molecules. This led to misinterpretation of the results, as there was no conclusive way to differentiate the modification reaction with the side products of the reaction. Therefore, to minimize these types of side reactions, a milder Lewis base had to be used as the stabilizer. The stabilizer selected for this purpose was sodium citrate. The three carboxyl groups of citrate act together to help stabilize the NP [14,55,59]. Interference of the modifying group with the oxygen of the carboxylic groups was not observed.

Therefore, for all modification reactions in our laboratory, sodium citrate was used as the stabilizer for the NPs.

RuBP modified CdSe nanoparticles:

The rich chemistry for $Ru(bipy)_2Cl_2$ complexes have been used in the design of coordinative supramolecules [94,95]. The two chloride ligands are quite labile and the resulting Ru-E (E = S, Se) bonds are very strong which make the choice of this complex very suitable to study surface modification reactions. In addition, Ru (II) forms a series of complexes with heterocyclic compounds like bipyridine and phenantroline [94,95]. This extends the family of Ru complexes that can be used for the modification reaction.

CuBM modified CdS nanoparticles:

The modification of surface sites of CdS using CuBM was investigated by Tong Ni and is described in Reference 55 and 76. Some of the new results of this experiment will be discussed here. The UPS experiments were performed by Nicholas Materer (Department of Chemistry, Oklahoma State University, Stillwater, Oklahoma) on CuBM modified CdS NPs. The details of this experiment are given in Reference 55. The result from this experiment is used to explain some of the observations in the CdSe modification reaction.

RuBP modified In_2S_3 nanoparticles:

In_2S_3 NPs are quite different from the other NPs studied in our lab previously, due to the greater number of chalcogen atoms compared to the metal atoms in the unit cell [15]. Since the modification reaction utilizes the chalcogen atom on the surface, this type of modification offers very interesting surface chemistry to investigate.

The TEM data are adapted from Reference 55. Gordon Gainer at the Center for Laser and Photonics Research, (Oklahoma State University, Stillwater, Oklahoma) performed the time resolved photoluminescence experiments). Details of the instrumentation are described in Reference 15 and 55. Juvencio Robles (Facultad de Quimica, University of Guanajuato, Noria Alta s/n, Guanajuato, Mexico), Stefan Müssig (in Oklahoma State University on a research exchange program from University of Hamburg, Germany) and Nicholas Kotov (Oklahoma State University) carried out the theoretical calculations and molecular modeling studies. Details of the software and methodology are given in Reference 55.

B. Modification reactions

B.1. CdSe_citrate NPs modified with RuBP

To 3 mL of CdSe NP solution, 60 μL of 3mM aqueous solution of RuBP was added. The solutions were mixed and immediately introduced in the UV-vis spectrophotometer to monitor the modification reaction with time. There are changes in the spectra with time and the reaction comes to completion within 60 minutes of mixing, after which there was no more significant changes in the spectrum. The ratio of Cd^{2+}: RuBP was calculated to be 1:24 (m/m). The experiment was also carried out with different molar ratios, 1:12 (m/m) and 1:6 (m/m), of the modifier on the same sized NPs (CdSe - 30:1) and also on different sized NPs (CdSe - 10:1, CdSe – 4:1). All of these modification reactions showed similar trends and the results are discussed below.

B.2. CdS_citrate NPs modified with CuBM

The details of this experiment are explained in Reference 55. In brief, 60 μL of 3 mM CuBM solution was added to a mixture of 1.5 mL water and 1.5 mL CdS NP solution. The sample was then introduced in the spectrophotometer. The changes in the reaction were monitored *in-situ* for 20 minutes, after which there were no more changes in the spectra. The ratio of the NPs to modifier was changed and also tried on different sized NPs, all of which showed similar trends in the modification reaction.

B.3. In_2S_3_citrate nanoparticles modified with RuBP

To 3 mL In_2S_3 NP solution, 60 μL of 3mM aqueous solution of RuBP was added to study the modification reaction. The UV-vis spectra were monitored until there were no more observable changes in the reaction, which was about 60 minutes. The ratio of NP

to modifier was changed and the UV-vis absorption monitored for the modification reaction.

C. Results of RuBP modified CdSe_citrate NPs

C.1. Structure of modified NPs

The stabilizer molecule, citrate, is bound to the metal sites on the surface of the NP and the chalcogen site is accessible for the RuBP to bind to the NP. During the reaction, the two labile chloride molecules in RuBP are displaced and ruthenium with the two bipyridine units binds to the surface of the NP. Since the citrate on the metal site is not involved in the reaction, the stability of the NP is not affected. In the case of CuBM modified CdS NPs, a water molecule was displaced from the mixed ligand complex. This resulted in the attachment of Cu with a bipyridine and malonate unit on the surface of CdS NPs [55,76].

C.1.a. Optical absorption spectrum:

The UV-vis absorption is a convenient tool to monitor the modification reaction. Since the UV spectra of the NP and the modifier are distinct, the evolution of spectra of the modified NP can be monitored by *in-situ* UV-vis absorption spectroscopy. The reaction was first tried on the CdSe (30:1) with 60μl of 3mM aqueous solution of RuBP. The important changes in the UV-vis spectrum, as seen in Figure 28 are:

* blue-shift of the 290 nm peak of RuBP to 285 nm,

* red shift of the semiconductor NP core at 510 nm and,

* new shoulder at 370 nm.

The evolution of the modification reaction can clearly be monitored by the in-situ UV-vis absorption measurements, as shown in Figure 28. The peak shift of 490 nm to

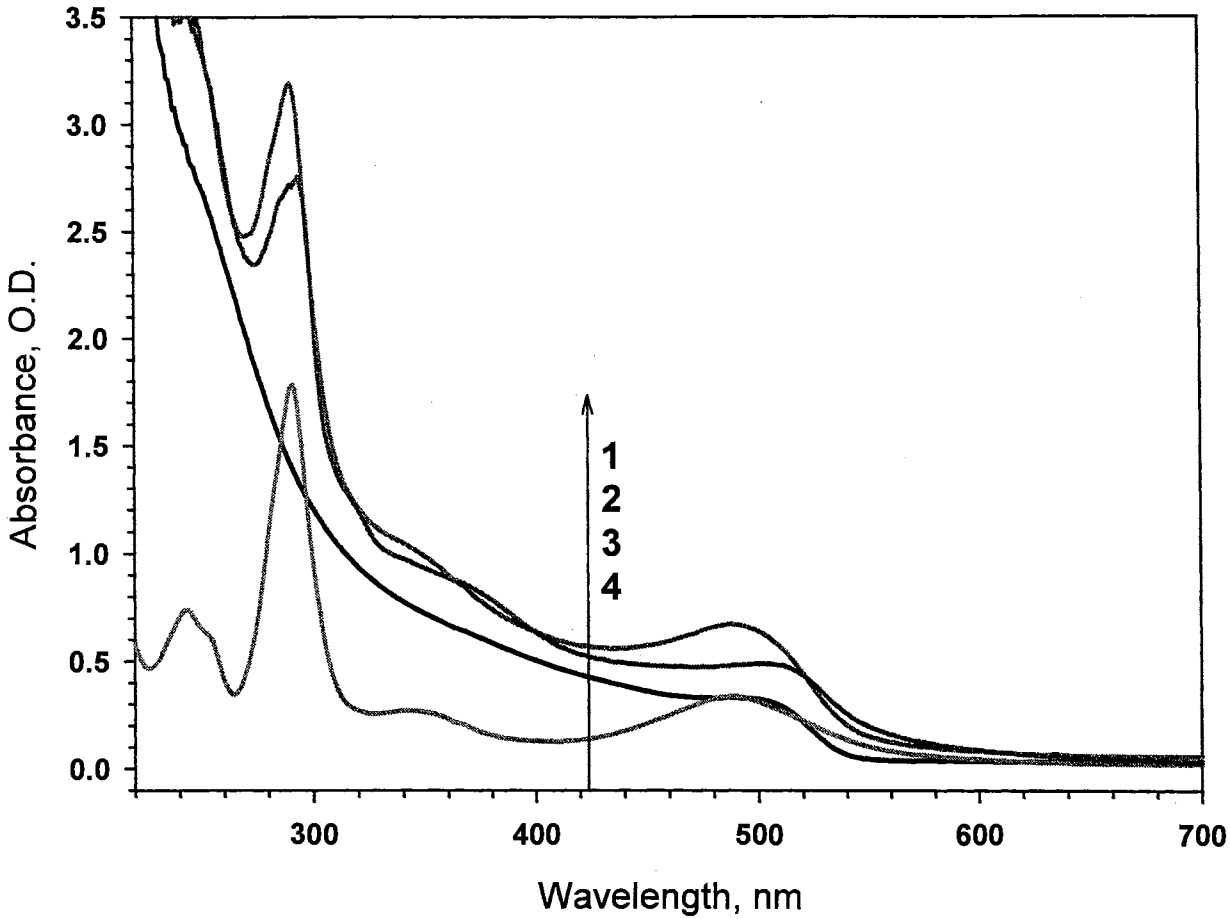

Figure 28. Absorption spectrum of RuBP modified CdSe NPs: 1) the arithmetic sum of the NP and RuBP, 2) after modification, 3) CdSe NP, and 4) RuBP

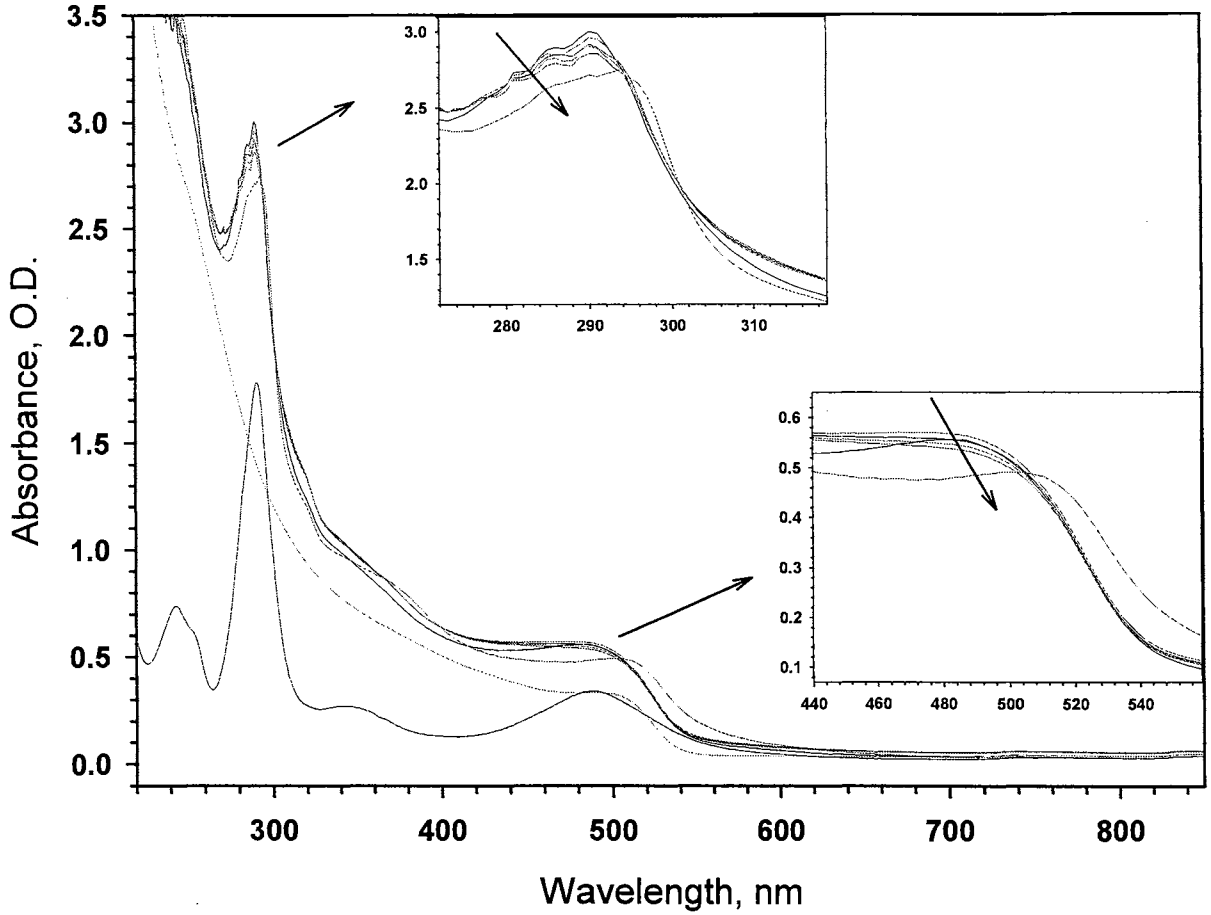

Figure 29. Evolution of the modification reaction with time

510 nm for the NP core is accompanied by a decrease in the absorption maxima. If the modification reaction resulted in the growth of the NP, it would lead to a red shift in the absorption spectra but not decrease in the absorption maxima. It suggests that this shift is not due to the increase in the size of the NP but rather a phenomenon related to the NP core. It has been previously reported in literature that RuS_2 can be synthesized from $RuCl_3$ in the presence of H_2S at high temperature[101,102] The optical spectrum of these materials is in the visible region of the spectrum but do not overlap with the region of the NP in our case. Since the experiment was performed at room temperature, this rules out the possibility of the formation of a layer of RuS_2 on the surface of CdSe NP to account for the red shift in the absorption spectrum in Figure 28. Similar observations were observed during the CuBM modification of CdS NP [55,76]. Therefore, this red shift of the CdSe band edge is attributed to the perturbations of the electronic levels of the core, possibly due to expansion of the delocalization volume available for the CdSe core.

The new peak/shoulder at 370 nm is distinct and does not interfere with the NP or the RuBP peaks. This could arise from new states being formed due to the mixing of the atomic orbitals of the two species. This new peak is seen in all the modification reaction with different ratios of RuBP, Figure 30. This further confirms the possibility of new electronic states arising from mixing of the energy states of NP and RuBP. To study the effect of selonourea on RuBP, RuBP solution was reacted with N,N,dimetylselenourea under similar experimental conditions. This is shown in Figure 31. The most important feature is a 210 nm peak from selenourea that is blue shifted to 205 nm after addition to RuBP, as shown in the inset of Figure 31. This blue shift could be in agreement with the other observations that this is due to the Ru – Se bond formation.

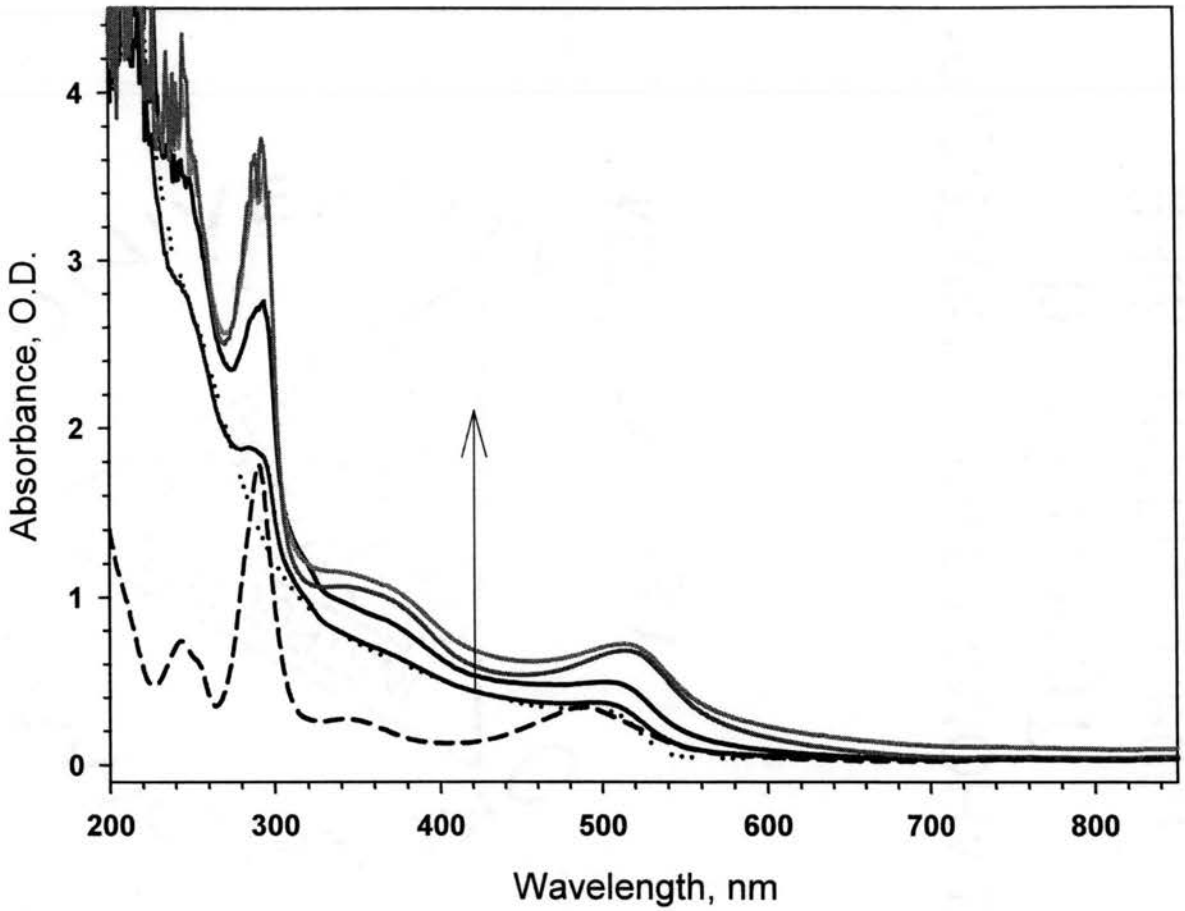

Figure 30. CdSe NPs modified with different ratios of RuBP. The arrow indicates increasing concertration from 1:12, 1:24, 1:36 and 1:30, respectively.
(.....) is CdSe NPs and (------) is RuBP solution.

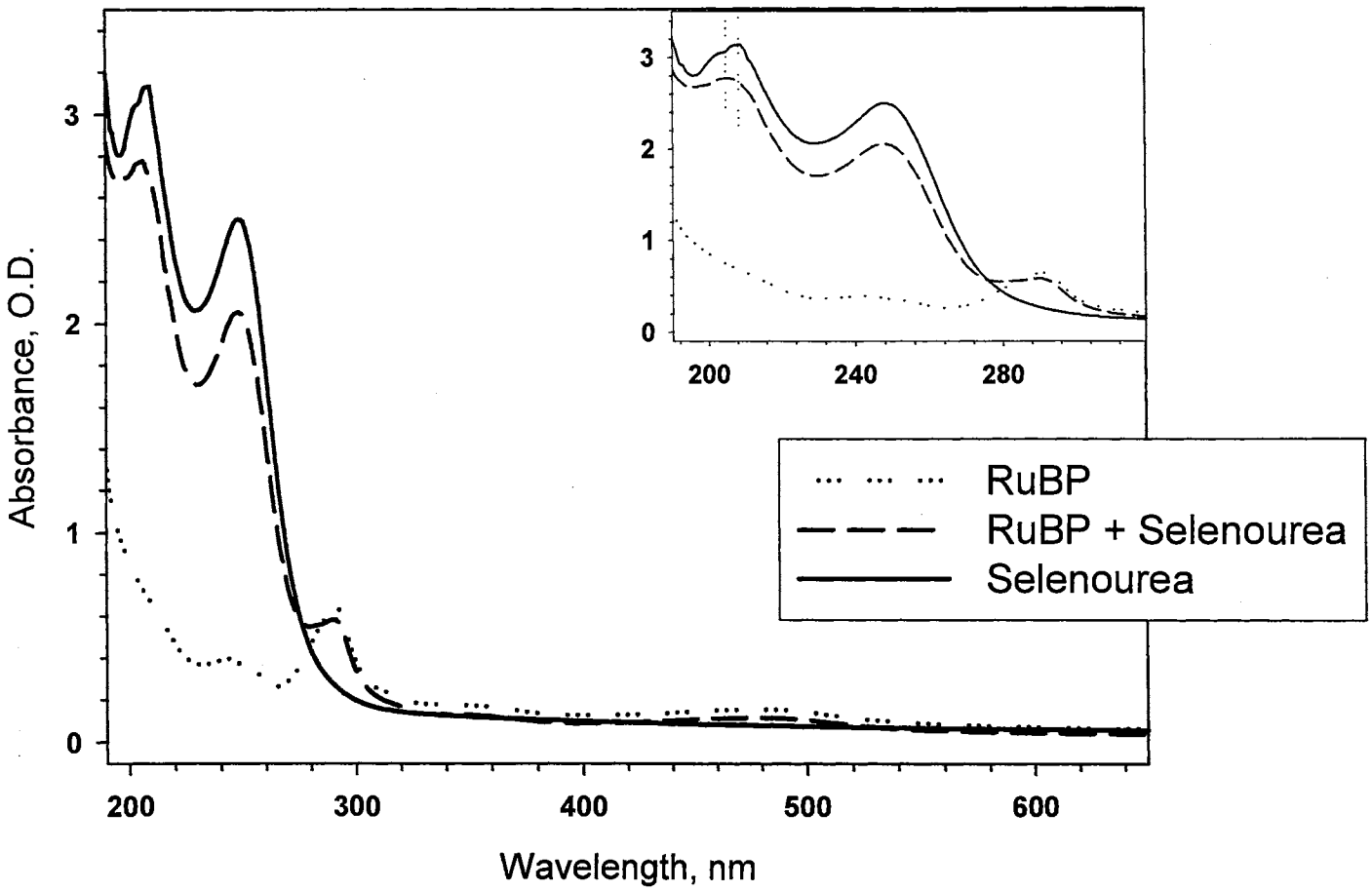

Figure 31. Absorption spectrum of 1) RuBP, 2) RuBP with selenourea and 3) selenourea
Inset: Blow up of the 200 - 320 nm range

The modified NPs were dialyzed against water for 24 hours and the UV-vis absorption measured after that. This is shown in Figure 32. The spectrum of the dialyzed sample still shows the peaks that were observed after the modification reaction, namely the 290 nm peak from RuBP and red shifted CdSe band gap edge (see Figure 28). There is a significant decrease in the intensity of the RuBP peak of the spectrum suggesting that the attachment and detachment of RuBP is reversible to some extent. Based on the decrease in the absorption maxima of the 290 nm peak, it is estimated that the initial CdSe:RuBP ratio of 1:24 decreased to 1:15. In addition to this, the band gap edge is blue shifted to an intermediate level between that of the naked CdSe and modified NP. If the red shift of NP after modification was due to growth of the NP, after dialysis this peak should have reverted back to the original position before modification, but this is not observed. Hence, it further proves the formation of intermediate energy levels.

C.1.b. Transmission Electron Microscopy:

TEM images of CdS NPs and CuBM modified CdS NPs were recorded and no significant changes were seen before and after the modification reaction. [55] This shows that there was no growth in the size of the NP. This observation further confirms the formation of new electronic levels as seen in the red shift of the band gap in the UV-vis absorption. (See Figure 28). The UV-vis results of CuBM – modified CdS NPs and RuBP – modified CdSe NPs are very similar with respect to the red shift of the band gap absorption after modification. Due to the similarities in the CdS and CdSe systems, the explanations used for CdS NPs can be extended to that of CdSe NPs. The TEM images before and after modification are shown in Figure 33.

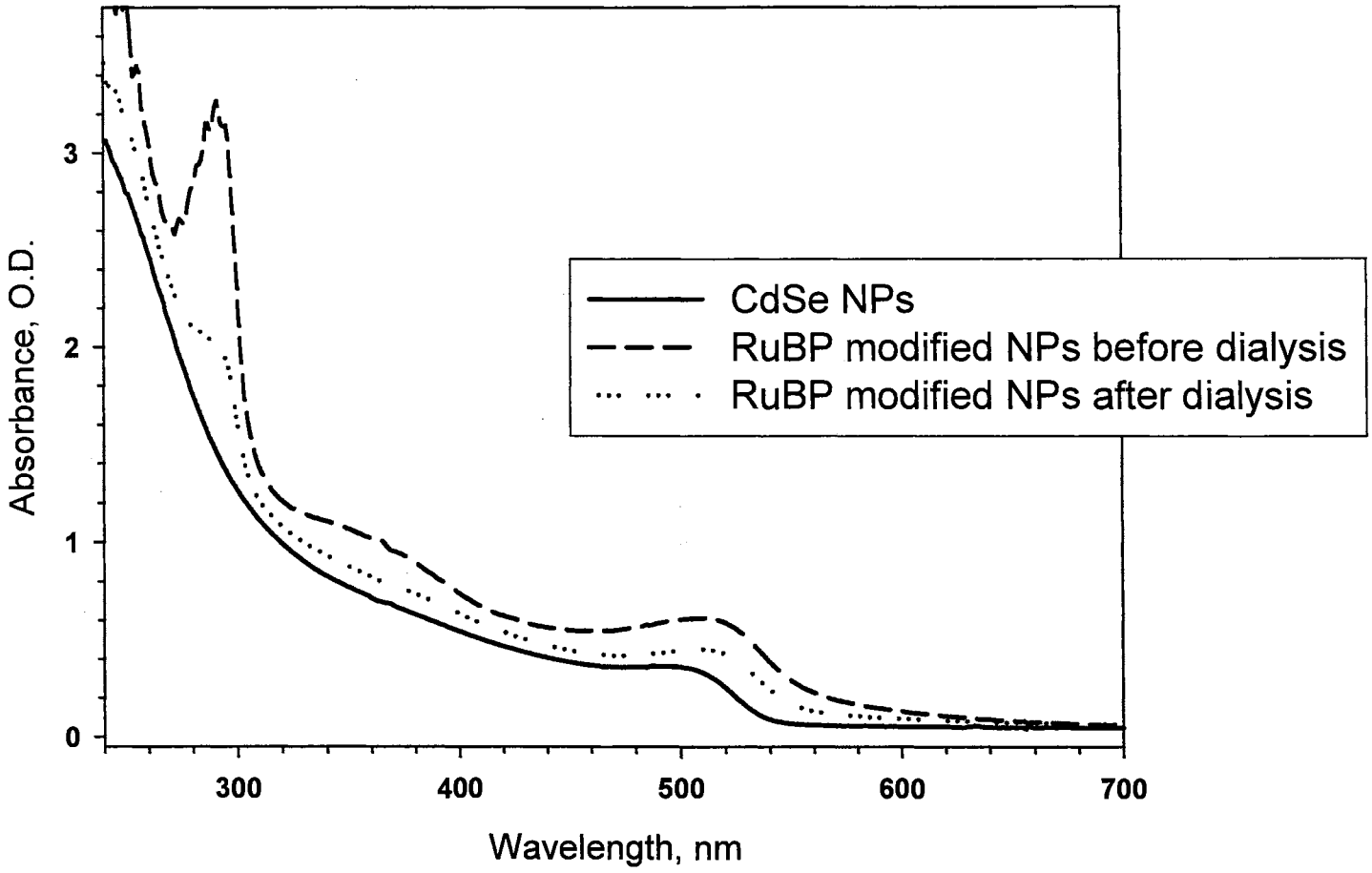

Figure 32. RuBP modified CdSe NPs before and after dialysis

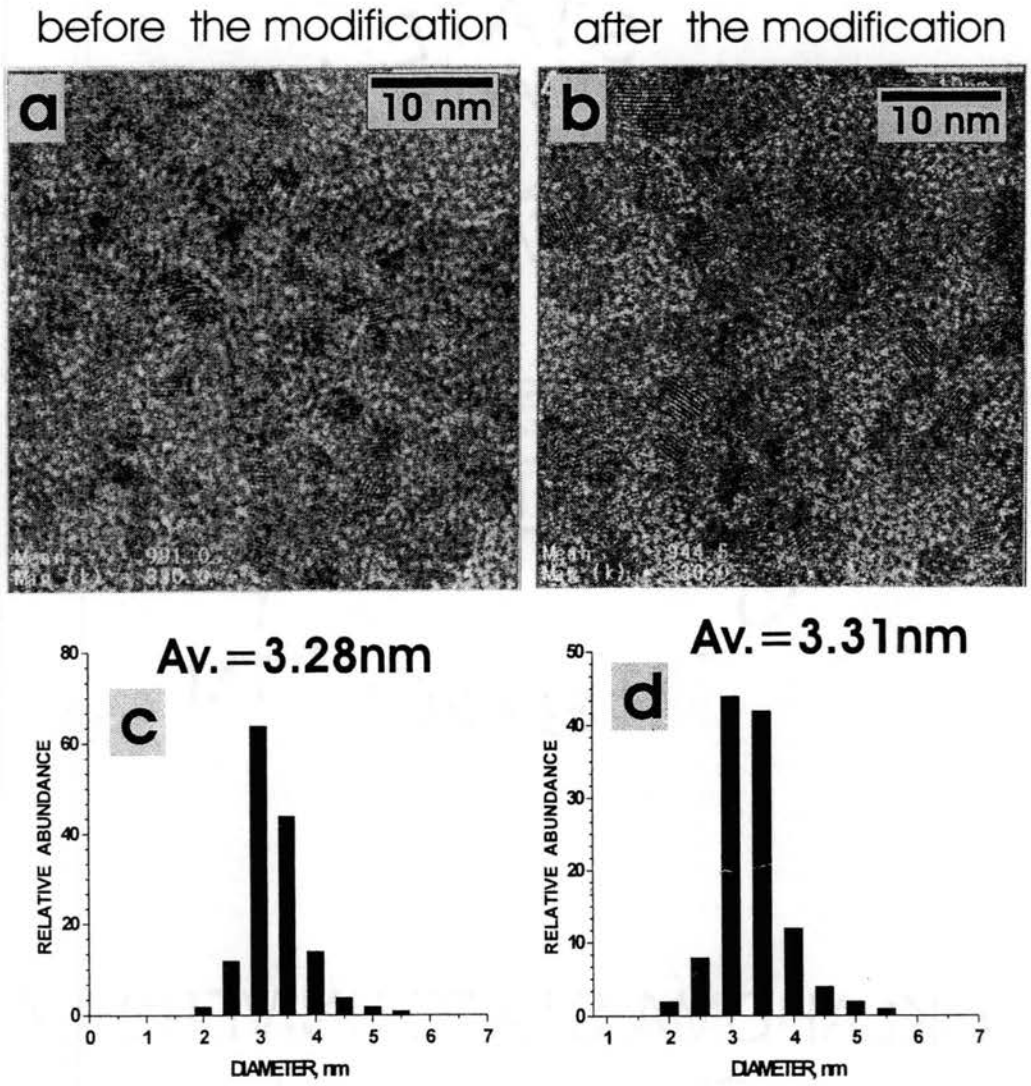

Figure 33. Transmission electron microscopy images of CdS NPs before (a) and after (b) modification NP:CuBM molar ratio of 1:60. Size distribution before (a) and after (b) modification. (Adapted from Reference 55, 76)

Based on the above observations, the model structure of the modified NP can be represented as in Figure 34.

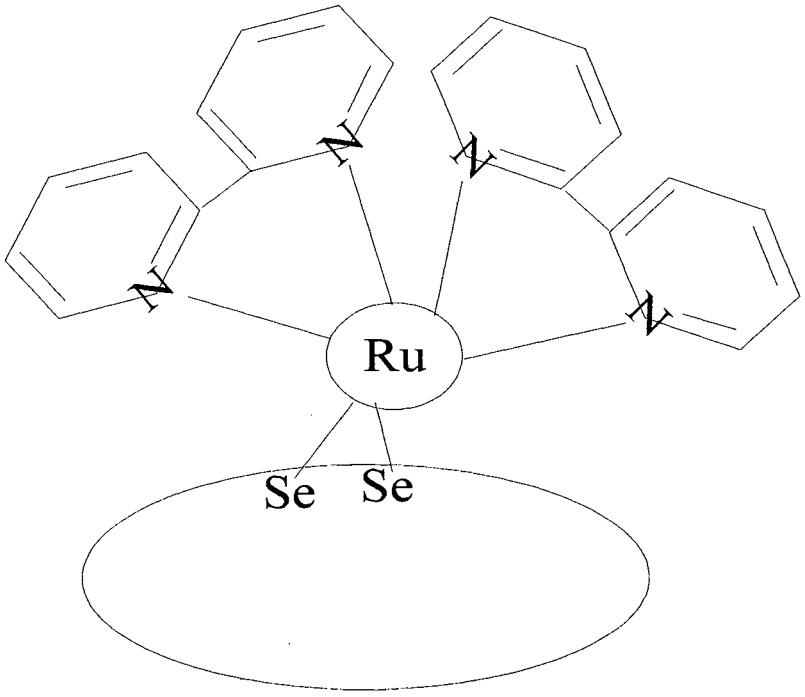

Figure 34. Proposed structure of RuBP modified CdSe NP supramolecule

C.2. Optical properties of RuBP-modified CdSe NPs

The UV-vis absorption spectrum clearly shows the effect of modification on the nature of the electronic states. The appearance of a new shoulder, red shift and decrease in the absorption edge of the NP core reveal the perturbation of energy levels in the CdSe NP core. These results were further corroborated by steady state luminescence and time resolved photoluminescence studies.

C.2.a. Steady state luminescence:

The modification reaction was also monitored by measuring the steady state luminescence before and after modification of the CdSe NPs with RuBP. The naked CdSe NPs have two distinct emission peaks, the excitonic emission in the 535-600 nm

and trapped emission in 665-735 nm regions. Upon surface modification, there is a strong decrease in the excitonic and trapped emission peaks, as shown in Figure 35. This development is seen in the modification reaction with different ratios of RuBP on CdSe (Figure 36), and also in differently sized CdSe NPs (Figure 37).

Surface modification of NPs via organic or inorganic capping occurs by binding of the modifier to lower energy sites that are responsible for non radiative decay. Removal of such defects enhances the excitonic emission. This phenomenon is not observed in the case of RuBP modified CdSe NPs, which makes them quite unique. Chalcogen site surface modification most likely creates new photophysical pathways for the excitation energy dissipation, which is reflected by reduced emission intensity. This is further investigated by the TRPL studies. The luminescence of the modification reaction with different CdSe:RuBP ratio is shown in Figure 36. It can be seen that as the ratio of Cd^{2+}: RuBP increases from 1:0 to 1:24 (m/m), the trapped emission completely disappears, indicating complete quenching of the surface states.

As with the UV-vis absorption spectra, the luminescence of the modification reaction was measured before and after dialysis. This is shown in Figure 38. The UV-vis absorption studies suggested that the adsorption of RuBP is reversible, due to the recovery of the peaks after dialysis to positions that were seen before modification. However, this was not observed in the luminescence measurements. The trapped emission peak should have recovered, resulting in an increase in intensity after the dialysis. But, this was not observed and on the contrary, it decreased in intensity. In addition, there is no recovery of the excitonic emission peak. This is unlike the previous chalcogen site modification reactions of CdS NPs with CuBM where, recovery of the

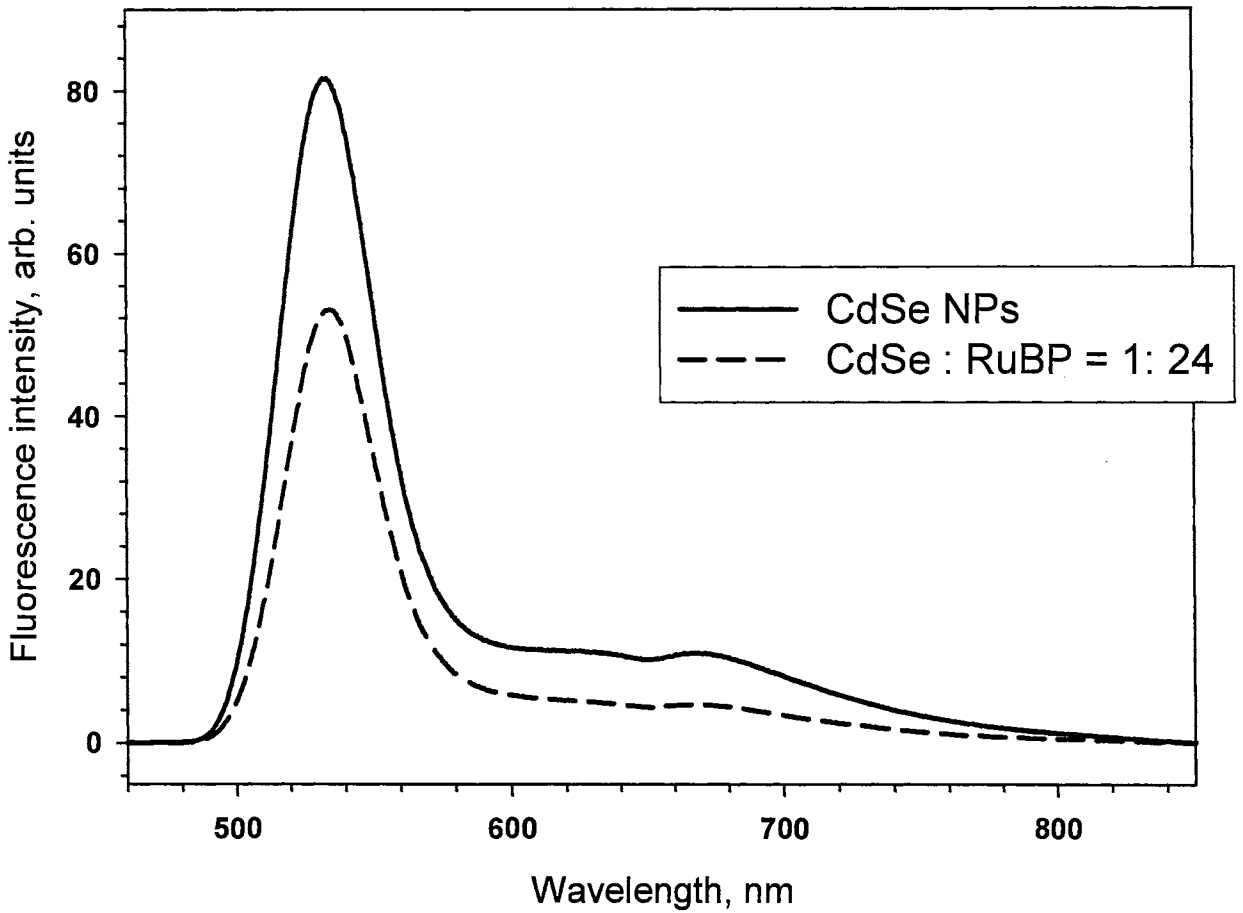

Figure 35. Luminescence spectrum of CdSe NPs and RuBP modified CdSe NPs

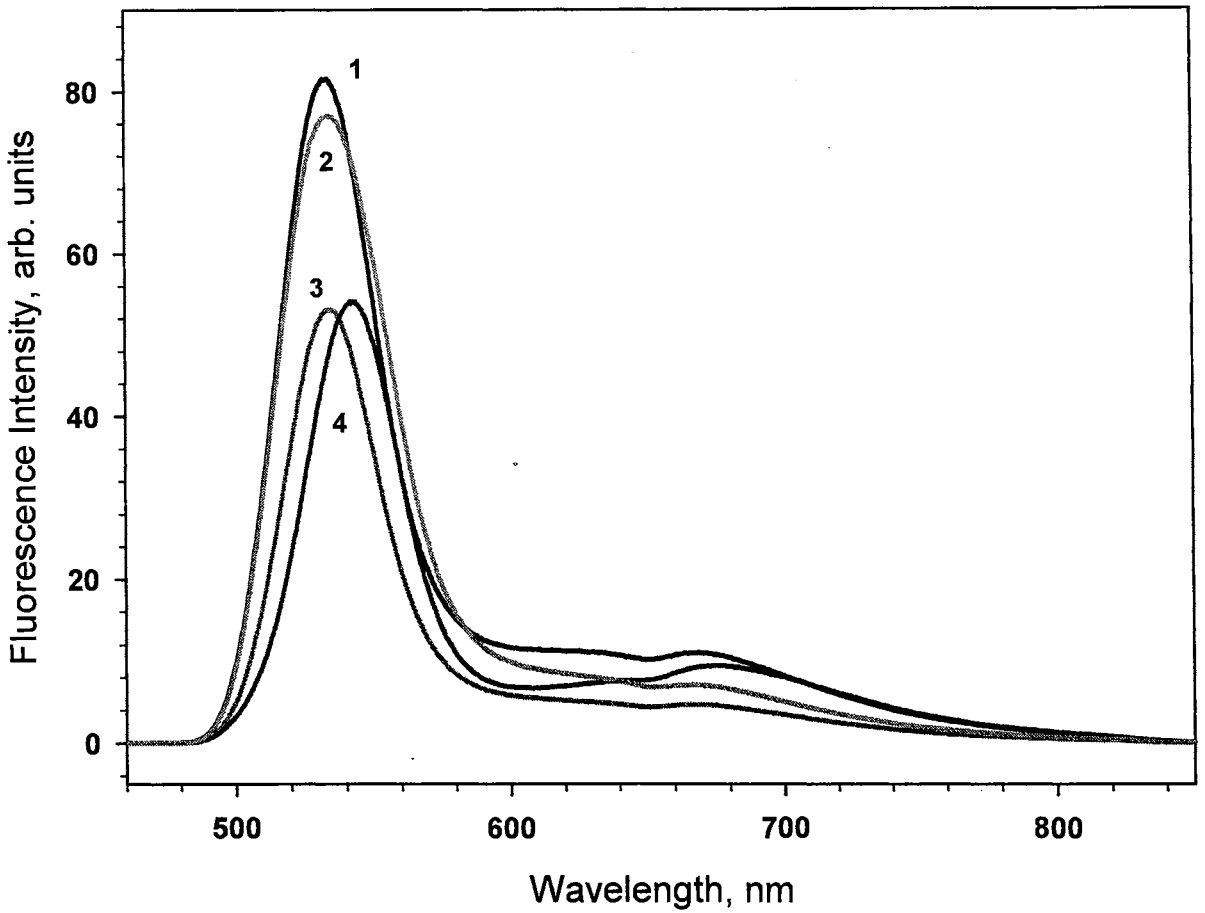

Figure 36. Modification reaction on CdSe NPs with different ratios of RuBP. 1) CdSe NPs, CdSe:RuBP ratios of 2) 1:12, 3) 1:24 and 4) 1:18, respectively

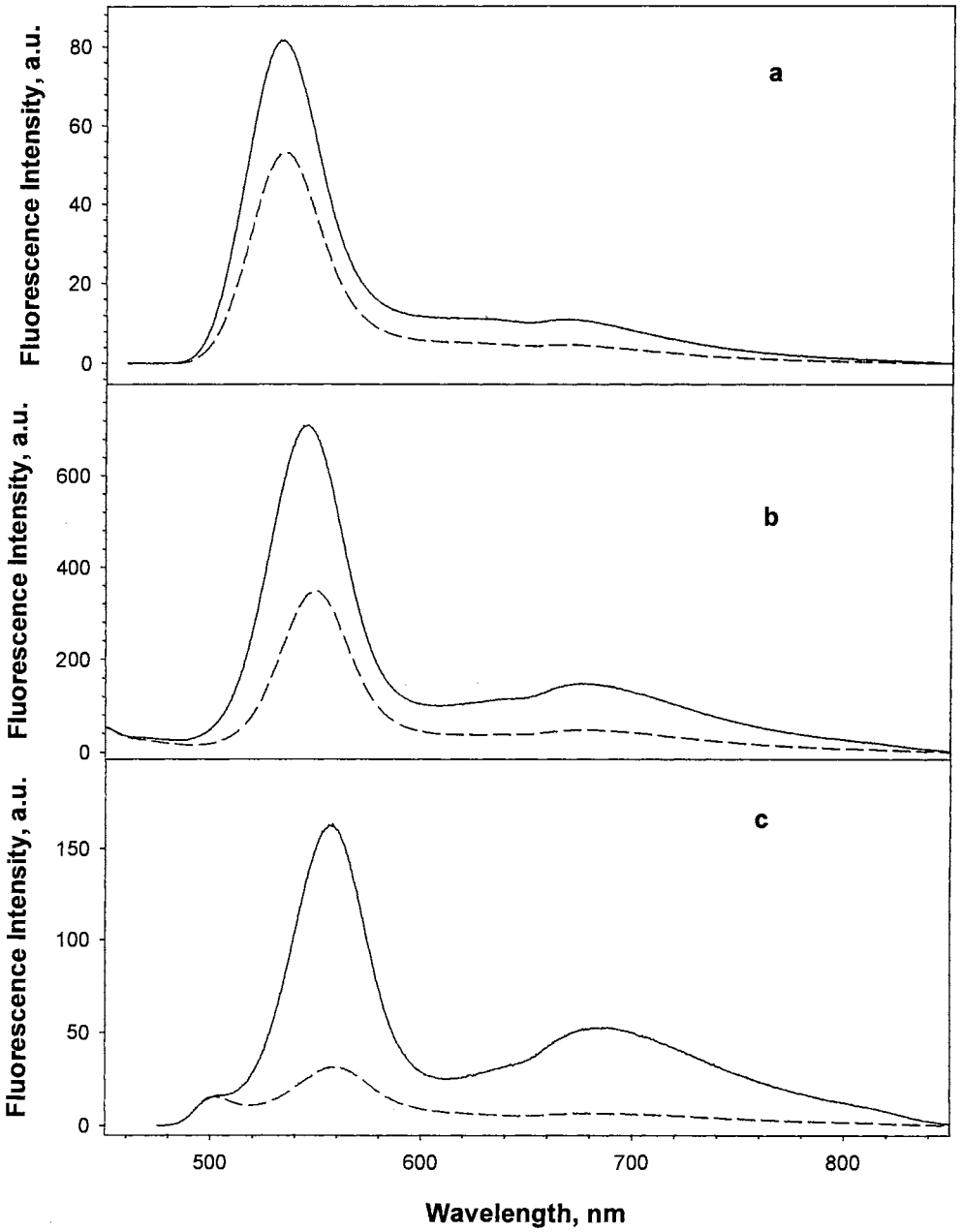

Figure 37. Luminescence spectra of different sized CdSe and RuBP modified CdSe NPs a) CdSe (30:1), (b) CdSe (10:1) and c) CdSe (4:1). (___) before modification and (-----) after modification.

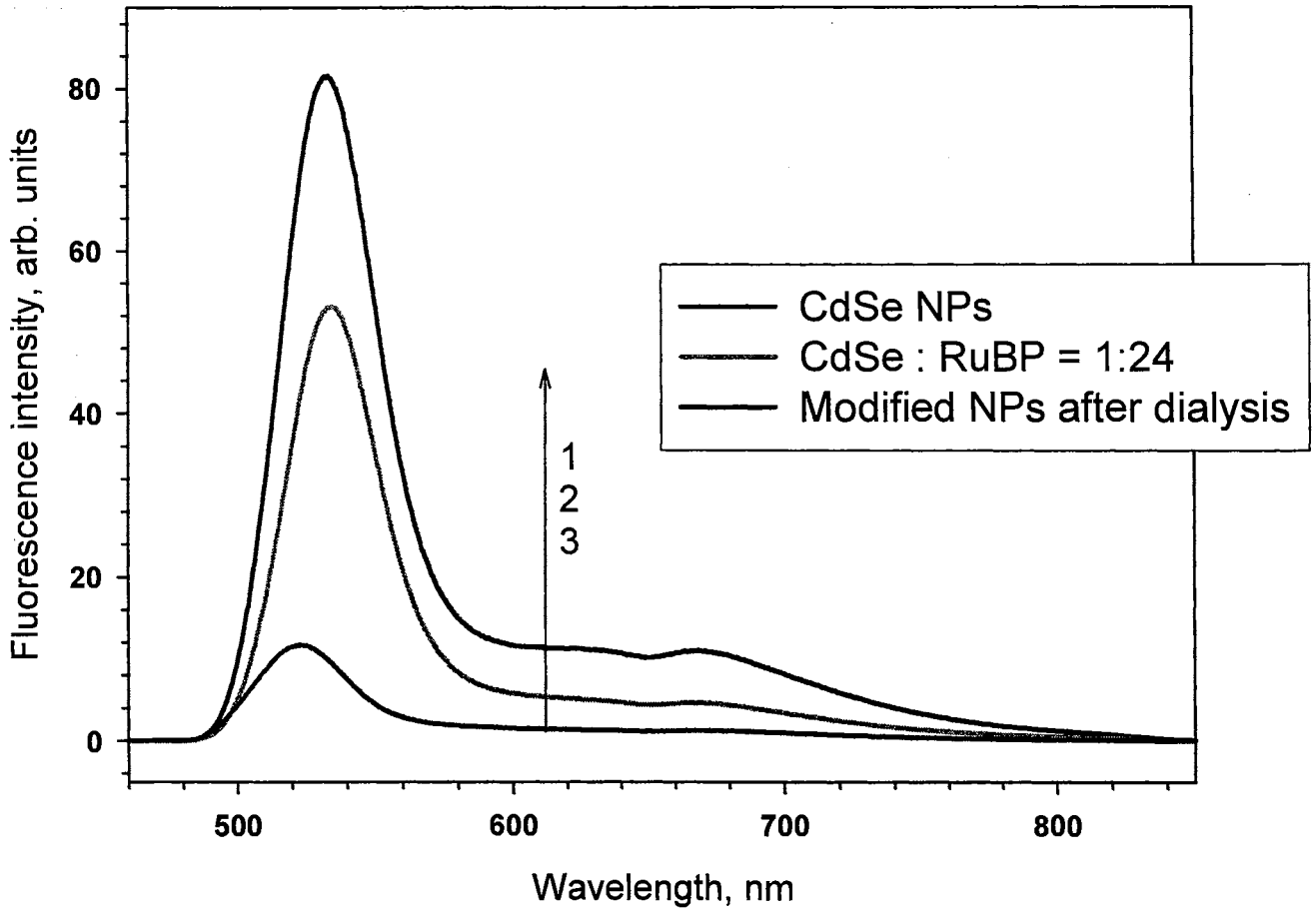

Figure 38. Steady state luminescence of CdSe and RuBP modified NPs : 1) CdSe NPs, 2) after modification and, 3) modified NP after dialysis

trapped emission peaks was seen[55,76]. It can be suggested that during the dialysis, some of the RuBP is partially removed from the surface of CdSe. However, the dialysis and removal of the modifier also result in partial oxidation of the surface of CdSe and hence, luminescence quenching.

C.2.b. Time Resolved Photoluminescence (TRPL):

Time resolved photoluminescence was used to further understand the effects of surface modification on the NPs. The trapped emission results from the recombination of charge carriers trapped in the surface and defects of NPs. The lifetime of these emissions will undergo changes when there is surface modification of some kind. It was observed that the lifetime increased from 54 ns for naked NPs to 67 ns for RuBP modified NPs Table 3, whereas the intensity of emission peak decreased. This observation is unique because it contradicts the accepted scheme of dynamic quenching mechanism for NPs, which result in decrease in both the lifetime and intensity due to nonradiative processes [75]. In some instances, such as static quenching, the lifetime may remain the same for the quenched electronic state being determined by unassociation with quencher molecules, but it never increases [75].

Table 3. Lifetime of CdSe NPs and RuBP modified CdSe NPs

Sample	Life time, ns (540 nm peak)	Life time, ns (670 nm peak)
Unmodified CdSe	2.3	54
CdSe +RuBP 1:6 (m/m)	2.3	53
CdSe + RuBP 1:12 (m/m)	2.1	60
CdSe +RuBP 1:24 (m/m)	1.7	67

The explanation for the effect of lifetime elongation is that there is the formation of new delocalized electronic states involving the NPs and the modifying group. The formation of the new levels is seen in the excitation spectrum of modified NPs, Figure 44. The excitation spectrum registered at 675 nm coincides with the absorption spectrum of the absorption spectrum of the unmodified NPs, repeating all the features Figure 39, trace b. In addition, the new band at 370 nm that was observed in the absorption spectrum (Figure 28) is also seen here. All these observations confirm the formation of new levels due to the delocalization of electronic states of CdSe NPs and RuBP.

As mentioned earlier, the HOMO states of the NPs are made up of the orbitals from chalcogen atoms and the atomic orbital of cadmium contribute to the LUMO states. In the case of the supramolecule formed by the RuBP modification of CdSe NPs, there is more contribution to the LUMO states from the metal center of RuBP. This observation is based on the results from the excitation spectrum in Figure 39 and 40. In the excitation spectrum registered at 675 nm after the attachment of RuBP, the characteristic peak of RuBP at 290 nm is seen. The peaks in Figure 40, trace 4 and 5 are not as distinct as compared to the UV absorption of free RuBP in water Figure 40, trace 1, which is due to the formation of Ru – Se bond. This peak shows that there are indeed some LUMOs, which have contributions from the RuBP complex and the excitation of the supramolecules to these LUMOs result in the trapped emission in the 665-735 nm region. The excitation spectrum also shows that the emissive state can be populated from both the CdSe and RuBP sides. (Figure 40, trace 4 and 5). This can be seen by the presence of

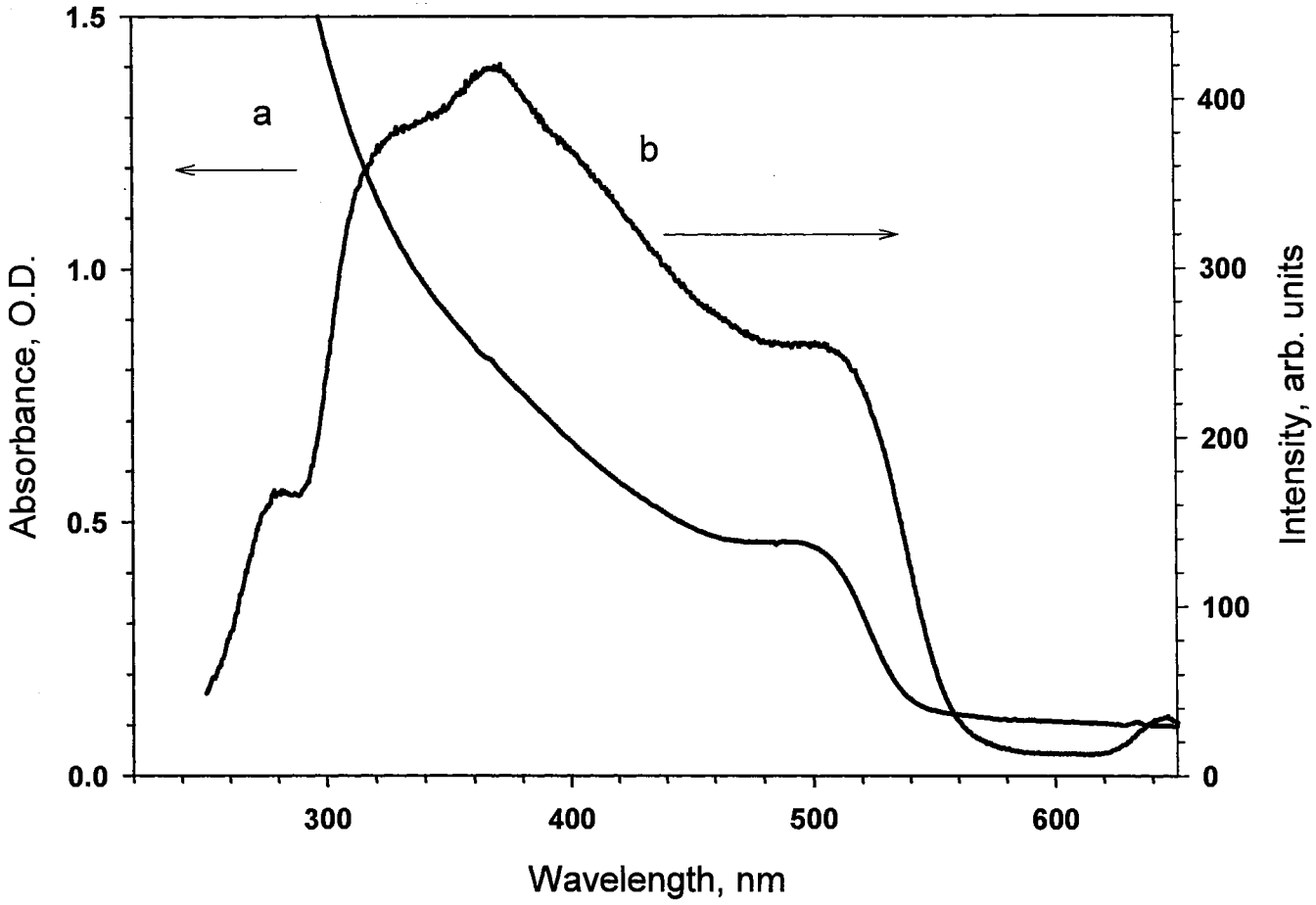

Figure 39. a) Absorption spectrum of unmodified CdSe NPs and b) excitation spectrum of RuBP modified CdSe NPs

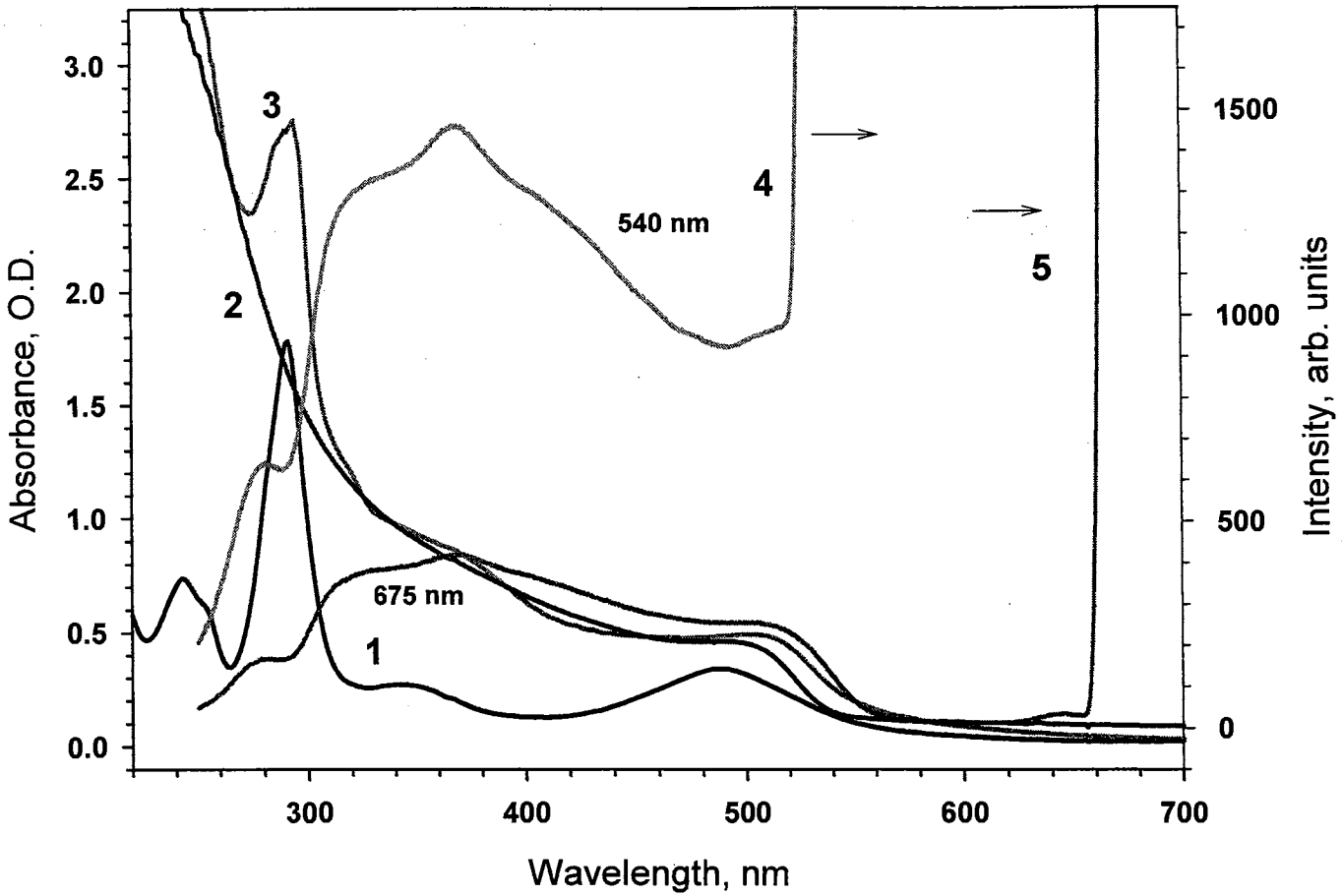

Figure 40. Optical spectrum of NPs. Absorption spectra of 1) RuBP, 2) CdSe and 3) RuBP modified CdSe NPs. Excitation spectra of modified CdSe 4) λ_{em} = 540 nm and 5) λ_{em} = 675 nm

absorption features of both CdSe (absorption edge at 540 nm) and RuBP (peak at 275 nm). The population of these emissive states should be facilitated by the delocalized orbitals.

C.2.c. Molecular modeling studies

Another approach to understand the excitation transfer between the NP and the modifier was through theoretical calculations [96,97]. In spite of good hardware and software available for calculations, all the atoms in the NP cannot be considered for the model. Therefore, as reported earlier, a small cluster model was used to simulate the NP – modifier system.

The model shown in Figure 41-structure a, is only a representation of a small part of the NP surface and consists of four Se atoms and five Cd atoms. The RuBP molecule is attached to the surface of the NP through the Se atoms. Optimized geometry was obtained for this particular model. We initially obtained a semiempirical PM3 optimized geometry. Other models with different arrangements of atoms were tried but the geometry failed to converge.

Upon completion of the calculations, the distributions of electronic states were obtained, as shown in Figure 41-structure b, c. The HOMO levels are situated on the Se atoms. The p-orbitals of Se are coupled to the valence band of the NP core. This results in expansion of the delocalization area for the charge carriers in the valence band. This explains the red shift seen in the UV-vis absorption seen in the case of RuBP modified CdSe NPs (See Figure 28). Even though the HOMO level is concentrated in the CdSe part of the supramolecule, it can be clearly seen that there is a definite contribution from the aromatic bipyridine group of the modifier to these HOMO levels. This is possible

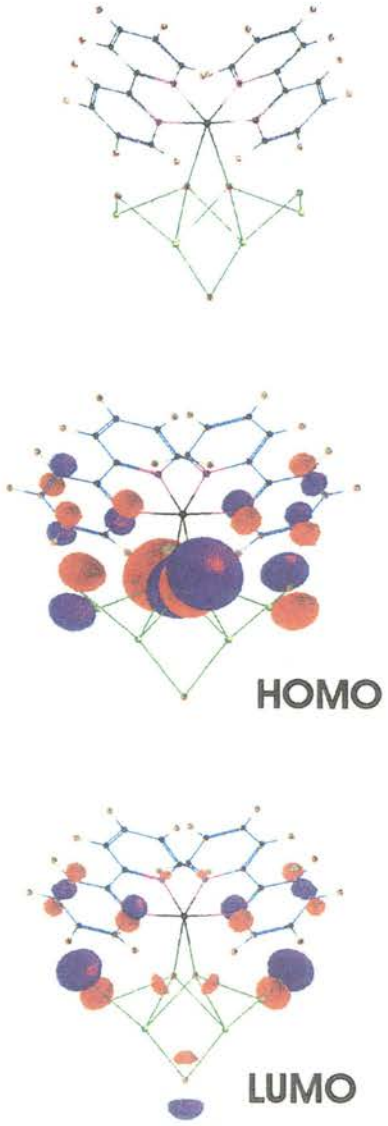

Figure 41. Molecular structure and the orbitals of CdSe – RuBP model cluster computed at PM3 level of theory. Atoms are color coaded as follows: Cd (green with yellow dots), Se (red with green dots), Ru (black), C (blue), H (red with blue dots), and N (pink). The positive and negative regions of the orbitals are depicted as red and blue clouds.

only when there is mixing of the electronic states of NP and the modifier. Similarly, the LUMO levels have contributions from Cd atoms on the surface of the NP and the aromatic bipyridine group of the modifier. From the PM3 molecular modeling studies, it is clear that there is a definite contribution to the HOMO and LUMO levels from both the CdSe and the RuBP molecules. This is made possible by the intermixing of the atomic orbitals in the supramolecule. This relaxation of the orbitals should result in the elongation of lifetime of the trapped exiton and this was confirmed by the time resolved photoluminescence experiments (See above).

Ultraviolet Photoelectron Spectroscopy (UPS)

The signature of the delocalized states is difficult to see in UV-vis absorption, but it can be seen in the UPS spectra of the modified NPs. In the case of CdS NPs modified by CuBM, the UPS experiments clearly demonstrated the reorganization of the electronic states upon modification. There are a lot of similarities in the case of CdSe and CdS system with respect to the surface modification via the chalcogen site, as seen in the UV-vis, TRPL, PM3 molecular modeling studies. The results obtained from the UPS studies on CuBM modified CdS NPs can be used to understand the electronic nature of the modified CdSe NPs. The important characteristics seen for the naked NPs in the UPS spectrum in Figure 42,a, are the strong peak at 12.5 eV and a weak shoulder at 16.5 eV. Upon modification with CuBM there is a formation of a new strong peak at 18 eV and disappearance of the 16.5 eV peak, as seen in Figure 42, b. In addition, the onset of the UPS signal, which represents the top of the valence band of CdS, shifts to a lower binding energy from 9 eV in naked NPs to 8 eV in modified NPs. A similar shift is noticed

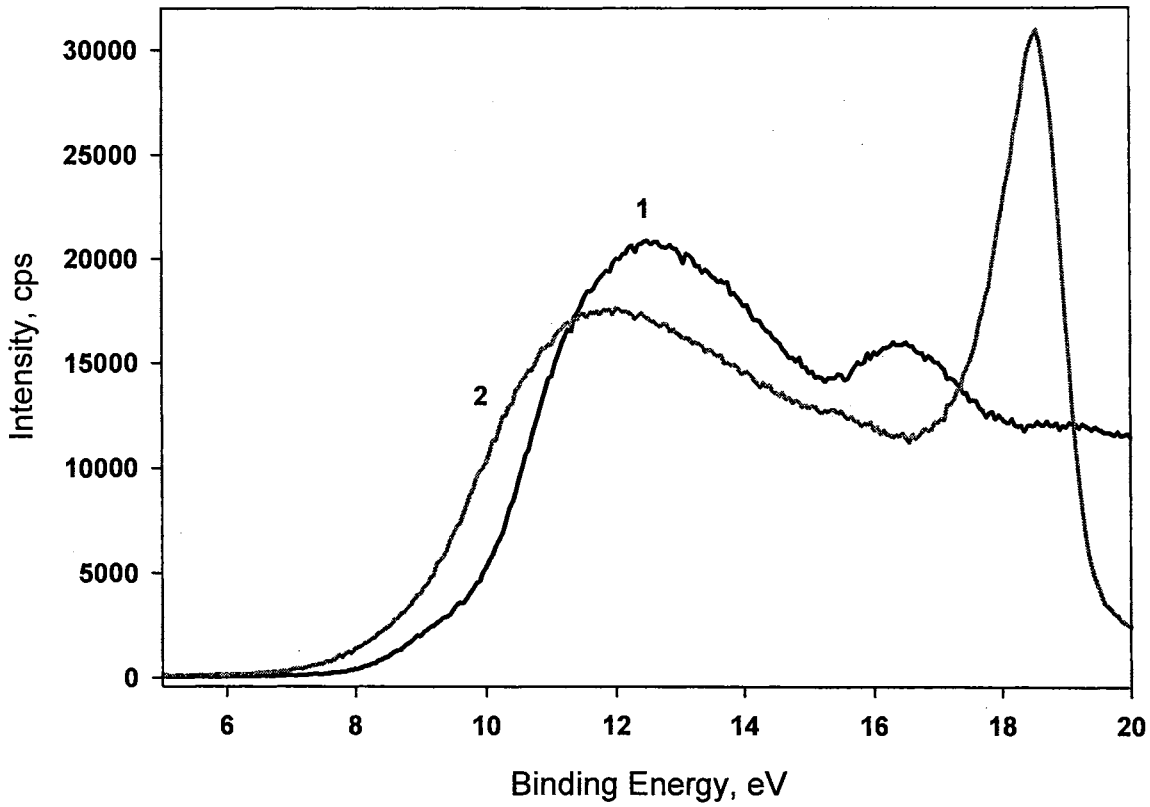

Figure 42. UPS spectra of CdS NPs 1) before and 2) after modification with CuBM

in the UPS peak, from 12.5 eV to 11.5 eV. It is essential to note that there is a very low photoelectron ejection cross section in the case of II-VI semiconductors and typically a signal cannot be seen when excited with a regular He UV light source. For the surface states, synchrotron UPS setups are normally used. The delocalizations involving the aromatic systems of the new surface states should significantly increase the UPS cross-section as compared to the parent states. Hence, the red shift seen in the UPS is attributed to the formation of new electronic states.

It can be concluded from the results of UV-vis absorption, X-ray photoelectron spectroscopy, steady state luminescence, time-resolved photoluminescence and the PM3 molecular modeling studies that upon surface modification, there is formation of new electronic states with contributions from both the NP core and the aromatic group of modifier through the metal atom. This results in the formation of a new supramolecule with delocalized surface states. Such systems would be of great interest for the many applications of the NPs.

D. Results of RuBP modified In_2S_3_citrate NPs

One of the main differences in the surface modification reaction via the chalcogen sites in the case of In_2S_3 NP and previously reported CdS and CdSe NPs, is the increased number of chalcogen atoms on the surface. Since the ratio of chalcogen to atom in the unit cell is greater, the probability of available sites on the surface for modification increases. This, in principle should increase the feasibility of this kind of modification reaction. As discussed in Chapter III, In_2S_3 can accommodate guest atoms in the vacant interstitial sites and improve its magnetic and semiconductor properties. Therefore, this extends of family of NPs available for chalcogen site surface modification reaction and further widens the scope of application for these NPs. Results of the surface modification of In_2S_3 NPs with RuBP are discussed below.

D.1. Structure of modified NPs

D.1.a. Optical absorption spectrum:

In-situ UV-vis absorption was used to monitor the changes in the modification reaction. The NP has a peak at 305 nm and RuBP has characteristic peaks at 290, 350, 490 and 650 nm. The UV-vis absorption spectrum of the modification reaction is shown in Figure 43 and the changes seen are:

* blue shift of the RuBP peak from 490 nm to 450 nm
* complete disappearance of the 650 nm RuBP peak
* shoulder at 320 nm decreases
* blue shift of the RuBP peak from 290 nm to 285 nm

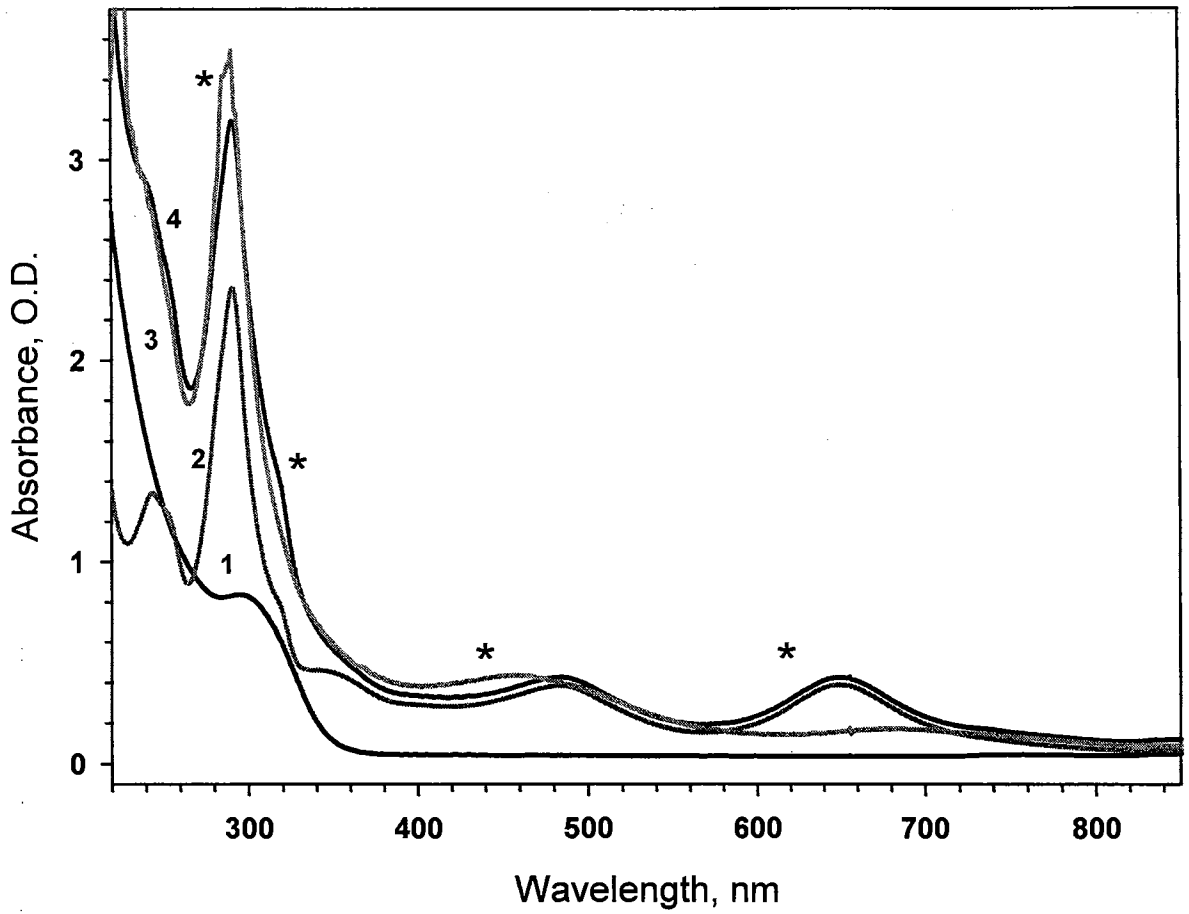

Figure 43. UV-vis absorption spectra of 1)In_2S_3 NPs, 2) RuBP, 3)RuBP modified In_2S_3 NPs and 4) arithmetic sum of In_2S_3 NP and RuBP

Changes to the semiconductor core arising from the modification reaction are not very distinct, due to the overlap of the NP and RuBP peaks. One of the limitations of this reaction was the inability to observe the modification reaction on different sized NPs. The various synthetic conditions for In_2S_3 NP synthesis always resulted in the same sized NP. Hence, the modification reaction could not be followed with respect to the changes in the NP core. The RuBP still underwent significant changes in the UV-vis spectrum, which was used to study the modification reaction.

The effect of Na_2S on the UV-vis spectra of RuBP was studied by mixing a solution of RuBP and Na_2S. This is shown in Figure 44. It is clearly seen that upon addition of Na_2S, the RuBP peak at 240 nm is blue shifted to 220 nm. This peak is not due to the Na_2S peak or a result of mixing to these two solutions but rather due to the formation of new electronic states. In addition, there is no significant change in the position of the 350 nm and 490 nm peak upon mixing with Na_2S. In the case of the modification reaction, these peaks are significantly blue shifted, Figure 43. This could be facilitated by the formation of new electronic states involving the orbitals of In_2S_3 NPs and RuBP.

Different ratio of modifying group and NPs were used to study the modification reaction. The concentration of the NPs was kept constant and the amount of RuBP was changed from 1:0 to 1:48 (m/m). Irrespective of the ratio used for the modification, the same changes in the UV-vis spectrum were observed in all the reactions. These are plotted in Figure 45. The UV-vis spectra were more characteristic for modification reaction in some of the samples as compared to others. One explanation for this is that for a given size of NP, there is a fixed number of chalcogen atoms on the surface. Once these

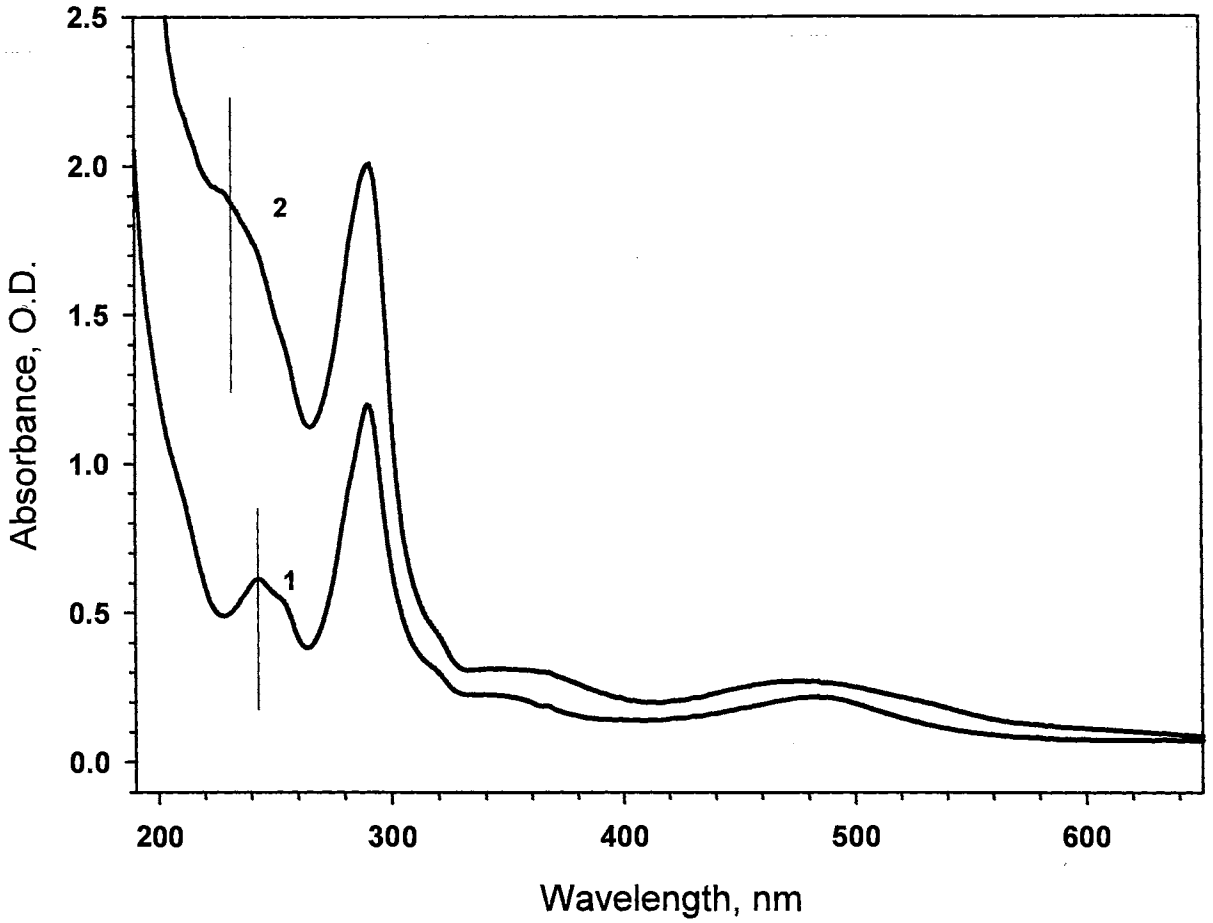

Figure 44. Absorption spectrum of 1) RuBP and 2) mixture of RuBP and Na_2S

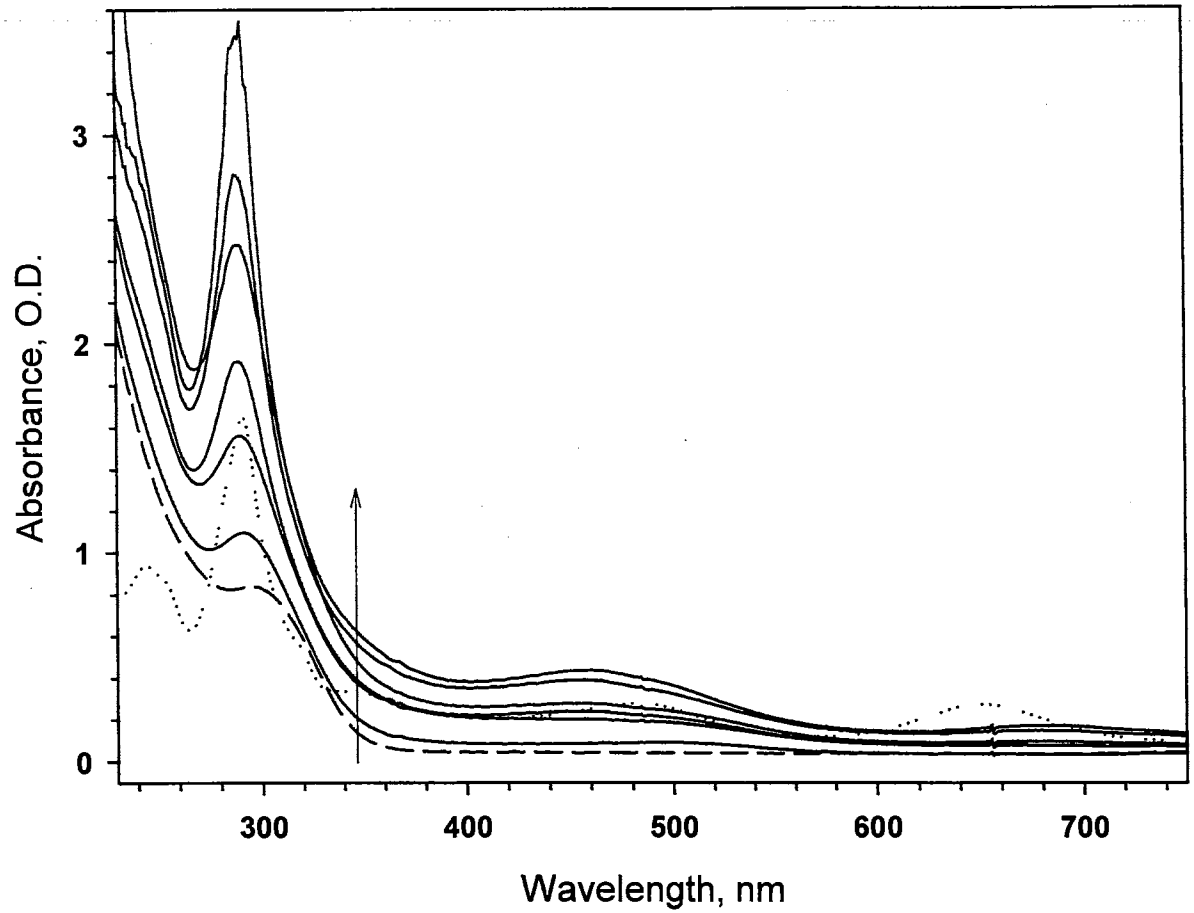

Figure 45. UV-vis absorption spectra of In_2S_3 NP, 60 µl RuBP and modified NPs with different ratios of RuBP. The arrow indicates increase in concentration.

sites are occupied or attached to the RuBP, additional RuBP cannot react with In_2S_3 and therefore will not significantly change the spectrum. In the case of RuBP modified In_2S_3 NPs, this ratio was found to be 1:24 NP: RuBP (m/m).

D.2. Optical properties of modified NPs

The UV-vis absorption measurements clearly demonstrated the effect of modification on the nature of electronic states of the NPs. Blue shift of the peaks associated with RuBP and formation of new peaks, which could be due to the formation of new energy levels. Steady state luminescence and time resolved photoluminescence experiments were used to support these results.

D.2.a. Steady state luminescence

As explained earlier in this chapter, the modification reaction was carried out on the citrate stabilized NPs. The surface of In_2S_3 NPs stabilized by sodium citrate was modified with RuBP. The characteristic features for the In_2S_3 NPs, seen in the steady state luminescence are: a) a very broad excitonic emission band and b) no trapped emission peaks. This is shown in Figure 46. Upon addition of different ratios of RuBP, there is an increase in the intensity of the excitonic emission, as shown in Figure 47. It has been reported in literature that surface modification of NPs helps eliminate some of the defects that are responsible for non-radiative decay and thereby enhancing the excitonic emission [47,36]. This is indeed observed in the case of RuBP modified In_2S_3 NPs. This is very different from the results obtained for similar type of chalcogen site surface modification involving CdS NPs [55,76] and CdSe NPs (see above). In the case of CuBM modified CdS NPs, upon surface modification, there was no change in excitonic emission peak and a strong decrease in the trapped emission bands. For RuBP modified CdSe NPs,

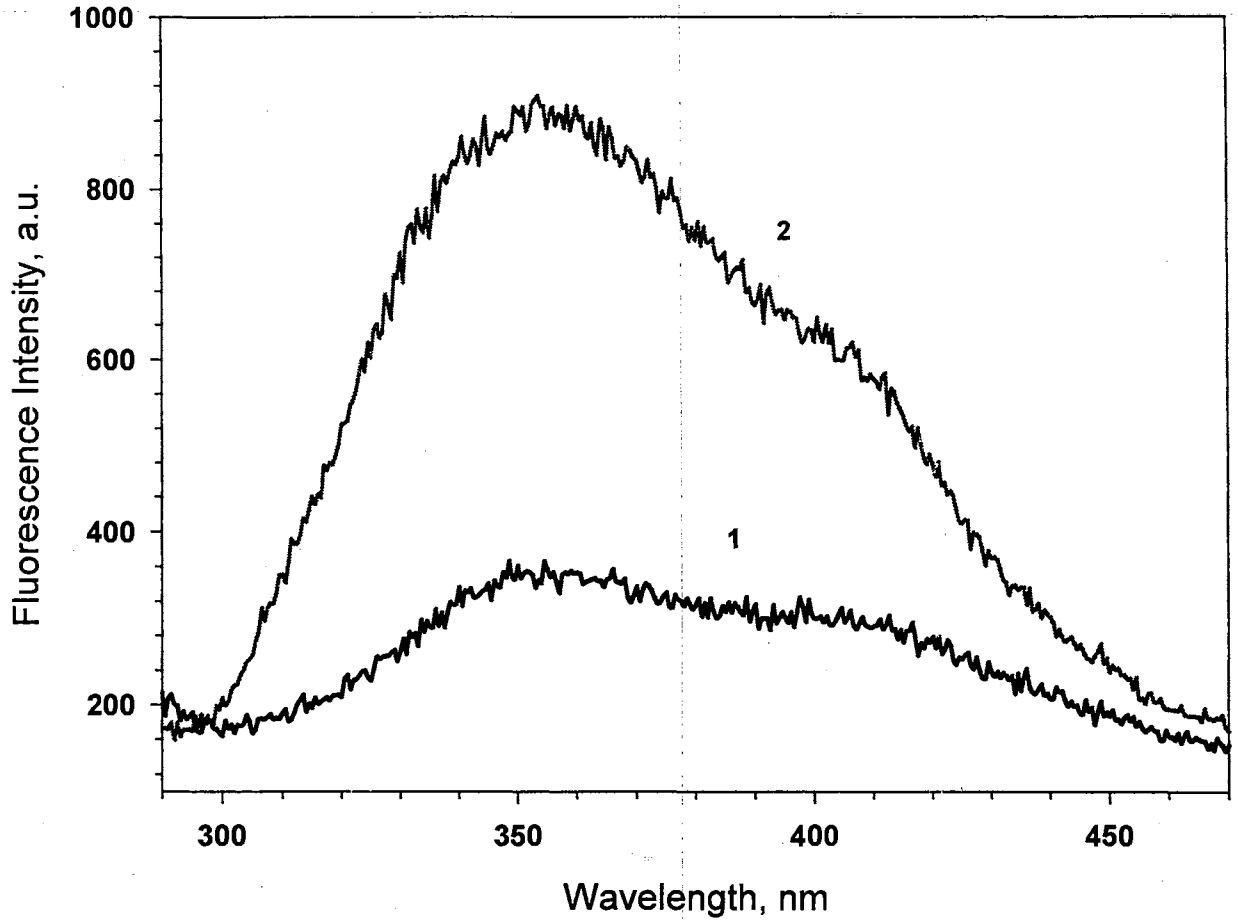

Figure 46. Steady state luminescence of In_2S_3 NPs 1) before modification and 2) after modification with RuBP

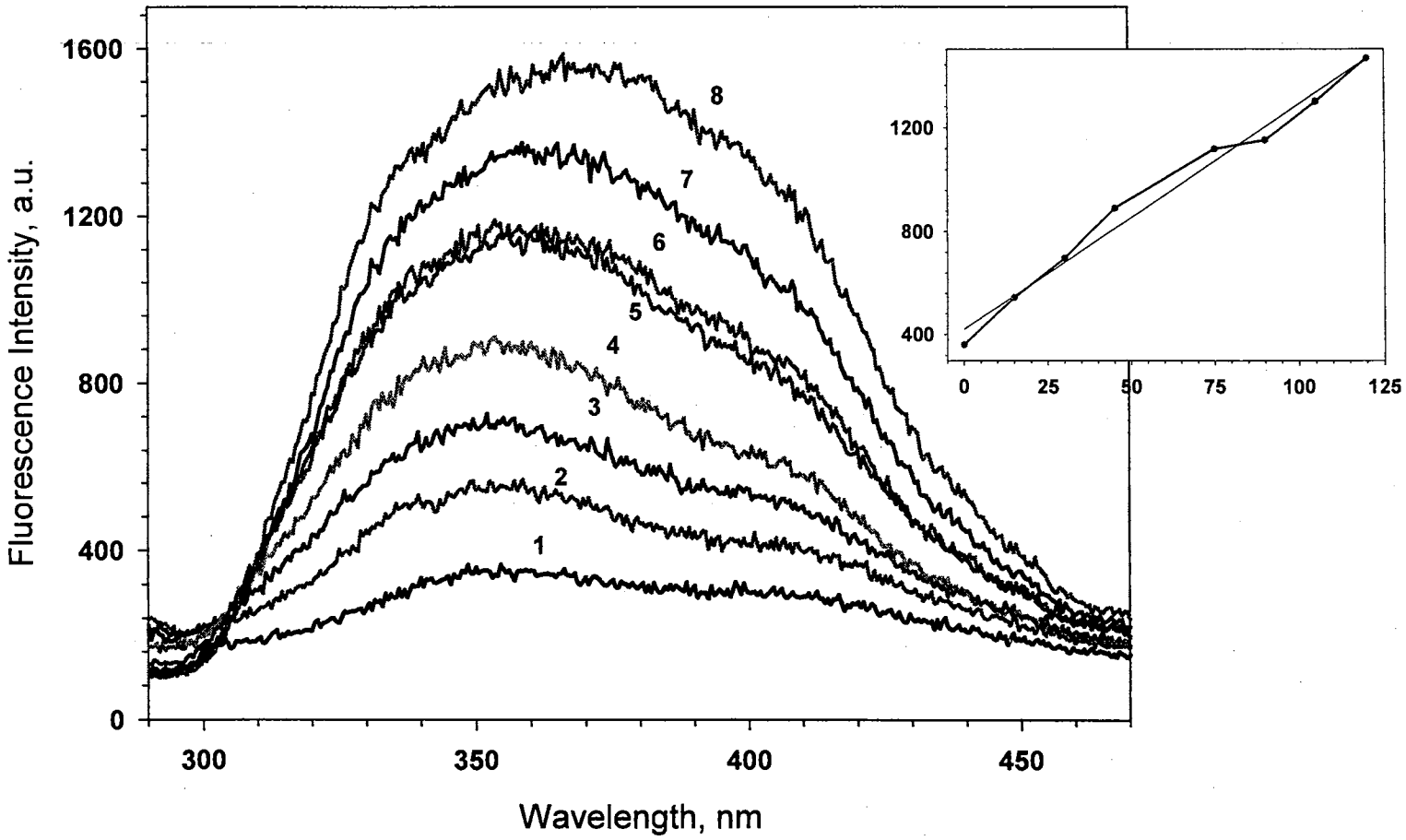

Figure 47. Steady state luminescence of In_2S_3 and In_2S_3 NP modified with different ratios of RuBP 1) In_2S_3 NP, NP:RuBP ratio of 2) 1:6, 3)1:12, 4)1:18, 5)1:24, 6)1:30, 7)1:42 and 8) 1:48, respectively. Inset: Fluorescence intensity *vs* concentration of RuBP, with linear curve fit

there was decrease in both the excitonic and trapped emission peaks. Based on the UV-vis absorption data, the increase in emission could also be due to the formation of new electronic states involving the NPs and the modifier.

D.2.b. Time Resolved Photoluminescence

Time resolved photoluminescence was used to understand the photophysical pathways for the exciton dissipation. The lifetime of emissions should undergo changes when there is surface modification of the NPs. The lifetime increased from 188 ps for naked NPs to 323 ps for (1: 24 m/m) RuBP modified NPs. The lifetime NPs and the different ratios of modifier – NP are in Table 4.

Table 4. Lifetime of In_2S_3 NPs and RuBP modified In_2S_3 NPs

Sample	Life time, ps
Unmodified In_2S_3	188
In_2S_3 +RuBP 1:6 (m/m)	196
In_2S_3 +RuBP 1:12 (m/m)	210
In_2S_3 +RuBP 1:18 (m/m)	244
In_2S_3 +RuBP 1:24 (m/m)	323
In_2S_3 +RuBP 1:30 (m/m)	303
In_2S_3 +RuBP 1:36 (m/m)	308
In_2S_3 +RuBP 1:42 (m/m)	333
In_2S_3 +RuBP 1:48 (m/m)	228

It can be seen that there is a linear increase in the lifetime with increasing concentration of RuBP from 1:0 to 1: 24 (m/m). This is in agreement with the increase in luminescence as seen in Figure 47. There was no observable trend for the ratios 1:30 – 1:48 in contradiction of the results obtained in the luminescence studies. One explanation for this could be the instability of the NPs to the strong laser pulse used in the TRPL measurement.

The excitation spectra of the NPs and modified NPs could be compared to the UV-vis absorption spectra to study the formation of these new electronic states. This was done in the CuBM – CdS [55,76] and RuBP – CdSe NP systems. However, this experiment could not be carried out with the RuBP system. The excitation wavelength selected for the steady state emission was in the 220-260 nm range. This wavelength is not ideal for this NP system because, this wavelength can excite the organic species in the solution and they tend to overlap with the peaks of NPs. Therefore, the excitation spectrum will have contributions from all the species in the solution and resulting in a broad featureless spectrum. This was indeed the case in In_2S_3 NPs and RuBP modified In_2S_3 NP system.

Future directions:

One of the limitations of this modification reaction was the broad size distribution of the citrate stabilized In_2S_3 NPs. It would be desirable to have a narrow size distribution to understand the photophysics of these nanoclusters. Since the peak of RuBP coincides with the absorption edge of the NPs, it would be desirable to follow the modification reaction on a different sized NPs. Larger sized NPs would be desirable as they would require a longer excitation wavelength, where the interference from organic species will

be minimized. This will be useful to study the excitation spectrum of the NPs and modified NPs.

E. Conclusions

Citrate stabilized CdSe and In_2S_3 NPs were synthesized and the surface modification with RuBP, via the E-site, was achieved. The modification resulted in mixing of the energy states of NP and RuBP and lead to the formation of new energy levels. This was observed by changes in the UV-vis absorption, luminescence, excitation spectrum, TRPL and XPS measurements. In the case of CdSe NPs, the important observation was the increase in the lifetime of trapped emission in spite of decrease in peak intensity after modification. This was due to the formation of new delocalized electronic states involving CdSe NPs and RuBP. Surface modification of In_2S_3 NPs led to passivation of the surface resulting in an increase in the excitonic emission peak. This research demonstrated the effect of surface modification on the luminescence properties of newly synthesized In_2S_3 and CdSe nanocolloids. This type of surface modification helps understand the surface of the NPs and opens new pathways to synthesize supramolecules with rich photochemistry.

Conclusions

Stable, water soluble CdSe NPs were synthesized. The unique features of the sodium citrate stabilized NPs were the narrow size distribution and relatively easy method to control the size of the NP formed. In addition, the starting material for the synthesis was cadmium perchlorate, which is less toxic when compared to dimethyl cadmium that is generally used to prepare CdSe NPs. The ability to synthesize these NPs in water opens the way for a variety of new applications for these materials. The CdSe NPs is very useful for core-shell modification reaction due to the lability of the stabilizer.

In_2S_3 NPs were synthesized by the colloidochemical method as stable aqueous dispersions, which had not been attempted so far in literature. These NPs were synthesized as stable dispersions with a variety of stabilizer molecules. The structure and properties of these NPs were very distinct from the previously studied CdSe NPs. Luminescence from semiconductor NPs are reported only in the visible region, but In_2S_3 fluoresce in the UV region and therefore extending the optical window for applications of NP materials. The ability of In_2S_3 to accommodate guest atoms can be used to improve the properties of these NPs.

New approach to the surface modification reactions of semiconductor NPs was attempted. The chalcogen site of the NP on the surface was used to modify the NP by the addition of mixed ligand complexes. Citrate stabilized CdSe and In_2S_3 NPs were modified by Ruthenium bis-bipyridine dichloride complex. The modification reaction resulted in the formation of a supramolecule with new energy levels. The formation of these bands was observed by the changes in the UV-vis absorption, steady state luminescence, excitation spectrum and the time resolved photoluminescence. In the case of CdSe NPs,

upon modification the lifetime of emission for the trapped emission increased with increasing concentration of modifier. This is explained by the formation of new delocalized electronic states involving the orbitals of CdSe NPs and RuBP. In the case of In_2S_3 NPs, modifications of NP lead to the passivation of the surface resulting in increase in the luminescence intensity. Thus, NPs with different surface properties behave differently to the modification reaction. This helps us to understand the surface properties of the NPs. The modification reaction can be used to make new supramolecule complexes with rich photochemistry.

REFERENCE

1) Alivisatos, A. P., Perspectives on the Physical Chemistry of Semiconductor Nanocrystals, *J.Phys.Chem.* **1996**, 100, 13226-13239

2) Alivisatos, A. P. *Science (Washington, D.C.)* **1996**, 271, 933-937.

3) Y.Wang and N.Herron. Nanometer-Sized Semiconductor Clusters: Materials Synthesis, Quantum Size Effects, and Photophysical Properties. *J.Phys.Chem.*, **1991**, 95, 525-532.

4) Eychmueller, A., Structure and Photophysics of Semiconductor Nanocrystals, *J.Phys.Chem.B,* **2000**, 104, 6514-6528.

5) Tito Trindade, Paul O'Brien, and Nigel L.Pickett. Nanocrystalline Semiconductors: Synthesis, Properties, and Perspectives, *Chem.Mater.*, **2001**, 3, 3848-3858.

6) Vossmeyer, T.; Katsikas, L.; Giersig, M.; Popovic, I. G.; Diesner, K.; Chemseddine, A.; Eychmueller, A.; Weller, H., CdS Nanoclusters: Synthesis, Characterization, Size Dependent Oscillator Strength, Temperature Shift of the Excitonic Transition Energy, and Reversible Absorbance Shift, *J.Phys.Chem*, **1994**, 98, 7665-7673.

7) Henglein, A., Small-particle research: physicochemical properties of extremely small colloidal metal and semiconductor particles, *Chem.*Rev, **1989**, 89, 1861-1873.

8) a) Dinega, D. P.; Bawendi, M. G., A Solution-Phase Chemical Approach to a New Crystal Structure of Cobalt, *Angew.Chem., Int.Ed.*, **1999**, 38, 1788-1791.

b) Pileni, M. P.; Ninham, B. W.; Gulik-Krzywicki, T.; Tanori, J.; Lisiecki, I.; Filankembo, A., Direct Relationship Between Shape and Size of Template and Synthesis of Copper Metal particles, *Adv.Mater.(Weinheim, Ger.)*, **1999**, 11, 1358-1362.

c) Petit, C.; Cren, T.; Roditchev, D.; Sacks, W.; Klein, J.; Pileni, M. P., Single Electron Tunneling Through Nano-Sized Cobalt Particles, *Adv.Mater.(Weinheim, Ger.)* **1999**, 11, 1198-1202.

d) Henglein, A.; Giersig, M., Formation of Colloidal Silver Nanoparticles: Capping Action of Citrate, *J.Phys.Chem.B*, **1999**, *103*, 9533-9539.

e) Henglein, A., Chemisorption Effects on Colloidal Lead Nanoparticles, *J.Phys.Chem.B*, **1999**, 103, 9302-9305.

9) a) Madhusudan Reddy, K.; Gopal Reddy, C. V.; Manorama, S. V., Preparation, Characterization, and Spectral Studies on Nanocrystalline Anatase TiO_2, *Journal of Solid State Chemistry*, **2001**, 158(2), 180-186.

b) Koktysh, Dmitry S.; Liang, Xiaorong; Yun, Bo-Geon; Pastoriza-Santos, Isabel; Matts, Robert L.; Giersig, Michael; Serra-Rodriguez, Carmen; Liz-Marzan, Luis M.; Kotov, Nicholas A., Biomaterials by design: Layer-by-layer assembled ion-selective and biocompatible films of TiO_2 nanoshells for neurochemical monitoring, *Advanced Functional Materials*, **2002**, 12(4), 255-265.

10) a) Leroux, Jean Christophe; Allemann, Eric; Doelker, Eric; Gurny, Robert, New approach for the preparation of nanoparticles by an emulsification-diffusion method, *Eur. J. Pharm. Biopharm.*, **1995**, 41(1), 14-18.

b) Nakache, Evelyne; Poulain, Nathalie; Candau, Francoise; Orecchioni, Anne-Marie; Irache, Juan Manuel, Biopolymer and polymer nanoparticles and their biomedical applications, Editor(s): Nalwa, Hari Singh, *Handbook of Nanostructured Materials and Nanotechnology*, **2000**, 5, 577-635.

11) a) Mamedova, Nataliya N.; Kotov, Nicholas A.; Rogach, Andrey L.; Studer, Joe, Albumin-CdTe Nanoparticle Bioconjugates: Preparation, Structure, and Interunit Energy Transfer with Antenna Effect, *Nano Letters*, **2001**, 1(6), 281-286.

b) Goldman, Ellen R.; Mattoussi, Hedi; Tran, Phan T.; Anderson, George P.; Mauro, J. Matthew, Bioconjugates of luminescent CdSe-ZnS quantum dots with engineered recombinant proteins: novel self-assembled tools for biosensing, *Materials Research Society Symposium Proceedings*, **2001**, 642(Semiconductor Quantum Dots II), J2.8/1-J2.8/6.

c) Sondi, Ivan; Siiman, Olavi; Koester, Steven; Matijevic, Egon, Preparation of aminodextran-CdS nanoparticle complexes and biologically active antibody-aminodextran-CdS nanoparticle conjugates, *Langmuir,* **2000**, 16(7), 3107-3118.

12) a) Jung, T.; Kamm, W.; Breitenbach, A.; Kaiserling, E.; Xiao, J. X.; Kissel, T., Biodegradable nanoparticles for oral delivery of peptides: is there a role for polymers to affect mucosal uptake?, *European Journal of Pharmaceutics and Biopharmaceutics*, **2000**, 50(1), 147-160.

b) Mattoussi, Hedi; Mauro, J. Matthew; Goldman, Ellen R.; Anderson, George P.; Sundar, Vikram C.; Mikulec, Frederic V.; Bawendi, Moungi G., Self-Assembly of CdSe-ZnS Quantum Dot Bioconjugates Using an Engineered Recombinant Protein, *J. Am. Chem. Soc.*, **2000**, 122(49), 12142-12150.

c) Tran, Phan T.; Goldman, Ellen R.; Mattoussi, Hedi; Anderson, George P.; Mauro, J. Matthew, Bioconjugates of luminescent CdSe-ZnS quantum dots with an engineered two-domain protein G for use in fluoroimmunoassays, *Proceedings of SPIE-The International Society for Optical Engineering,* **2001**, 4258(Nanoparticles and Nanostructured Surfaces: Novel Reporters with Biological Applications), 1-7.

d) Alivisatos, A. P.; Johnsson, K. P.; Peng, X.; Wilson, T. E.; Loweth, C. J.; Bruchez, M. P., Jr.; Schultz, P. G. *Nature (London)*, **1996**, 382, 609-611.

13) Murray, C. B.; Norris, D. J.; Bawendi, M. G., Synthesis and characterization of nearly monodisperse CdE (E = sulfur, selenium, tellurium) semiconductor nanocrystallites, *J.Am.Chem.Soc.*, **1993**, 115, 8706-8715

14) Andrey L.Rogach, Dattatri K.Nagesha, John W.Ostrander, Michael Giersig, and Nicholas A.Kotov, Raisan Bun-Type composite Spheres of Silica and Semiconductor Nanocrystals, *Chem.Mater.*, **2000**, 12(9), 2676-2685.

15) Dattatri K.Nagesha, Xiaorong Liang, Arif A.Mamedov, Gordan Gainer, Margaret A.Eastman, Michael Giersig, Jin-Joo Song, Tong Ni, and Nicholas A.Kotov, In_2S_3 Nanocolloids with Excitonic Emission: In_2S_3 vs CdS Comparative Study of Optical and Structural Characteristics, *J.Phys.Chem.B*, **2001**, 105(31), 7490-7498.

16) Rogach, A. L.; Katsikas, L.; Kornowski, A.; Su, D.; Eychmueller, A.; Weller, H. *Ber.Bunsen-Ges.* **1996**, *100*, 1772-1778.

17) Nedeljkovic, J. M., Nenadovic, M. T., Micic, O. I., and Nozik, A. J., Enhanced photoredox chemistry in quantized semiconductor colloids, *J.Phys.Chem.*, **1986**, 90, 12.

18) Kumar, K. N. P., Keizer, K., Burggraaf, A. J., Okubo, T., Nagamoto, H., and Morooka, S. Nature (London) 358, 48. 1992.

19) Sbervegliere, G., Depero, L. E., Ferroni, M., Guildi, V., Martinelli, G., Nelli, P., Perego, C., and Sangaletti, L. Adv.Mater.(Weinheim, Ger.) 28, 1416. 1989.

20) a) Marcel Bruchez Jr., Mario Moronne, Peter Gin, Shimon Weiss, and A.Paul Alivisatos, Semiconductor Nanocrystals as Fluorescent Biological Labels. *Science*

(Washington, D.C.), **1998**, 281, 2013-2016.
b) Warren C.W.Chan and Shuming Nie, Quantum Dot Bioconjugates for Ultrasensitive Nonisotopic Detection, *Science (Washington, D.C.)*, **1998**, 281, 2016-2018.
c) Santra, Swadeshmukul; Zhang, Peng; Wang, Kemin; Tapec, Rovelyn; Tan, Weihong, Conjugation of Biomolecules with Luminophore-Doped Silica Nanoparticles for Photostable Biomarkers, *Analytical Chemistry*, **2001**, 73(20), 4988-4993.

21) a) Maraveyas, A.; Myers, M.; Stafford, N.; Rowlinson-Busza, G.; Stewart, J. S.; Epenetos, A. A., Radiolabeled antibody combined with external radiotherapy for the treatment of head and neck cancer: reconstruction of a theoretical phantom of the larynx for radiation dose calculation to local tissues, *Cancer Res.*, **1995**,55(5), 1020-1027
b) Hughes, O.D.; Bishop, M. C.; Perkins, A. C.; Wastie, M. L.; Denton, G.; Price, M. R.; Frier, M.; Denley, H.; Rutherford, R.; Schubiger, P. A.,Targeting superficial bladder cancer by the intravesical administration of copper-67-labeled anti-MUC1 mucin monoclonal antibody C595, *Journal of Clinical Oncology*, **2000**, 18(2), 363-370.
c) van Hof, Arjan C.; Molthoff, Carla F. M.; Davies, Quentin; Perkins, Alan C.; Verheijen, Rene H. M.; Kenemans, Peter; den Hollander, Wim; Wilhelm, Abraham J.; Baker, Terry S., Biodistribution of 111Indium-labeled engineered human antibody CTMO1 in ovarian cancer patients: influence of protein dose, *Cancer Res.*, **1996**, 56(22), 5179-5185.
d) Plut, Edward M.; Hinkle, George H., 111In-capromab pendetide: The evolution of prostate specific membrane antigen and the nuclear imaging of its 111In-labelled murine antibody in the evaluation of prostate cancer, *BioDrugs*, **2000**, 13(6), 437-447.
e) Hassfjell, Sindre; Brechbiel, Martin W., The Development of the α-Particle Emitting Radionuclides 212Bi and 213Bi, and Their Decay Chain Related Radionuclides, for Therapeutic Applications, *Chemical Reviews*, **2001**, 101(7), 2019-2036.
f) Whitlock, Jenny L.; Roeske, John C.; Dietz, Mark L.; Straus, Chris M.; Hines, John J.; Horwitz, E. Philip; Reba, Richard C.; Rotmensch, Jacob., Radionuclide Therapy for the Treatment of Microscopic Ovarian Carcinoma: An Overview., *Industrial & Engineering Chemistry Research*, **2000**, 39(9), 3135-3139

g) Geldof, Albert A.; De Rooij, Laurens; Versteegh, Richard T.; Newling, Donald W. W.; Teule, Gerrit J. J., Combination 186Re-HEDP and cisplatin supra-additive treatment effects in prostate cancer cells, *Journal of Nuclear Medicine*, **1999**, 40(4), 667-671.
h) Anderson, Peter M.; Wiseman, Gregory A.; Dispenzieri, Angela; Arndt, Carola A. S.; Hartmann, Lynn C.; Smithson, William A.; Mullan, Brian P.; Bruland, Oyvind S., 1) High-dose samarium-153 ethylene diamine tetramethylene phosphonate: Low toxicity of skeletal irradiation in patients with osteosarcoma and bone metastases, *Journal of Clinical Oncology*, **2002**, 20(1), 189-196.
i) Foss, Francine M.; Raubitscheck, Andrew; Mulshine, James L.; Fleisher, Thomas A.; Reynolds, James C.; Paik, Chang H.; Neumann, Ronald D.; Boland, Cynthia; Perentesis, Patricia; Brown, Margaret R.; Frincke, James M.; Lollo, Charles P.; Larson, Steven M.; Carrasquillo, Jorge A, Phase I study of the pharmacokinetics of a radioimmunoconjugate, 90Y-T101, in patients with CD5-expressing leukemia and lymphoma, *Clinical Cancer Research*, **1998**, 4(11), 2691-2700.
22) a) Zhang, Ming; Bando, Y.; Wada, K., Sol-gel template preparation of TiO_2 nanotubes and nanorods, *J. Mater.Sci. Lett.*, **2001**, 20(2), 167-170.
b) Dong, Wenting; Zhu, Congshan, Use of ethylene oxide in the sol-gel synthesis of α-Fe_2O_3 nanoparticles from Fe(III) salts, *J.Mater.Chem.*, **2002**, 12(6), 1676-1683.
23) Sooklal, K., Cullum, B. S., Angel, S. M., and Murphy, C. J., Photophysical Properties of ZnS Nanoclusters with Spatially Localized Mn^{2+}, *J.Phys.Chem.*, **1996**, 100, 4551.
24) a) Hakimi, F.; Bawendi, M. G.; Tumminelli, R.; Haavisto, J. R., *US Patent* 5, 260, 957, **1993**.
b) Klimov, V.I.; Mikhailovski, A. A.; Xu, Su; Hollingsworth, J. A.; Leatherdale, C. A.; Eisler, H.-J.; Bawendi, M. G.; Optical gain and stimulated emission in nanocrystal quantum dots, *Science*, **2000**, 290(5490), 314-317
c) Klimov, V. I., Mikhailovski, A. A., McBranch, D. W., Leatherdale, C. A., and Bawendi, M. G., Mechanism for interband energy relaxation in semiconductor quantum dots: The role of electron-hole interactions, *Phys.Rev.B*, **2000**, 61, R13349.
d) Klimov, V. I., Schwarz, Ch. J.; McBranch, D. W.; Leatherdale, C. A.; Bawendi, M. G.; Ultrafast dynamics of inter- and intraband transitions in semiconductor nanocrystals: Implications for quantum-dot lasers. *Phys. Rev. B.*, **1999**, 60(4), R2177-R2180.

25) Borgarello, E., Kiwi, J., Pelizzetti, E., Visca, M., and Graetzel, M., *Nature (London)*, **1981**, 289, 158.

26) O'Regan, B., Moser, J., Anderson, M., and Graetzel, M., Vectorial electron injection into transparent semiconductor membranes and electric field effects on the dynamics of light-induced charge separation, *J.Phys.Chem.*, **1990**, 94, 8720

27) a)Vogel, R., Hoyer, P., and Weller, H., Quantum-Sized PbS, CdS, Ag_2S, Sb_2S_3, and Bi_2S_3 Particles as Sensitizers for Various Nanoporous Wide-Bandgap Semiconductors, *J.Phys.Chem.*, **1994**, 98, 3183.

b) Ginley, D. S.; Curtis, C. J.; Ribelin, R.; Alleman, J. L.; Mason, A.; Jones, K. M.; Matson, R. J.; Khaselev, O.; Schulz, D. L., Nanoparticle precursors for electronic materials, *Materials Research Society Symposium Proceedings*, **1999**, 536 (Micro-crystalline and Nanocrystalline Semiconductors--1998), 237-244.

28) Petit, C.; Pileni, M. P., Synthesis of cadmium sulfide in situ in reverse micelles and in hydrocarbon gels, *J.Phys.Chem.* **1988**, 92, 2282-2286.

29) P.Llanos and J.K.Thomas., Cadmium Sulfide of Small Dimensions Produced in Inverted Micelles, *Chem.Phys.Lett.*, **1986**, 125(3), 299-302.

30) Spanhel, L.; Haase, M.; Weller, H.; Henglein, A., Photochemistry of colloidal semiconductors. 20. Surface modification and stability of strong luminescing CdS particles, *J.Am.Chem.Soc.*, **1987**, 109, 5649-5655.

31) Arcoleo, V.; Goffredi, M.; Liveri, V. T. *J.Therm.Anal.Calorim.*, **1998**, 51, 125-133.

32) Gutierrez, M.; Henglein, A. *Ultrasonics* **1989**, *27*, 259-261.

33) a) Zhu, J.; Koltypin, Y.; Gedanken, A., General Sonochemical Method for the Preparation of Nanophasic Selenides: Synthesis of ZnSe Nanoparticles, *Chem.Mater.*, **2000**, 12 , 73-78.

b) Malik, M. Azad; O'Brien, Paul; Revaprasadu, Neerish, A Simple Route to the Synthesis of Core/Shell Nanoparticles of Chalcogenides, *Chem. Mater.*, **2002**, 14(5), 2004-2010.

c) Talapin, Dmitri V.; Shevchenko, Elena V.; Kornowski, Andreas; Gaponik, Nikolai; Haase, Markus; Rogach, Andrey L.; Weller, Horst, A new approach to crystallization of CdSe nanoparticles into ordered three-dimensional superlattices, *Adv. Mater.* (Weinheim, Germany), **2001**, 13(24), 1868-1871.

d) Haubold, Stephan; Haase, Markus; Kornowski, Andreas; Weller, Horst, Strongly luminescent InP/ZnS core - shell nanoparticles, *Chem. Phys. Chem.*, **2001**, 2(5), 331-334.
34) Chandler, R. R.; Coffer, J. L., Stabilizer-mediated photoluminescence quenching in quantum-confined cadmium sulfide clusters, *J.Phys.Chem.*, **1993**, 97, 9767-9770.
35) Rajh, T.; Micic, O. I.; Nozik, A. J., Synthesis and characterization of surface-modified colloidal cadmium telluride quantum dots, *J.Phys.Chem.*, **1993**, 97, 11999-12003.
36) Hines, M. A.; Guyot-Sionnest, P., Synthesis and Characterization of Strongly Luminescing ZnS-Capped CdSe Nanocrystals, *J.Phys.Chem.*, **1996**, 100, 468-471.
37) Wang, Y.; Herron, N., Photoluminescence and relaxation dynamics of cadmium sulfide superclusters in zeolites, *J.Phys.Chem.*, **1988**, 92, 4988-4994.
38) Wang, Y.; Herron, N., Optical properties of cadmium sulfide and lead (II) sulfide clusters encapsulated in zeolites, *J.Phys.Chem.*, **1987**, 91, 257-260.
39) Cassagneau, Thierry, Hix, G. B., Jones, D. J., Maireles-Torres, P., Rhomari, M., and Roziere, J. J., *J.Mater.Chem.*, **1994**, 4, 189.
40) Brenchley, M. E. and Weller, M. T., *Angew.Chem., Int.Ed.*, **1993**, 32, 1663.
41) Watzke, H. J. and Fendler, Janos H., Quantum size effects of in situ generated colloidal cadmium sulfide particles in dioctadecyldimethylammonium chloride surfactant vesicles, *J.Phys.Chem.*, **1987**, 91, 854.
42) Choi, K. M. and Shea, K. J., Amorphous Polysilsesquioxanes as a Confinement Matrix for Quantum-Sized Particle Growth. Size Analysis and Quantum Size Effect of CdS Particles Grown in Porous Polysilsesquioxanes, *J.Phys.Chem.*, **1994**, 98, 3207.
43) Nirmal, M.; Murray, C. B.; Bawendi, M. G., Fluorescence-line narrowing in CdSe quantum dots: Surface localization of the photogenerated exciton, *Phys.Rev.B: Condens.Matter*, **1994**, 50, 2293-2300.
44) Shinojima, H., Yumoto, J., Uesugi, N., Omi, S., and Asahara, Y., Microcrystallite size dependence of absorption and photoluminescence spectra in CdS_xSe_{1-x}-doped glass, *Appl.Phys.Lett.*, **1989**, 55, 1519.
45) Fischer, C. H.; Lilie, J.; Weller, H.; Katsikas, L.; Henglein, A. *Ber.Bunsen-Ges.Phys.Chem.* **1989**, 93, 61-64.
46) Eychmueller, A.; Katsikas, L.; Weller, H., Photochemistry of semiconductor colloids.

35. Size separation of colloidal cadmium sulfide by gel electrophoresis, *Langmuir*, **1990**, 6, 1605-1608.

47) Dmitri V.Talapin, Andrey L.Rogach, Andreas Kornowski, Markus Haase, and Horst Weller, Highly Luminescent Monodisperse CdSe and CdSe/ZnS Nanocrystals Synthesized in a Hexadecylamine-Trioctylphosphine Oxide-Trioctylphosphine Mixture, *Nanoletters*, **2001**, 1(4), 207-211.

48) a) Katari, J. E. B.; Colvin, V. L.; Alivisatos, A. P., X-ray Photoelectron Spectroscopy of CdSe Nanocrystals with Applications to Studies of the Nanocrystal Surface, *J.Phys.Chem.*, **1994**, 98, 4109-4117.

b) Kulkarni, S. K.; Winkler, U.; Deshmukh, N.; Borse, P. H.; Fink, R.; Umbach, E., Investigations on chemically capped CdS, ZnS and ZnCdS nanoparticles, *Applied Surface Science*, **2001**, 169-170, 438-446.

c) Winkler, U.; Eich, D.; Chen, Z. H.; Fink, R.; Kulkarni, S. K.; Umbach, E., Detailed investigation of CdS nanoparticle surfaces by high-resolution photoelectron spectroscopy, *Chem. Phy. Lett.*, **1999**, 306(1,2), 95-102.

49) Sachleben, J. R.; Wooten, E. W.; Emsley, L.; Pines, A.; Colvin, V. L.; Alivisatos, A. P., NMR studies of the surface structure and dynamics of semiconductor nanocrystals, *Chem.Phys.Lett.*, **1992**, 198, 431-436.

50) a) Ladizhansky, V.; Hodes, G.; Vega, S., Surface Properties of Precipitated CdS Nanoparticles Studied by NMR, *J.Phys.Chem.B*, **1998**, 102, 8505-8509.

b) Ladizhansky, V.; Hodes, G.; Vega, S., Solid State NMR Study of Water Binding on the Surface of CdS Nanoparticles, *J.Phys.Chem.B*, **2000**, 104, 1939-1943.

51) a) Torimoto, Tsukasa; Kontani, Hironori; Shibutani, Yoshihiro; Kuwabata, Susumu; Sakata, Takao; Mori, Hirotaro; Yoneyama, Hiroshi, Characterization of Ultrasmall CdS Nanoparticles Prepared by the Size-Selective Photoetching Technique, *J. Phys. Chem.B*, **2001**, 105(29), 6838-6845.

b) Rice, Cynthia; Tong, YuYe; Oldfield, Eric; Wieckowski, Andrzej; Hahn, Francoise; Gloaguen, Frederic; Leger, Jean-Michel; Lamy, Claude, In Situ Infrared Study of Carbon Monoxide Adsorbed onto Commercial Fuel-Cell-Grade Carbon-Supported Platinum Nanoparticles: Correlation with 13C NMR Results, *J. Phys. Chem.B*, **2000**, 104(24), 5803-5807.

c) L. R. Becerra, C. B. Murray, R. G. Griffin, Bawendi, M. G., Investigation of the surface morphology of capped CdSe nanocrystallites by ^{31}P nuclear magnetic resonance, *J. Chem. Phys.*, **1994**, 100 (4), 3297-3300.

d) Chen, Shuang; Liu, Weimin; Yu, Laigui, Study on the structure of PbS nanoparticles coated with dialkyldithiophosphate, *J. Mater.Res.*, **1999**, 14(5), 2147-2151.

52) Daniele Gerion, Fabien Pinaud, Shara C.Williams, Wolfgang J.Parak, Daniele Zanchet, Shimon Weiss, and A.Paul Alivisatos, Synthesis and Properties of Biocompatible Water-Soluble Silica-Coated CdSe/ZnS Semiconductor Quantum Dots, *J.Phys.Chem.B*, **2001**, 105, 8861-8871.

53) a) Lakowicz, J. R.; Gryczynski, I.; Gryczynski, Z.; Murphy, C. J., Luminescence Spectral Properties of CdS Nanoparticles, *J.Phys.Chem.B*, **1999**, 103(36), 7613-7620.

b) Lakowicz, J. R.; Gryczynski, I.; Gryczynski, Z.; Nowaczyk, K.; Murphy, C. J., Time-Resolved Spectral Observations of Cadmium-Enriched Cadmium Sulfide Nanoparticles and the Effects of DNA Oligomer Binding, *Anal.Biochem.*, **2000**, 280, 128-136.

54) Lakowicz, Joseph R.; Gryczynski, Ignacy; Gryczynski, Zygmunt; Nowaczyk, Kazimierz; Murphy, Catherine J., Time-Resolved Spectral Observations of Cadmium-Enriched Cadmium Sulfide Nanoparticles and the Effects of DNA Oligomer Binding, *Anal. Biochem.*, **2000**, 280(1), 128-136.

55) Tong Ni, Dattatri K.Nagesha, Juvencio Robles, Nicholas F.Materer, Stefan Mussig, and Nicholas A.Kotov, CdS Nanoparticles Modified to Chalcogen Sites: New Supramolecular Complexes, Butterfly Bridging, and Related Optical Effects, *J.Am.Chem.Soc.*, **2002**, 124(15), 3980-3992.

56) Haesselbarth, A.; Eychmueller, A.; Eichberger, R.; Giersig, M.; Mews, A.; Weller, H., Chemistry and photophysics of mixed cadmium sulfide/mercury sulfide colloids, *J.Phys.Chem.*, **1993**, 97, 5333-5340.

57) Lifshitz, E.; Porteanu, H.; Glozman, A.; Weller, H.; Pflughoefft, M.; Echymueller, A., Optically Detected Magnetic Resonance Study of CdS/HgS/CdS Quantum Dot Quantum Wells, *J.Phys.Chem.B*, **1999**, 103, 6870-6875.

58) Mews, A.; Eychmueller, A.; Giersig, M.; Schooss, D.; Weller, H., Preparation, characterization, and photophysics of the quantum dot quantum well system cadmium sulfide/mercury sulfide/cadmium sulfide, *J.Phys.Chem.*, **1994**, 98, 934-941.

59) Correa-Duarte, M. A.; Giersig, M.; Liz-Marzan, L. M., Stabilization of CdS semiconductor nanoparticles against photodegradation by a silica coating procedure, *Chem.Phys.Lett.*, **1998**, 286, 497-501.

60) Caruso, F., Nanoengineering of Particle Surfaces, *Adv.Mater.(Weinheim, Ger.)*, **2001**, 13, 11-22.

61) Sullivan B.P., Salmon D.J., and Meyer T.J., Mixed phosphine 2,2'-bipyridine complexes of ruthenium, *Inorg.Chem.*, **1978**, 17, 3334-3341.

62) Suresh E and Bhabdhade M.M. Acta Crystallogr. C53, 193-195. 1997.

63) Cordero, S. R., Carson, P. J., Estabrook, R. A., Strouse, G. F., and Buratto, S. K., Photo-Activated Luminescence of CdSe Quantum Dot Monolayers, *J.Phys.Chem.B*, **2000**, 104, 12137-12142.

64) Peng, X. G., Wickham, J., and Alivisatos, A. P., Kinetics of II-VI and III-V Colloidal Semiconductor Nanocrystal Growth: "Focusing" of Size Distributions, *J.Am.Chem.Soc.*, **1998**, 120, 5343-5344.

65) Micic, O. I. and Nozik, A. J., Synthesis and characterization of binary and ternary III-V quantum dots, *J.Lumin.*, **1996**, 70, 95-107.

66) Motte, L. and Pileni, M. P., Influence of Length of Alkyl Chains Used To Passivate Silver Sulfide Nanoparticles on Two- and Three-Dimensional Self-Organization, *J.Phys.Chem.*, **1998**, 102, 4104-4109.

67) Penner, R. M. *Acc.Chem.Res.*, **2000**, 33, 78-86.

68) Wilcoxon, J. P., Newcomer, P. P., and Samara, G. A., Synthesis and optical properties of MoS_2 and isomorphous nanoclusters in the quantum confinement regime, *J.Appl.Phys.*, **1997**, 81, 7934-7944.

69) Wilcoxon, J. P.; Newcomer, P. P.; Samara, G. A., Strong quantum confinement effects in semiconductors: FeS_2 nanoclusters, *Solid State Commun.* **1996**, 98, 581-585.

70) Becker, R. S., Zhou, G. D., and Elton, J., Preparation and photoelectrochemistry of p-mercury indium telluride (HgIn2Te4) and p- and n-cadmium indium telluride ($CdIn_2Te_4$), *J.Phys.Chem.*, **1986**, 90, 5866-5870.

71) Odenweller, T. and Grabner, E. W., *Ber.Bunsen-Ges.Phys.Chem.*, **1988**, 92, 1330-1334.

72) Mikulec, F. V., Kuno, M., Bennati, M., Hall, D. A., Griffin, R. G., and Bawendi, M.

G., Organometallic Synthesis and Spectroscopic Characterization of Manganese-Doped CdSe Nanocrystals, *J.Am.Chem.Soc.*, **2000**, 122, 2532.

73) Norris, D. J., Yao, N., Charnock, F. T., and Kennedy, T. A., *Nanoletters* 1, 3-7. 2001.

74) Kamat, P., Dimitrievich, N. M., and Fessenden, R. W., Photoelectrochemistry in particulate systems. 7. Electron-transfer reactions of indium sulfide semiconductor colloids, *J.Phys.Chem*, **1988**, 92, 2324-2329.

75) Lakowicz, Joseph R. Principles of Fluorescent Spectroscopy. 1986. New York, Plenum Press.

76) Tong Ni. Synthesis, Property Study and Modification of II-VI Sulfide Semiconductor Nanoparticles. Thesis . 2002. Oklahoma State University.

77) Bawendi, M. G., Carroll, P. J., Wilson, William L., Brus, L. E., Luminescence properties of CdSe quantum crystallites: Resonance between interior and surface states, *J. Chem. Phys.*, **1992**, 96 (2), 946-954.

78) Peng, Xiaogang, Wickham, J., Alivisatos, A. P., Kinetics of II-VI and III-V Colloidal Semiconductor Nanocrystal Growth: "Focusing" of Size Distributions, *J. Am. Chem. Soc.*, **1998**, 120, 5343-5344.

79) a) Nosaka, Y.; Ohta, N.; Miyama, H., Photochemical kinetics of ultrasmall semiconductor particles in solution: effect of size on the quantum yield of electron transfer, *J. Phys. Chem.* **1990**, *94*, 3752-3755

b) Becker, R. S.; Zhou, G. D.; Elton, J., Preparation and photoelectrochemistry of *p*-mercury indium telluride ($HgIn_2Te_4$) and p- and n- cadmium indium telluride ($CdIn_2Te_4$), *J. Phys. Chem.* **1986**, *90*, 5866-5870

c) Herrero, J.; Ortega, J., n-Type indium sulfide (In_2S_3) thin films prepared by gas chalcogenization of metallic electroplated indium: photoelectrochemical characterization, *Sol. Energy Mater.* **1988**, *17*, 357-368

d) Hodes, G.; Engelhard, T.; Turner, J. A.; Cahen, D., Slurry painted copper indium sulfide ($CuInS_2$ and $CuIn_5S_8$) layers: preparation and photoelectrochemical characterization, *Sol. Energy Mater.* **1985**, *12*, 211-219

e) Kambas, K.; Anagnostopoulos, A.; Ves, S.; Ploss, B.; Spyridelis, J., Optical absorption edge investigation of cadmium indium sulfide ($CdIn_2S_4$) and b-indium sulfide compounds, *Phys. Status Solidi B* **1985**, *127*, 201-208

f) Yoshida, T.; Yamaguchi, K.; Toyoda, H.; Akao, K.; Sugiura, T.; Minoura, H.; Nosaka, Y., *Proc.- Electrochem. Soc.* **1997**, *97-20*, 37-57.

g) George, J.; Joseph, K. S.; Pradeep, B.; Palson, T. I., Reactively evaporated films of indium sulfide, *Phys. Status Solidi A* **1988**, *106*, 123-131.

80) a) Kim, W. T.; Kim, C. D. Optical energy gaps of β-indium sulfide (In_2S_3) thin films grown by spray pyrolysis, *J. Appl. Phys.* **1986**, *60*, 2631-2633

b.Tagirov, V. I.; Ismailov, I. M.; Khusein, A. K. Study of absorption band edge of indium sulfide (In_6S_7), *Fiz. Tekh. Poluprovodn.* **1978**, *12*, 2027-2028

c. Kambas, K. Near band-edge optical investigation of α-indium sesquiselenide and α-indium sulfide selenide (α-In_2S_3-xSe_x) mixed crystals, *Physica B (Amsterdam)* **1989**, *160*, 103-107

d. Kim, C. D.; Lim, H.; Park, H. L.; Park, H. Y.; Kim, J. E.; Kim, H. G.; Kim, Y. G.; Kim, W. T., Optical absorption of cobalt ($^{2+}$) ions in indium sulfide (In_2S_3) thin films, *Thin Solid Films* **1993**, *224*, 69-73.

81. Diehl, R.; Nitsche, R., Vapor and flux growth of γ-indium sulfide, a new modification of indium sesquisulfide, *J. Crystal Growth* **197 3**, *20*, 38-46.

82. Bessergenev, V. G.; Bessergenev, A. V.; Ivanova, E. N.; Kovalevskaya, Yu. A., Study of In_2S_3 thin films by diffraction of synchrotron radiation, *J. Solid State Chem.* **1998**, *137*, 6-11

83. *Powder Diffraction File Sets 1-5 (Revised)*; Joint Committee on Powder Diffraction Standards, 1845 Walnut St., Philadelphia, PA, 1967; pp 5-0729-5-0731.

84.a. Bhira, L.; Essadi, H.; Belgacem, S.; Couturier, G.; Salardenne, J.; Barreaux, N.; Bernede, J. C., Structure and photoelectrical properties of sprayed β-In_2S_3 thin films, *Phys. Status Solidi* **2000**, *181*, 427-435.

b. Yu, S.; Shu, L.; Qian, Y.; Xie, Y.; Yang, J.; Yang, L., Hydrothermal preparation and characterization of nanocrystalline powder of β-indium sulfide, *Mater. Res. Bull.* **1998**, *33*, 717-721.

85. O'Brian, P.; Walsh, J. R.,*Thin Solid Films* **1998**, *315*, 57-61

86. Lokhande, C. D.; Ennaoui, A.; Patil, P. S.; Giersig, M.; Diesner, K.; Muller, M.; Tributsch, H., Chemical bath deposition of indium sulfide thin films: preparation and characterization, *Thin Solid Films* **1999**, *340*, 18-23.

87. Diehl, R.; Nitsche, R., Vapor and flux growth of γ- indium sulfide, a new modification of indium sesquisulfide, *J. Crystal Growth* **197 3**, *20*, 38-46.

88. Gusten, H.; Rinke, M.; Wirth, H. O., *Appl. Phys. B* **1988**, *45*, 279.

89. http://www.lambdaphysik.com/productspectrum/index.asp.

90) Cherepy, N. J., Liston, D. B., Lovejoy, J. A., Deng, H., Zhang, J. Z., *J. Phys. Chem. B*, **1998**, 102, 770-776.

91. Dabbousi, B. O.; Rodriguez-Viejo, J.; Mikulec, F. V.; Heine, J. R.; Mattoussi, H.; Ober, R.; Jensen, K. F.; Bawendi, M. G., (CdSe)ZnS Core-Shell Quantum Dots: Synthesis and Characterization of a Size Series of Highly Luminescent Nanocrystallites, *J. Phys. Chem. B* **1997**, *101*, 9463-9475.

92. Peng, X. G.; Schlamp, M. C.; Kadavanich, A. V.; Alivisatos, A. P., Epitaxial Growth of Highly Luminescent CdSe/CdS Core/Shell Nanocrystals with photostability and Electronic Accessibility, *J. Am. Chem. Soc.* **1997**, *119*, 7019-7029.

93. Norris, D. J.; Bawendi, M. G.; Brus, L. E., Optical properties of semiconductor nanocrystals (quantum dots), *Mol. Electron.* **1997**, 281-323.

94. a. Leif Hammarström, Francesco Barigelletti, Lucia Flamigni, Maria Teresa Indelli, Nicola Armaroli, Giuseppe Calogero, Massimo Guardigli, Angelique Sour, Jean-Paul Collin, and Jean-Pierre Sauvage, A Study on Delocalization of MLCT Excited States by Rigid Bridging Ligands in Homometallic Dinuclear Complexes of Ruthenium(II), *J. Phys. Chem. A*, **1997**, 101(48), 9061-9069. b. Grosshenny, V.; Harriman, A.; Romero, F. M.; Ziessel, R., Electron Delocalization in Ruthenium(II) and Osmium(II) 2,2'-Bipyridyl Complexes Formed from Ethynyl-Bridged Ditopic Ligands, *J. Phys. Chem.* **1996**, *100*, 17472-17484.

c. Boyde, S.; Strouse, G. F.; Jones, W. E., Jr.; Meyer, T. J., The effect of MLCT excited states of electronic delocalization in the acceptor ligand, *J. Am. Chem. Soc.* **1990**, *112*, 7395-7396.

95) a) Strouse, G. F.; Schoonover, J. R.; Duesing, R.; Boyde, S.; Jones, W. E. J.; Meyer, T. J., Influence of Electronic Delocalization In Metal-to-Ligand Charge Transfer Excited States, *Inorg. Chem.* **1995**, *34*, 473-487.

b) Li, C.; Hoffman, M. Z., Electron Localization or Delocalization in the MLCT Excited States of $Ru(bpy)_3^{2+}$ and $Ru(phen)_3^{2+}$. Consequences to Their Photochemistry and

Photophysics in Fluid Solution, *Inorg. Chem.* **1998**, *37*, 830-832.

c) Aarnts, M. P.; Stufkens, D. J.; Wilms, M. P.; Baerends, E. J.; Vlcek, A., Jr.; Clark, I. P.; George, M. W.; Turner, J. J., A combined spectroscopic, photophysical and theoretical (DFT) study of the electronically excited inorganometallic complexes [Ru(E)(E')(CO)2(iPr-DAB)] (E = Cl, Me, SnPh3, PbPh3; E' = GePh3, SnR3, PbR3 (R = Me, Ph); iPr-DAB = N,N'-diisopropyl-1,4-diaza-1,3-butadiene): evidence of an exceptionally long-lived 3sp* excited state for [Ru(SnPh3)2(CO)2(iPr-DAB)], *Chem.-Eur. J.* **1996**, *2*, 1556-1565.

96) Diaz, David; Rivera, Mario; Ni, Tong; Rodriguez, Juan-Carlos; Castillo-Blum, Silvia-Elena; Nagesha, Dattatri; Robles, Juvencio; Alvarez-Fregoso, Octavio-Jaime; Kotov, Nicholas A.; Conformation of Ethylhexanoate Stabilizer on the Surface of CdS Nanoparticles, *J. Phys. Chem. B*, **1999**, 103(45), 9854-9858.

97) Diaz, David; Robles, Juvencio; Ni, Tong; Castillo-Blum, Silvia-Elena; Nagesha, Dattatri; Alvarez-Fregoso, Octavio-Jaime; Kotov, Nicholas A.; Surface Modification of CdS Nanoparticles with MoS42-: A Case Study of Nanoparticle-Modifier Electronic Interaction, *J. Phys. Chem. B*, **1999**, 103(45), 9859-9866.

98) Jana, Nikhil R.; Gearheart, Latha; Murphy, Catherine J.; Seeding growth for size control of 5-40 nm diameter gold nanoparticles, *Langmuir*, **2001**, 17(02), 6782-6786.

99) Mahtab, Rahina; Harden, H. Hydrick; Murphy, Catherine, J.; Temperature- and Salt-Dependent Binding of Long DNA to Protein-Sized Quantum Dots: Thermodynamics of "Inorganic Protein"-DNA Interactions, *J. Am. Chem. Soc.*, **2000**, 122(1), 14-17.

100) Murphy, Catherine J.; CdS Nanoclusters Stabilized by Thiolate Ligands: A mini-review, *J. Cluster Science*, **1996**, 7(3), 341-350.

101) Ashokkumar, M.; Kudo, A.; Sakata, T.; Synthesis and characterization of RuS_2 nanocrystallites. *J. Mater. Sci.*, **1995**, 30(11), 2759-2764.

102) Berhault, G.; Lacroix, M.; Breysse, M.; Mauge, F.; Lavalley, J.C.; Nie, H.; Qu, L.; *J. Catal.*, **1998**, 178, 555.

VITA

Dattatri Jois Kudanalli Nagesha 2

Candidate for the Degree of

Doctor of Philosophy

Dissertation: SYNTHESIS AND CHARACTERIZATION OF CdSe AND In_2S_3 SEMICONDUCTOR NANOPARTICLES AND THEIR SURFACE MODIFICATION USING $Ru(bipy)_2 Cl_2$ COMPLEX

Major Field: Chemistry

Biographical:

Education: Graduated with Bachelors in Science from A.M. Jain College, Madras University, in 1995. Obtained a Masters in Science degree from Indian Institute of Technology, Chennai, in 1997. Completed the requirements for the Doctor in Philosophy degree in Chemistry at Oklahoma State University in December 2002.

Experience: Employed by the Oklahoma State University, Department of Chemistry as a graduate teaching assistant and research assistant, 1997 to present.

Professional Memberships: American Chemical Society, Materials Research Society, Phi Lambda Upsilon